



JIMMA UNIVERSITY
JIMMA INSTITUTE OF TECHNOLOGY
SCHOOL OF GRADUATE STUDIES
FACULTY OF MECHANICAL ENGINEERING
DESIGN OF MECHANICAL SYSTEM

**ANALYZING THE EFFECT OF OXIDE SCALE GROWTH ON CREEP BEHAVIOR
AND RUPTURE TIME OF SUPERHEATER TUBE BOILER**

A thesis submitted to School of Graduate Studies, Jimma University, Jimma Institute of Technology, Faculty of Mechanical Engineering in Partial Fulfillment of the Requirements for the Degree Master of Science in Design of Mechanical System

By
Ermiyas Tefera Yigletu

June 2, 2023
Jimma, Ethiopia

JIMMA UNIVERSITY
JIMMA INSTITUTE OF TECHNOLOGY
SCHOOL OF GRADUATE STUDIES
FACULTY OF MECHANICAL ENGINEERING
DESIGN OF MECHANICAL SYSTEM

Analyzing the Effect of Oxide Scale Growth on Creep Behavior and Rupture Time of
Superheater Tube Boiler

A thesis submitted to School of Graduate Studies, Jimma University, Jimma Institute of
Technology, Faculty of Mechanical Engineering in Partial Fulfillment of the
Requirements for the Degree Master of Science in Design of Mechanical System



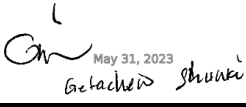
Main Advisor: Dr.-Ing. Mesay Alemu (Assoc. Prof.)
Co-Advisor: Dr. Johnson Santhosh (Asst. Prof.)

June 2, 2023
Jimma, Ethiopia

JIMMA UNIVERSITY
JIMMA INSTITUTE OF TECHNOLOGY
POST GRADUATE PROGRAM


This is to certify that the thesis prepared by Ermiyas Tefera Yigletu, entitled: **“Analyzing the Effect of Oxide Scale Growth on Creep Damage and Rupture Time of Superheater Tube Boiler”** and submitted in partial fulfillment of the requirements for the degree of masters of Science in Mechanical Engineering (Design of Mechanical System) complies with the regulations of the university and meets the accepted standards with respect to the originality and quality.

Approved by the Examining Committee:

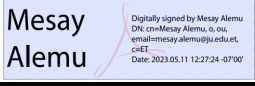

Dr.-Ing. Mesay Alemu (Assoc.Prof.) Advisor	 Signature	<u>May 31, 2023</u> Date
Dr. Johnson Santhosh (Asst.Prof.) Co-Advisor	 Signature	<u>May 31, 2023</u> Date
Dr.-Ing. Getachew Shunki (Assoc.Prof.) External Examiner	 Signature	<u>May 31, 2023</u> Date
Mr. Addisu Kidanemariam (Asst.Prof.) Internal Examiner	_____ Signature	_____ Date
Mr. Firew Tullu Chairman	_____ Signature	_____ Date

DECLARATION

I declare that this research entitled “Analyzing the Effect of Oxide Scale Growth on Creep Behavior and Rupture Time of Superheater Tube Boiler” is my original work and has not been submitted as a requirement for the award of any degree in Jimma University or elsewhere.

Ermiyas Tefera Yigletu Name	 Signature	May 31, 2023 Date
--------------------------------	--	----------------------

As research Adviser, I hereby certify that I have read and evaluated this thesis paper prepared under my guidance, by Ermiyas Tefera Yigletu entitled “ANALYZING THE EFFECT OF OXIDE SCALE GROWTH ON CREEP BEHAVIOR AND RUPTURE TIME OF SUPERHEATER TUBE BOILER” and recommend and would be accepted as a fulfilling requirement for the Degree Master of Science in Design of Mechanical System.

Dr.-Ing. Mesay Alemu (Assoc.Prof.) Advisor	 Signature	May 31, 2023 Date
Dr. Johnson Santhosh (Asst.Prof.) Co-Advisor	 Signature	May 31, 2023 Date
Mr. Firew Tullu Chairman	 Signature	May 31, 2023 Date

ACKNOWLEDGMENT

First and foremost, I would like to dedicate my deepest gratitude to my advisor Dr. Mesay Alemu and Co-Advisor Dr. Johnson Santhosh for their valuable advice by commenting and directing to accomplish this through their effort.

Deepest gratitude also for the Design of mechanical system head and also the staff members of the Faculty of Mechanical Engineering, who share their knowledge and assistance and play a great role in the success of this thesis work.

Special thanks also go to the friends and colleagues who have given advice, motivation and inspiration during this work.

ABSTRACT

One way of increasing boiler efficiency is by increasing the working pressure and temperature of steam. But higher operating temperature and pressure leads to the formation and growth of steam side oxide scale. The growth of oxide scale reduces the heat transfer from flue gas to steam and overheating the tube. The accumulated stress and strain due to oxide growth can cause scale exfoliation or failure when the strain exceed the critical strain. The failure of oxide scale can cause obstructing tube bends, eroding the nozzle, and eroding the first stage of the turbine's blades. Due to growth of oxide scale the metal tube overheating and it leads to creep damage of the tube. T92(SA213-T92) is one type of high alloy ferritic (Martensitic) steels and it is the preferred choice material for high temperature and pressure application of superheater boiler tube, thus the mechanism and kinetics of oxidation, the growth of oxidation, thermos-mechanical stress-strain and effect of oxide scale growth on creep behavior should be studied. Analytical and numerical approaches are applied in this research. For analytical computation, develop a mathematical model and computed by using python. The numerical is computed by numerical (finite element simulation) software of ABAQUS. The rate of oxide growth of T92 alloy steel is computed at different steam temperature (600°C and 650°C) and flue gas temperature (800°C, 900°C and 1000°C), based on the analytical and numerical result the oxide growth rate at 650°C steam temperature is higher and the oxide scale growth is more affected by the increase of steam side temperature than flue gas temperature. Around 178µm the thermo-mechanical hoop strain become 1.503×10^{-3} and it cross the critical strain in tension curve, which means the oxide scale start cracking. Under constant internal pressure and elevated temperature for a long period of time the material accounts secondary creep behavior and computed by using Norton's law (power creep law) and time-hardening rule. Based on the analytical and numerical result, the creep hoop stress and strain rate in increasing due to the increase of oxide scale, and after 10000 working hour of superheater boiler tube the maximum creep hoop stress become 169.2 MPa and the maximum creep strain rate become $8.612 \times 10^{-1} \text{ hr}^{-1}$. The creep rupture time is calculated based on LMP and with the Norton's Law of minimum creep strain rate relation. Based on LMP prediction 73% reduction of rupture time when the boiler tube has 242µm oxide scale thickness as compared to the oxide scale of 96µm. The result from both analytical approach and numerical (FEM) have a good agreement with other literatures.

Key words: Steam side oxide scale, Elastic stress-strain, thermal (thermo-mechanical) stress-strain, critical strain, crack initiation, creep stress, creep strain rate, creep rupture time.

Table of Contents

DECLARATION	ii
ACKNOWLEDGMENT	iii
ABSTRACT	iv
Table of Contents	vi
List of Table	viii
List of Figure	x
List of Symbols	xi
1 INTRODUCTION	1
1.1 Background	1
1.2 Research questions	8
1.3 Problem statement	9
1.4 Objectives	10
1.4.1 General Objective	10
1.4.2 Specific Objectives	10
1.5 Scope of the study	11
1.6 Significance of the study	11
1.7 Structure of the Thesis	12
2 LITERATURE REVIEW	13
3 MATERIAL AND METHODS	20
3.1 Material for Superheater boiler tube	20
3.2 Research methodology	24
3.2.1 Selection of Appropriate Approach	24
3.2.2 Tools or Techniques	24
3.2.3 Method of oxide scale growth prediction	26
4 HIGH TEMPERATURE OXIDATION AND MATHEMATICAL MODELING	29
4.1 Steam-side oxidation	29
4.1.1 Oxidation Mechanics (Formation)	30
4.1.2 Oxidation Kinetics	32
4.2 Oxidation of Ferritic steel	35
4.2.1 Oxidation of high alloy ferritic (Martensitic) steel (T92)	35
4.3 Mathematical Modeling	38

4.3.1	Heat transfer Analysis	38
4.3.2	Estimation of oxide scale growth	47
4.4	Stress analysis of steam side oxide scaled boiler tube	47
4.4.1	Derivative of Equilibrium Equation	49
4.4.2	Elastic stress and strain	49
4.4.3	Thermo-Mechanical (Thermal) stress and strain	52
4.4.4	Failure of oxide scale	55
4.5	Creep stress and Strain rate of Metal	56
4.5.1	Predict creep rupture time	60
4.6	Numerical (Finite Element) Method Simulation	62
4.6.1	Finite Element Simulation/Modeling Procedure	62
5	RESULT AND DISCUSSION	67
5.1	Oxidation kinetics	67
5.1.1	Estimation of oxide scale growth at different temperature	67
5.1.2	Compare the effect of steam and flue gas temperature	71
5.2	Result of stress and strain	75
5.2.1	Result of Elastic stress and strain at different oxide scale	77
5.2.2	Result of Thermal stress and strain at different oxide scale	82
5.2.3	Result of Failure of Oxide scale	89
5.3	Result of Creep Analysis	90
5.3.1	Result of creep rupture time	94
6	CONCLUSION AND RECOMMENDATION	97
6.1	Conclusion	97
6.2	Recommendation	99
	REFERENCES	100
A	APPENDIX	108
A.1	Properties of T92 alloy steel and steam side oxide	108
B	APPENDIX	110
B.1	Python code for predicting oxide scale growth	110
B.2	Python code for Elastic radial and hoop stress-strain	115
B.3	Python code for Thermo-Mechanical radial and hoop stress-strain	118
B.4	Python code for Creep stress and strain rate	122

List of Tables

3.1	Chemical composition (wt.%) of selected Ferritic steels [27,42,46]	22
3.2	Chemical composition (wt.%) of selected Ferritic steels	23
3.3	Chemical composition (wt.%) of selected Ferritic steel for this research . .	24
4.1	Value of the parabolic rate constant K_p value for oxide thickness	37
4.2	Parameters of the steady state heat transfer stiffness matrix	45
4.3	The time used in the iterative procedure	47
4.4	Mesh convergence result	65
5.1	The value of h_g at different temperature	67
5.2	The value of h_s at different temperature and free from oxide scale condition	67
5.3	Oxide growth at each iterative step when $h_g = 220.03, T_s = 600^\circ\text{C}$ and $T_g =$ 800°C	68
5.4	Oxide growth at each iterative step when $h_g = 227.78, T_s = 600^\circ\text{C}$ and $T_g =$ 900°C	69
5.5	Oxide growth at each iterative step when $h_g = 234.64, T_s = 600^\circ\text{C}$ and $T_g =$ 1000°C	69
5.6	Oxide growth at each iterative step when $h_g = 220.03, T_s = 650^\circ\text{C}$ and $T_g =$ 800°C	70
5.7	Oxide growth at each iterative step when $h_g = 227.78, T_s = 650^\circ\text{C}$ and $T_g =$ 900°C	70
5.8	Oxide growth at each iterative step when $h_g = 234.64, T_s = 650^\circ\text{C}$ and $T_g =$ 1000°C	71
5.9	summery of the effect of different temperature for the growth of oxide scale thickness	72
5.10	Summery of analytical and numerical result of elastic radial stress at dif- ferent oxide scale	77
5.11	Summery of analytical and numerical result of elastic hoop stress at dif- ferent oxide scale	78
5.12	Summery of analytical and numerical result of elastic radial strain at dif- ferent oxide scale	79
5.13	Summery of analytical and numerical result of elastic hoop strain at dif- ferent oxide scale	80
5.14	Analytical and numerical result of thermal radial stress at different oxide scale	82
5.15	Summery of analytical and numerical result of thermal hoop stress at dif- ferent oxide scale	83
5.16	Summery of analytical and numerical result of thermo-mechanical radial strain at different oxide scale	84

5.17	Summery of analytical and numerical result of thermo-mechanical hoop strain at different oxide scale	85
5.18	Summery of analytical and numerical result of creep radial, hoop and von mises stress at different oxide scale thickness	91
5.19	Summery of analytical and numerical result of creep radial and hoop strain at different oxide scale thickness	91
5.20	Summery of analytical and numerical result of radial and hoop creep strain rate at different working time	92
5.21	Summery of creep rupture time due to growth of oxide scale thickness using LMP	94
5.22	Summery of creep rupture time due to growth of oxide scale thickness using power law rupture	94
A.1	Geometry of T92 superheater tubes	108
A.2	Thermo-physical properties of metal and oxide	108
A.3	Thermo- physical properties of steam	108
A.4	Thermo- physical properties of flue gas	108
A.5	Oxide scale and Temperature of boiler tube for a given time	109
A.6	Creep parameter of T92 steel at temperature of 600°C of steam	109

List of Figures

1.1	Failure of Boiler tubes [2-4]	2
1.2	Creep curve obtained at constant temperature under constant load	5
1.3	Schematic representation of superheater with steam side oxide scale	7
3.1	Research Methodology	25
3.2	Flow chart of the iterative procedure	28
4.1	Schematic representation of the oxidation process. Adapted from[49,52]	30
4.2	Schematic representation of the metal-scale-gas system[50]	31
4.3	Oxidation mechanisms of ions transfer in high temperature. Cation mobile (a) and Anion mobile (b) [50,51]	32
4.4	Mass gain curve versus time for the three-oxidation kinetics law	33
4.5	Summary of oxide scale morphologies formed on chromium containing steels in high temperature steam.	35
4.6	Schematic representation of oxidation mechanism of T92 alloy steel	36
4.7	Optical micrographs showing oxide scale cross-section of T92 steel on the steam side after exposure at 650°C for (a) 25 h (b) 250 h and (c) 1000 h. [55]	36
4.8	Summarized oxide thickness of T92 steels with time in temperature range between 600 and 750 C, based on Table 4.1	37
4.9	Arrangement and geometry of superheater tubes.	39
4.10	Schematic representation of the steam-side oxide scale and the discretization model.	40
4.11	Discretize representation of the steam side oxide with dimensional representation.	42
4.12	Applied stress acting on circumferential and longitudinal direction of the tubes[67]	48
4.13	Radial representation of oxide scaled boiler tube	49
4.14	Schematic representation of displacement stress element	50
4.15	Representation of criteria for oxide failure in an Exfoliation Diagram[12]	56
4.16	Two-dimensional part model boiler tube	63
4.17	Quadrilateral mesh surface of the oxide scale boiler tube at 242.82 μm of oxide scale thickness at different mesh size (a) 0.2 mm, (b) 0.1mm, (c) 0.05mm, and (d) 0.025mm	66
5.1	Simulation result of Temperature distribution at 60.0686 μm of oxide scale thickness	68
5.2	Summery of oxide scale thickness as a function of time with the steam temperature of 600°C for different flue gas temperature	70
5.3	Summery of oxide scale thickness as a function of time with the steam temperature of 650°C for different flue gas temperature	71

5.4	Comparison the effect of flue gas and steam temperature for the growth of oxide scale	72
5.5	Temperature at relevant surfaces	74
5.6	The experimental and calculated value of oxide scale thickness at 600°C of steam temperature after 1000hr exposure	74
5.7	The experimental and calculated value of oxide scale thickness at 650°C of steam temperature after 1000hr exposure	75
5.8	Simulation result of Elastic hoop stress at 242.82 μm of oxide scale thicknes	76
5.9	Simulation result of Elastic hoop strain at 242.82 μm of oxide scale thickness	77
5.10	Numerical results of elastic radial and hoop stress vs total thickness of tube	79
5.11	Numerical results of elastic radial and hoop strain vs total thickness of tube	80
5.12	Maximum of elastic radial and hoop strain at different oxide scale thickness	81
5.13	Maximum of elastic radial and hoop stress at different oxide scale thickness	82
5.14	Numerical results of thermos- radial and hoop stress vs total thickness of tube	84
5.15	Numerical results of thermo-mechanical radial and hoop strain vs total thickness of tube	85
5.16	Maximum of thermal radial and hoop strain at different oxide scale thickness	86
5.17	Maximum of thermal radial and hoop stress at different oxide scale thickness	87
5.18	Comparison between analytical and numerical value of stress	88
5.19	Damage map showing critical strains and maximum elastic strains of oxide scale	89
5.20	Damage map showing critical strains and maximum thermal strains of oxide scale	90
5.21	creep stress of metal versus radial direction of tube (a) and at different oxide scale (b)	92
5.22	Creep strain rate vs working time	93
5.23	Stress vs rupture time	95
5.24	Comparison between predicted and experimental value of rupture time . .	95
A.1	Thermal expansion of T92 alloy and oxide scale at different temperature .	109

List of Symbols

$\dot{\varepsilon}_{\theta}^c$	Radial creep strain rate (hr^{-1})
K_p	proportional constant of parabolic law
μ_g	dynamics viscosity of gas
ε_{θ}	Hoop strain
Pr_s	Prandtl Number of steam
Pr_g	Prandtl Number of gas
$\dot{\varepsilon}_r^c$	Radial creep strain rate (hr^{-1})
C_g	specific heat of the gas
C_s	specific heat of the steam
h_g	Convection coefficient of the gas
h_s	Convection coefficient of the steam
K_g	thermal conductivity of gas
K_s	thermal conductivity of steam
p	Larson – miller parameter
r_0 or c	Radius of outer tube (m)
r_n or b	Radius of oxide/metal interface surface (m)
r_x or a	Radius of inner tube (inner radii of oxide scale) (m)
t	Service time (in hour)
T_g	Flue gas temperature ($^{\circ}C$)
T_m	Melting (recrystallization) temperature ($^{\circ}C$)
T_s	steam temperature ($^{\circ}C$)
T_{ave}	Average temperature ($^{\circ}C$)
u	Displacement
α_j	thermal expansion coefficient of j th layer (oxide and metal)

E_{met}	Young's modulus of Metal (GP_a)
E_{ox}	Young's modulus of Oxide (GP_a)
μ_S	dynamics viscosity of steam
σ_e	Von mises stress or equivalent stress (MP_a)
σ_r	Radial stress (MP_a)
σ_z	Axial stress (MP_a)
σ_θ	Hoop stress (MP_a)
ε_r	Radial strain
Re_g	Reynolds Number of gas
Re_S	Reynolds Number of steam
FEM	Finite Element Method
LMP	Larson – miller parameter
SSOS	Steam side oxide scale
$X(\delta_X)$	Thickness of steam side oxide scale (μm)

1. INTRODUCTION

1.1 Background

A boiler is a closed vessel that takes heat energy in the available form (for example, coal, oil, etc.) and converts the heat energy into the required purpose. Mainly used for heating water for producing steam in many power plant industries. In the modern power plant industries, the boiler has different accessories, the most commons are feed pump, injector, economizer, superheater, reheater, and air pre-heater.

Boiler tubes are important components of energy conversion systems that utilize thermal energy to transform water into high-pressure superheated steam, which is then fed to steam turbines to generate electricity. Understanding boiler-tube failures and tube service life could lead to significant improvements in boiler performance and availability, as well as a reduction in the severe economic loss associated with electricity generation.

Types of steam boilers differ in the way they burn fuel, the fuel they burn, or the steam cycle they use. As this thesis is concerned with the oxidation of steam-touched surfaces, it will be more useful to distinguish boiler types based on the steam cycle, because the steam-side oxidation is not directly influenced by the fuel burned or the method of combustion[1].

There are several different types of boilers, and the heat exchangers might be very different, but generally, the arrangement of the flue gas path is almost the same regardless. The heat exchanger transfers the heat generated by the combustion of fuel to the water/steam circulation in the boiler. It is critically important to exploit flue gas thermal energy as efficiently as possible in order to achieve high thermal efficiency.

Surfaces for heat exchange are categorized by purpose of use, such as evaporators, superheaters and reheaters, feedwater preheaters, economizers, and air preheaters. Typically, superheaters are exposed to the most severe conditions in a boiler, since they are exposed to the highest fluid temperatures and, subsequently, the highest metal temperatures. Materials for superheaters and reheaters should have sufficient heat resistance and creep strength. The statistical failure of boiler tubes is shown in Figure 1.1.

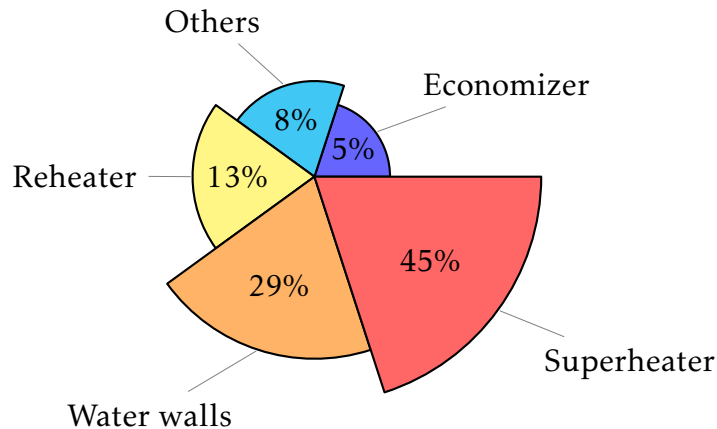


Figure 1.1: Failure of Boiler tubes [2-4]

In comparison to the other boiler tubes, the superheater boiler tube fails most of the time, as seen in Figure 1. So, in this thesis, choose a superheater boiler tube to investigate the failures.

Boiler tubes are prone to a variety of failure modes, such as short-term and long-term overheating (creep-rupture), surface pitting, stress corrosion cracking, and fatigue are the most common types of boiler tube failure these failures are led to the shutdown of the whole power plant. From these failures long term overheating (Creep) the most common and highly affect the life of boiler tube.

The main reason or cause of the failures of boiler tube in early-stage or before the expected lifetime is [2-6]

- The environmental condition means the working pressure and temperature or working in the corrosive environment and formation of oxide layers.
- The material properties or the micro structure of the tube
- Stress caused by internal fluid, external loads, due to bending of the tube, or welding those lowering the strength of the tube and it may easily attack by corrosion and form crack.

Short term overheating

During boiler startup, short-term overheat failures are the most common. When the tube metal temperature is exceptionally high due to a lack of cooling steam or water flow, failures occur. It's a type of fast failure caused by a loss of internal water or steam flow[3,4].

Stress corrosion cracking

In corrosion-resistant metals exposed to harsh conditions, stress corrosion cracking is a major concern. SCC is caused by three factors: (a) high tensile stress, either imposed (internal pressure or bending) or residual stress created during manufacturing or welding, (b) operating in a corrosive environment, and (c) a vulnerable material, such as one with insufficient mechanical qualities for the application.[2,4,6].

Fire side corrosion

It occurs on the boiler's outside surface. It's a very different process because it usually contains some kind of impurity deposit that contributes to the corrosion. The deposit is made up of additives and the fuel that was consumed. Due to the high steam temperature and reduced heat transfer coefficient of steam in superheaters and reheaters, the metal temperature is greatest. High metal temperatures and deposits caused by fly ash particles are the main causes of corrosion in this region. The deposits will also obstruct flue gas flow in the boiler, causing the boiler's internal energy consumption to rise and its efficiency to fall.

Steam side oxidation

The metal tubes contact with steam over a while the oxidation process begins and forms a layer this is called steam side oxidation. This layer form in the inside of the tube and reduce the thickness of the tube by forming a layer. On the steam side, temperature, pressure, and alloy composition all have an impact on oxidation behavior. Impurity deposits on the steam-side of a superheater tube are uncommon since steam impurity levels are closely controlled. Depending on the alloy composition, the scale created on the steam side is made up of different metal oxides. It commonly happens when materials are exposed to extremely high steam temperatures. The oxide scales that accumulate on the steam-side of the plant could cause serious failures and, as a result, lower plant availability. Due to steam-side oxidation, there are three basic forms of failure that can be identified. The first one is, oxidation-induced tube wall loss may increase hoop stresses and cause early creep failures in heat-exchanging tubes. Second, the insulating oxide scale may reduce thermal conductivity, resulting in higher metal temperatures and thus

faster creep and corrosion processes; this is commonly referred to as long-term overheating. The third point to consider is that when the oxide scale on the steam side thickens, it will be more likely to spall. The spalled oxide scale particles may lodge in the steam circulation and cause tube blockages, or they may cause erosion in turbine blades and nozzles if they enter the steam turbine. Steam-side oxidation is discussed more extensively in chapter 4.

Long term overheating

The focus of this study was on the second sort of steam side oxidation failure, known as boiler tube overheating. When the oxide layer forms reduce the cooling effect and also reduces the amount of heat transfer into the steam this leads to the hoop stress and the metal temperature increase[7,8]. The rise of the metal temperature over a long time of operation leads to creep. Creep is a function of time, temperature, and constant stress. It is a time-dependent deformation at elevated temperature and constant stress. Any metals subjected to a sustained load at a temperature slightly above their recrystallization temperature can experience creep[3,4]. The increase of operating temperature is increasing the boiler efficiency but this decreases the life of boiler because the increase temperature leads to creep[9]. Under creep conditions, the grain boundaries change from trans-granular to inter-granular. When this happens steady stress is considered with sufficient temperatures ($T \geq 0.4T_m$)[10].

Long term overheating (creep) due to formation of oxide scale mainly occurs in superheater and reheater boiler tubes after many years of use with high temperatures. Superheater boiler tubes are usually found in the boiler's final stages. Steam is conveyed at the highest pressure and temperature inside superheater tubes, which are exposed to high-temperature combustion gases. Mainly the creep life of the superheater boiler tube affected by the formation of oxide scale.

Creep

Creep is more severe in materials that are subjected to heat for long periods since creep is the time dependent deformations that occur when a material is subjected to high level of stresses at elevated temperature for prolonged period so when the time the boiler is exposed to much heat and pressure increases then the chances of creep are then automatically high and near melting point[11]. Unlike brittle fracture, creep deformation does not occur suddenly upon the application of stress. Instead, strain accumulates as a result of long-term stress. Creep deformation is "time-dependent" deformation.

Creep behavior or deformation

When the temperature and stress are modest, the primary creep regime predominates. Negligible initial creep strain will accrue in high-temperature alloys, but it is frequently not seen in studies. The primary creep regime was not considered since (a) it extends for a very limited time most time operating time less than 2000hr (b) the creep strain attained in this regime is very small[12]. When load and temperature are low to moderate, the secondary creep regime predominates. The most stable regime is one in which the prediction of creep deformation is straightforward due to a balance between strain-hardening and recovery mechanics. The tertiary creep phase takes control at intermediate-to-high temperature and stress. The creep-damage accumulation that does not occur linearly and contributes to both gross creep deformation and rupture is what defines this regime [13]. oxidation's impact on fracture initiation and propagation, which primarily occur during the tertiary creep stage [14].

It has been found from experiment that if a metal which creeps is subjected to a constant uniaxial stress, then the accumulation of creep strains with time has the form illustrated in as shown by Figure 1.2.

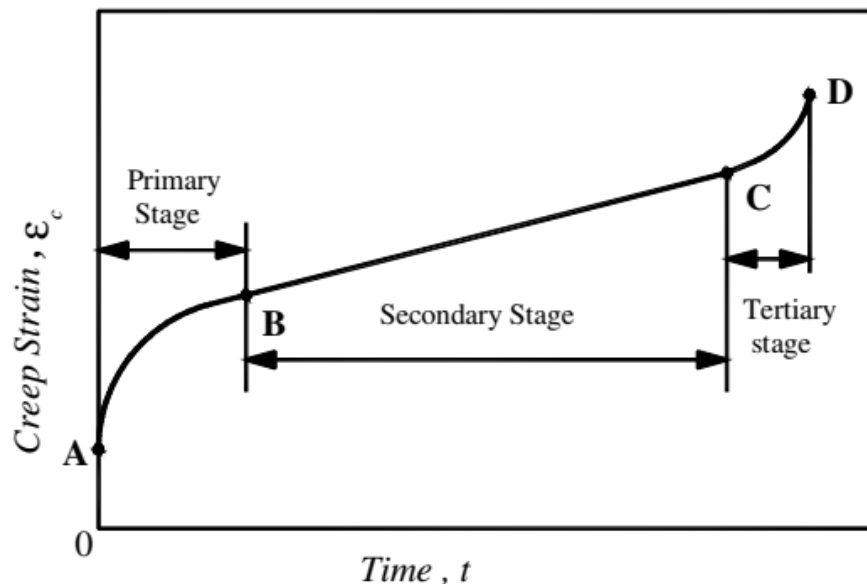


Figure 1.2: Creep curve obtained at constant temperature under constant load

The presence of oxide scale on the wall of the tubes increases the metal temperature which accelerates the damage mechanisms, thereby reducing the material's life.

Mechanisms of Creep

The creep mechanisms are often different between metals, plastics, rubber, concrete. Controlled by movement of dislocations, strong dependence on applied stress. Broadly categorized into two, those are diffusion of vacancies based on creep mechanisms example coble creep and the second one is dislocation based on creep mechanics example power law of creep.

Based on power law of creep, the creep strain rate of secondary stage creep of the material is calculated and predicted the rupture time. In this research creep power law is used to analysis the creep behavior of the oxide scaled boiler tube.

Creep Damage

Creep damage, which is shown in three different scales of damage micro, meso, and macro is the irreversible accumulation of flaws that lead to rupture. Atomic voids and dislocations manifest on the micro-scale, whereas damage that can be seen with the naked eye or with good vision manifests on the macro-scale. The impacts of micro-scale cracks, voids, and other dispersed deteriorations are averaged at the mesoscale by a representative volume element[13].

As exploitation conditions like temperature and pressure increase, the consideration of creep-damage processes is becoming more and more crucial in engineering practice. The provided constitutive equations and the selected structural analysis model have a significant impact on the precision of the mechanical state estimation (stresses, strains, and displacements). The most applicable creep damage models are the Continuum Damage Mechanics (CDM) and Kachanov-Rabotnov Model.

Continuum Damage Mechanics (CDM) based damage rate equations can provide accumulated damage, residual life, and rupture prediction given the applied stress and temperature. It is assumed that damage happens in a continuum (a homogeneous representative volume) thereby the expression continuum damage mechanics is coined.

The damage variable in the Kachanov-Rabotnov model is based on enhanced stress brought on by a local decrease in cross-sectional area. Microcracks, cavities, and voids are the cause of the decrease in cross-sectional area.

When boiler materials, such as T92 alloy steel, are subjected to oxidizing conditions,

such as in the "depleted zone" where the volume fraction of the "phase" is practically nil, the growth of the oxide scale has an effect on the microstructural stability of the material. The mechanical performance, creep behavior, durability, and damage kinetics of superalloys are thereby clearly affected by oxidation [11].

This thesis or study mainly focus on analyze how the growth of oxide scale affect the creep behavior of superheater tube boiler. So, in this study try to cover the creep behaviors and select the appropriate mechanism to show the creep behavior of oxide scaled boiler tube.

The increase of temperature and oxygen are the reason for the formation of steam side oxide scale in boiler tubes and also the other parameters implicate the oxidation reaction rate are geometry of the boiler, the steam gas and flue gas temperature, and the impurities of feed water are the main reasons[7,8,15].

- The thinner tube has less incremental scale formation
- The lower mass flow rate of steam will increase the oxide scale formation rate on the inner surface.
- The increase of steam and flue gas temperature is the result for large growth rate of steam side oxide scale.

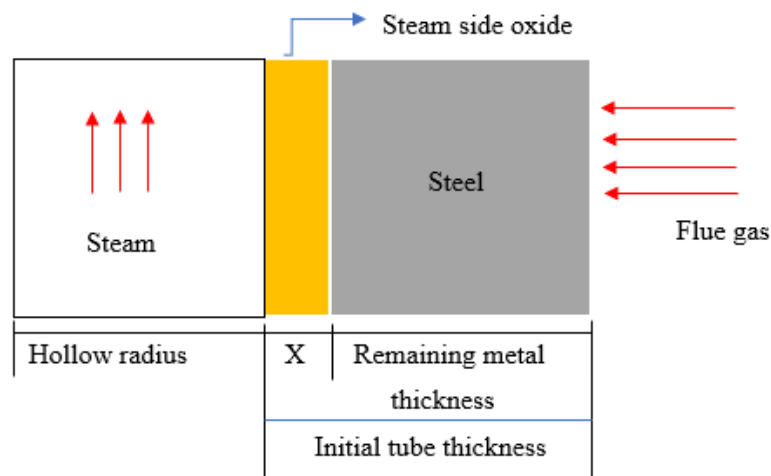


Figure 1.3: Schematic representation of superheater with steam side oxide scale

When the thickness of X increases the tube wall thickness is decreases. The main effect of growth of oxide scale is:

- Reduces the heat transfer into steam and also reduce the cooling effect this leads to overheating of the metal tube.
- Stresses that develop during scale growth at high temperature can lead to scale crack, buckling, and spallation. For superheater boiler tube it reducing flow, obstructing tube bends, eroding the nozzle, and eroding the first stage of the turbine's blades.
- Then the superheater work over a long period with high temperature and pressure condition the growth of oxide scale enhancing microstructure degradation and accelerating dislocation motion this condition accelerate creep's failure of the tube and reduce creep rupture time.

Therefore, understanding the steam oxidation processes, the growth rate of the oxide scale and factors influencing them is crucial for determining the creep behavior and remaining life of boiler tube this leads to improvement of power plant efficiency.

In boiler steam circulation systems, superheaters are subjected to the highest temperatures and pressures. As a result, good material selection is critical. Ferritic steel and Austenitic steels are the most frequent materials used for superheater boiler tubes. Chapters 2 and 3 go through the material features of superheater boiler tubes in greater detail.

In general, this research addressed the prediction of oxide scale at different flue and steam temperature, derive the equation of elastic and thermo-mechanical stress-strain at different oxide scale thickness, investigate the failure of oxide scale thickness, derive the equation to analyze the effect of oxide scale on creep behavior of metal by calculating the creep stress and strain rate of oxide scaled boiler tube and also predict creep rupture time. This work is carried out by reviewing several publications, building a mathematical model and computed by analytical equation and by using a numerical software.

1.2 Research questions

The main research questions raised in this study are.

- Which type of boiler tube mainly failed in sugar cane factories, Brewery company, chemical industries, and power plants?
- What are the main reasons for the failure of the boiler tube?
- What are the common materials used for boiler manufacturing?

- What are the mechanism and kinetics of steam side oxide?
- How can develop the mathematical model of superheater with SSOS?
- How to calculate the thickness of the oxide scale due to the variation of temperature?
- How can calculate the elastic and thermo-mechanical stress and strain of oxide scaled boiler tube and failure of oxide scale?
- How can the oxide scale affect the creep behavior and rupture time of the boiler tube?

1.3 Problem statement

In sugar cane factories, Brewery company, chemical industries, and thermal power plants the failure of boiler tubes is the main failure that leads to the shutdown of the industries. From different failure modes of boiler tube, steam side oxide scale is one of the main failure types. Many power plant industries try to increase the efficiency of boiler tube by increasing the temperature and pressure of steam and flue gas, this increment leads to the growth of oxide scale and overheating of boiler tube. So, study of the growth of steam side oxide scale and effect of the variation or increment of flue gas and steam temperature for the growth of oxide scale thickness is the crucial part to calculate the stress and strain of oxide and metal tube parts at different oxide scale thickness, to determine the failure of oxide scale, to calculate the creep stress and strain rate and rupture time of the metal part .

To predict or estimate the growth of steam side oxide scale, understanding of the mechanism and kinetics of oxide scale is important. Based on this in this research investigation of the oxidation mechanism and kinetics of T92 alloy steel is one of the objectives. For prediction of oxide scale growth, the researchers assume the growth of oxide is only in outward direction which means they are not consider the reduction of tube wall due to growth, but to obtain better result of estimated oxide scale, considering the growth of the scale in outward and inward direction of the metal tube, which means considering the reduction of thickness of the metal tube. Oxide scale failed due to different reason, like cracking, spalling and etc. To find out by which oxide failure reason the steam side scale oxide scale will be fail, it needs the calculating of elastic and thermal stress and strain of oxide scaled boiler tube at different oxide scale and compare the value with critical

stress and strain of each failure type. In this research, derive the equation of elastic and thermo-mechanical stress and strain of oxide scaled boiler tube and try to investigate the growth of stress and strain at different oxide scale those obtained from the prediction and compare the result to the critical stress and strain of different failure modes to predict the oxide exfoliation (failure of oxide).

Due to increase of oxide scale, the metal tube become hot (the change of temperature between outer surface of tube and oxide/metal interface surface is become small) this overheating of the boiler tube for long period of time leads to creep failure of boiler tube. Study the creep behavior of the tube at different oxide scale is crucial for determining the remaining life and rupture time of boiler tube. To solve this problem in this research drive equation to calculate the creep stress and strain rate and and rupture time of boiler tube.

1.4 Objectives

1.4.1 General Objective

Develop mathematical model to analyzing the effect of oxide scale growth on creep behavior and rupture time of superheater tube boiler by using analytical and numerical approaches.

1.4.2 Specific Objectives

1. Investigate oxide mechanism and kinetics of ferritic steel alloy at high temperature.
2. Develop the one-dimensional heat conduction equation using finite element model to calculate the temperature of each surface and estimate the growth of steam side oxide scale due to the variation of steam and flue gas temperature and compare the effect of steam and flue gas temperature for oxide growth.
3. Analysis Elastic and (thermo-mechanical) thermal stress due to steam side oxide scale growth and estimate the failure of oxide scale.
4. Develop mathematical equation for oxide scaled boiler tube and analysis creep stress and strain rate of T92 alloy steel superheater boiler tube due to growth of oxide scale and calculate the creep rupture time.

1.5 Scope of the study

The study focused to the investigation of oxide scale formation and its growth at high temperature by reviewing different articles and experimental values, the other one is to develop a finite element model to calculate 1D heat conduction equation to obtain the temperature at different nodal points, predict the steam side oxide scale growth at different steam and flue gas temperature for the given step of time, and finally, calculate the creep rupture life and predict the remaining life of superheater boiler tubes using analytical and numerical approaches.

The approaches follow to achieve the objectives are develop mathematical modeling (Finite element model or the stiffness matrix) of the one-dimensional heat conduction equation to calculate the temperature at different node or location of the boiler tube. This one computed by Python code or by developing the 2D model of boiler tube by using ABAQUS software to compute the heat transfer. The prediction of steam side oxide scale growth is computed by analytical calculation using Python software. The elastic, thermal and creep stress and strain are computed by using analytically and develop a 2D model of boiler tube with oxide scale by using ABAQUS software.

The effect of fireside corrosion in boiler tubes is not cover in this study and in this study the main concern is the effect of temperature variation for steam side oxide scale growth and how the steam side oxide scale affects the stress and creep behavior of the boiler tube. Finally, the result is validated with literature.

1.6 Significance of the study

The significance of the study is to give clear information for boiler designers about the mechanism and kinetics of T92 alloy steel to mitigate the failure of boiler due to steam side condition the other significance is give clear information for designers, quality controllers and researchers how to predict the growth of steam side oxide scale at different steam and flue gas temperature for a long operating time and also show how to analysis the elastic, thermal (thermo-mechanical) and creep stress and strain due to the growth of steam side oxide scale. Based on this information they can calculate the creep rupture life this helps for the power plant industry set the preventive action before early frailer of the boiler tube and also help the boiler manufacturer to select the appropriate material to increase the life time of boiler and the efficiency. The researcher uses this study as a reference to design a boiler tube with different condition and also get information how

to numerical analysis heat transfer, estimate the growth of steam side oxide scale, calculate the elastic, thermal and creep stress and strain by using analytical and numerical method.

1.7 Structure of the Thesis

This thesis has the following structure:

- Under chapter one, introductory part of the thesis it covers the different failure types of boiler tube is briefly discussed. Them also the research equations, the problem statement, objective of the research, scope of the study and significant of the study are also discussed in this chapter.
- The second chapter deals with literature review.
- In the third chapter the behavior of different materials, their chemical composition is discussed. The general method of this research and also the specific methods to achieve the goal of objective is briefly discussed under this chapter.
- The fourth chapter presents the finite element mathematical discretization for heat transfer problem of boiler tube and prediction of oxide scale equation is presented. Analytical elastic, thermal and creep stress and strain of oxide scaled boiler tube equation is derived in this chapter and also the failure of oxide scale and creep rupture time is discussed under this chapter. The final part of this chapter is covering the procedure of finite element simulation.
- Chapter five covers the result and discussion of the Analytical and numerical result of the thesis.
- Finally, chapter six gives a conclusion to the thesis, its contribution and possible future research directions.

2. LITERATURE REVIEW

This review of the pieces of literature is mainly focused on mathematical model or the general rules that developed and used by different researchers to analyze the creep behavior and life of the material the other one is focused on the numerical method specifically the FE approach how to develop the 2D and 3D model of boiler tubes, which commercial software is applicable, and how to analyze the creep behavior and remaining life by using this commercial software are the main things and also the specification of the material for the superheater boiler tube and other power plant equipment and also shows the effect of Cr concentration in the formation of oxide layer the other thing review in this paper is the method to predict oxide scale growth and the way to calculate creep rupture time of oxide scaled boiler tube.

Mathematical model

For Creep behaviour

The creep behavior of a boiler tube is investigated by using as a thick-walled cylinder subjected to internal and/or external pressure at a constant temperature and analyze the creep behavior by considering a normal boiler tube surface, i.e. surface with no soot or scale deposit and no crack and scar existing try to estimate the residual life using two approaches those are creep curve and life damage rule. The creep behavior and deformation classified in three stages primary, secondary and tertiary. The secondary stage deformation or creep behavior is calculated by using power (Norton's) creep law and time hardening law[3]. The limitation of this study is not considering the boiler tube with defects.

The formation of steam side oxidation and fireside corrosion degradation processes are affect the creep life of service exposed superheater boiler tube[7,8]. The oxide scale thickness method using heat transfer equations and the accelerated temperature method for creep life estimation are suggested to analyze the effect of oxide scales in creep behavior and remaining life analysis of boiler tube[7]. An empirical formula of Larsen-Miller formula and the Kachanov- Rabotnov creep damage model is used to analyze the remaining life of a boiler tube. The Larsen-Miller formula is used for calculating the thickness growth curve of the oxide scale, temperature change of boiler tubes, and the Von-Mises

stresses of the tubes. The Kachanov- Rabotnov creep damage model is used to investigate the creep damage of different materials and the creep life of the tubes[8].

Effect of sediment thickness on the remaining creep lifetime of 9Cr1Mo refinery furnace tubes described by Farid and Iraji [15]. Use the Larson-Miller parameter and Monkman-Grant coefficient to analyze the creep behavior and remaining life of furnace tubes by assuming the sediment thickness is 1mm and 2mm.

The creep crack growth behavior of the components and the material response was investigated by using compact tension(CT) specimen[16-18]. Continuum damage mechanics is used to analyze the effects of bending, cracking and hardening on microscopic scale. The increasing initial crack depth and specimen dimension promoted the crack growth rate, while the decreasing hold time accelerated the crack formation under a multi axial load condition.[16]. To reduce the complexity of the continuum damage model, develop the Mokamn-Grant model for uniaxial/multi-axial creep rupture and cracking rates for notched bar specimen[19,20]. The Continuum and Mokamn-Grant models are only analysis the creep behavior with load variation not consider the temperature effect but creep is affected by temperature.

For Stress, Strain and Steam side oxide scale Failure

Stresses arise within the scale as a result of several thermos mechanochemical reactions occurring during boiler operation and metal oxidation. The flat-plate model has historically been used extensively in stress calculation techniques to analyze oxide scale failure difficulties [21,22]. This model has an easy understanding physical meaning and can be simply programmed. The other stress analysis of the steam side oxide of boiler tube is by considering the influence of interface roughness of the oxide[23], they consider the interface has sinusoidal function. Another stress calculation model[24], the compound cylinder model can calculate the accurate stress distribution of compound cylinders. This model can be used to calculate the stress distribution of oxide scaled boiler tube by considering the metal and oxide part as a component of compound cylinder. The compound hollow cylinder model can obtain more accurate stress distribution in steam side oxide scale.

Oxide scale failure on the steam side of the superheater tube is reducing flow, obstructing tube bends, eroding the nozzle, and eroding the first stage of the turbine's blades. There are many critical failure strains for each of the various failure processes that could lead to the failure of the oxide scales, including through-scale cracking, interfacial crack

development, buckling, crack deflection toward surface, and spalling[25]. The oxide scale failure occurs when the stress and strain cross the critical strain. The Advanced Oxide Scale Failure Diagram (AOSFD) as failure criterion, a systematic analysis model for the failure behavior of steam-side oxide scales in T92 superheater tubes during unsteady thermal processes is established[22]. For critical failure strain of oxide scale due to tensile crack, develop three curves based on the ratio of physical defect size to oxide scale ratio is equal to 0.1, 0.25 and 1, and the most accepted one based on their work is 1. Finally, they conclude the failure probability of thicker steam-side oxide scales is higher. Hence, for tubes having operated for a long time or operating with higher steam temperature.

The above pieces of literature are trying to analyze the creep behavior with a different condition by using standard laws the main points are summarized below.

1. The continuum damage mechanics is more applicable to analyze the creep failure and crack growth of the compact tension specimen and also use to analyze the creep-fatigue interaction of the specimen.
2. Monkman-Grant model is simpler than the continuum damage model for analyzing the uniaxial/multiaxial creep rupture and growth.
3. The heat transfer equation and Larson-Miller formula are used to calculate the thickness of the oxide scale and the Larson-Miller parameter is also used to determine the remaining life of the material due to creep.
4. The creep damage rule and the Larson-Miller formula were used to investigate the creep damage of different materials and the creep life of the tubes.
5. The stress analysis of a boiler tube can be done by considering a flat plate model and compound cylinder model.
6. The Advanced Oxide Scale Failure Diagram is useful to develop oxide scale failure criterion, the most common one is tensile critical strain.

Numerical Method

The tube temperature and stress distribution by using the FE commercial software ANSYS Workbench 10.0. The method of FE analysis used here is known as the direct stiffness or displacement method[3]. Use very old ANSYS software and also the procedure is not clearly defined or described.

Develop the two-dimensional axisymmetric tube model by using ANSYS software and the FEM for simulating the model to obtain the thickness growth curve of the oxide scale, a temperature change of boiler tubes, and the Von-Mises stresses of the tubes. The oxide scale substrate interface temperature (T_m) is simulated by ANSYS. If the T_m is not equal to T change the value of T_m and again simulate using ANSYS until to get $T=T_m$ [8].

The commercial FE software ABAQUS is used to investigate the creep deformation of the oil refinery main furnace tubes. The researcher used a long tube to simulate the plane strain condition and tries to investigate the creep behavior of the tubes with and without sediment for the FE analysis consider inner wall sediment thicknesses: 1 and 2mm[15].

The numerical approach or the FEM is used ABAQUS software to analysis the cracked 2.25Cr-1.0Mo steel tubes of an oil refinery boiler tube. The FEA results showed tensile residual stress formed at welding zone due to non-alignment before tubes welding[26].

The above pieces of literature are trying to show the numerical methods use by different researchers the main points are summarized below.

1. The 2D and 3D model of the boiler tubes and the FE analysis is done by the commercial software of ANSYS and ABAQUS.
2. The tube temperature and the stress distribution are calculated by using the FE of the direct stiffness or displacement method.
3. FEM is used to calculate the thickness of the oxide scale at a variety of different conditions and also it helps to analyze the creep behavior and the remaining life of boiler tubes.
4. To make connectivity between the domain areas at oxide scale and metal interface the merge-size control should be smaller than the meshing size control.

Material

The safety of the boiler tubes is a primary concern in power plant industries. The main cause for the failure of boiler tubes is the selection of inappropriate material in the design and manufacturing stage. Many researchers are tries to solve this problem by suggesting the appropriate materials in the specific application. This review tries to cover the materials mostly applicable in different boilers.

The composition of Cr and Mo material for the application of boiler tubes. The basic difference between the materials is the percentage composition of Cr and Mo[6], [14], [16],[27]. The steels used at high temperature and pressure have been classified into four groups for use in the increasing order of operating temperature which include Carbon steels (0Cr), Low alloy ferritic (1-2.25Cr), High alloy ferritic (9-12Cr), and Austenitic steels (17-25Cr)[8,15,28-30].

9Cr-1Mo material to analyze the remaining creep life of furnace tube because the is applicable in producing heat exchangers and fired heater tubes in high temperature and pressure condition[15]. 2.25Cr-1Mo (T22) steel in the application of boiler tubes to estimate the effect of oxide scale in the creep life of boiler tubes by calculating the residual life[27,31].

Increasing the chromium content in the alloy increases its ability to resist oxide scale formation by forming a higher oxide layer. When steel is oxidized, it develops wustite, hematite, and magnetite scales. As chromium is added to the alloys, the inner layer (magnetite) of steel is replaced by a spinel of iron-chromium in ferritic (up to 3% Cr) or martensitic steel (9-12 percent Cr).So, the researcher concludes that the increase of chromium content in steel alloy increases the ability of the material to resist the concentration of oxide scale[32,33].

The above pieces of literature are trying to show the different materials use by different researchers the main points are summarized below.

1. The alloy of Cr and Mo steel is widely used in the design and manufacture of superheater boiler tubes.
2. 2.25Cr-1Mo (T22) steel is widely used for superheater boiler tubes and 9Cr1Mo steel is widely used for the furnace.
3. The seamless ferritic low-alloy steel SA213-T22 is cannot withstand a highly oxidizing environment within a high-temperature condition for a long period.
4. The increase of chromium content in steel alloy increases the ability of the material to resist the concentration of oxide scale

Prediction of oxide scale growth

In order to determine the growth of the oxide scale, the Arrhenius constant and activation energy of the material are obtained. These are substituted into oxidation kinetics laws, mostly parabolic laws. Although this method is more accurate to predict oxide scale growth, experimental data at different temperatures isn't available. To solve this problem researchers proposed Larsen-Miller parameter[27], [34], [35]. The Larsen-Miller equation is a function of temperature and time. The temperature is the average temperature, it is the average value of the inside temperature and the metal oxide interface temperature. At initial stage it means oxide free condition the average temperature is equal to the average of the inner and outer temperature of a tube[34] and others take the inner tube temperature as average temperature[35]. It is an iterative step for a given time, first calculate the average temperature of a tube without oxide scale by numerical method considering all thermal properties, when obtained the average temperature, they substitute the average temperature and the time into Larsen-Miller formula. After obtaining the Larsen-Miller value, then they substitute into oxide equation and obtained the oxide thickness at the first-time step. For the next time step include the oxide scale to calculate the average temperature and it these iterative steps continue until reach the required time. The equation is vary based on the material properties, for 1-2.25% Cr content material the formula is mentioned on[27,34] and for 9-12% Cr content material the formula is mentioned on[35]. The above literatures assumed the growth of the oxide scale is only in outward direction, it means the thickness of the metal part is not decrease due to the increment of the oxide scale.

The above pieces of literature are trying to show the prediction of oxide scale growth by analytical and numerical method by different researchers the main points are summarized below.

1. Prediction of oxide scale is the iterative step, output of the first is become input to the second, and it's continued until the final step.
2. They considered the oxide scale is grow in the out-ward direction
3. The formula of convection coefficient (h_s) of steam and Reynolds number of steam are not considering the oxide thickness, it means the h_s will be the same throughout the step.

Methods to predict creep rupture time

During a planned outage, it's crucial to monitor how superheater tubes are creeping. Superheater tubes must be cut out for sample and testing in the lab using a creep testing machine in order to assess creep progress. Due to the high expense of repairing and replacing the cut region, the destructive testing sampling procedure may not be a practicable method for the majority of power plants [25]. The residual life estimation of super heater tubes based on oxide scale thickness measurement is computed by Larsen-Miller parameter[31]. The researcher uses the Larsen-Miller parameter to predict oxide scale of low alloy ferritic steel and also for rupture time calculation use the relation of Larsen-Miller parameter and the rupture stress of the tube. From maximum elastic hoop stress, minimum diameter stress and Tresca reference stress they select maximum elastic Hoop stress criteria gives the most conservative value and hence is very widely used and only consider the effect of internal pressure. Other researcher proposes steady state creep rates with the Norton's Law of minimum creep strain rate relation[36].

Summary of the main research gap from the above literatures are

1. Stress analysis is computed by the concept of flat plate and compound cylinder, but for oxide scale boiler tube the Elastic stress, thermal stress and creep stress require some change and simplification from the compound cylinder stress analysis concept.
2. The effect variation of flue gas and steam temperature in the growth of steam side oxide scale is needed detail study.
3. The prediction of oxide scale considers only the outward growth of oxide, but high alloy ferritic steel the growth is in both inward and outward direction, so after each iterative step the thickness of the metal tube and the convection coefficient of steam should change. This consideration affects the accuracy of the prediction of steam side oxide scale growth.
4. The analytical and numerical method or procedure for analysis of creep behavior and rupture time of superheater boiler tube with SSOS condition is not clearly define.
5. The reason behind selection of the material and formation of oxide scale is not clearly define and also the mechanism and kinetics of oxide scale of materials like T92 alloy steel need detail study and documentation.

3. MATERIAL AND METHODS

3.1 Material for Superheater boiler tube

Increasing the temperature and pressure of the power plant is the most convenient way to improve the efficiency of the plant[37] and reduce pollutants or lower CO₂ emissions [38] by producing steam. The heat source for modern power plants comes from coal, gas, and fuel oil[39]. But in this thesis consider the power source is coal fire.

Steam is heated to a higher temperature in a convective superheater before it is delivered to the turbine to increase the efficiency of the plant. The goal of superheaters is to elevate steam temperature from saturation to the appropriate ultimate temperature, which in some situations can reach above 540 °C. In such activities, steam pressure typically varies from 10-100 bar[40]. Thermal efficiency and overall power production benefit from superheated steam. Those are the hottest part of the power plant, proper material selection is the challenged and crucial part to increase efficiency and safety of the plant[38]. There is some consideration to know before producing to material selection like the normal operating parameters (such as the nature of the fluids on both the tube and shell sides, flow rate, temperature, and pressure), startup and shutdown conditions, upset conditions, special conditions such as product purity requirements, hazardous effects of mixing shell and tube side fluids, radioactivity and associated maintenance, and so on. Many papers are describing the criteria for material selection.

Criteria for material selection [8,41-43]

1. High- Temperature mechanical strength
2. Creep and rupture resistance property
3. Corrosion and erosion resistance properties.
4. Cost of the material: it is important to choose the least expensive material
5. Thermal conductivity: the heat is easily flowing through the material
6. Availability and easy manufacturing

The increase in operating temperature is affecting the strength and the lifetime of boiler tubes. When the temperature increases the creep strength of the material is decreased and also the formation of an oxide layer in the inner and outer surface of the boiler increase which leads to the reduction of the wall thickness of the boiler tube and the reduction of heat transfer of the pipe[42]. It means the increasing temperature is a direct relation to the formation of oxide scale and creep So, the temperature variation is the main factor in the material selection. Material strength is the main concern in high-temperature working conditions. Therefore, understanding the steam oxidation processes and selecting the appropriate material is crucial for the improvement of power plant efficiency. Based on their micro structure and alloying elements the steel material is classified into different groups. Those are:

1. Ferritic Steels
2. Austenitic Steels

Ferritic Steels

The microstructure of ferritic steels is body-centered cubic (BCC)[44]. Because of their inexpensive cost, heat-resistant ferritic steels are preferred as superheater materials. Molybdenum and chromium are the most important alloying constituents in these steels. When compared to austenitic steels, ferritic steels have a higher heat transfer coefficient and a lower coefficient of thermal expansion.

Ferritic steel is mainly classified into two parts are Low alloy ferritic steels and High alloy ferritic (Martensitic) steels. Low alloy ferritic steels are 1-3 % Cr content and they exhibit good tensile strength at temperatures as high as 450°C, creep strength at temperatures as high as 550°C, and steam oxidation resistance. But when the temperature becomes above 550°C the material is not good to resist creep and corrosion. So, search for another material the Cr content is above 3% like high alloy ferritic steel. High alloy ferritic steels have 9-12% Cr used in high steam temperature and pressure conditions 620°C and 33MPa respectively, but when the steam temperature exceeds 620 °C, the oxidation resistance of ferrite steel cannot meet the operation requirements[45].

Table 3.1: Chemical composition (wt.%) of selected Ferritic steels [27,42,46]

Steel Grade	Chemical composition, wt.-%									
	C	Si	Mn	Cr	Mo	W	V	Nb	B	N
T22	0.05-0.15	0.5	0.3-0.7	2-2.5	0.9-1.2	-	-	-	-	-
T23	0.06	0.2	0.45	2.25	1	1.5				-
T91	0.1	0.24	0.4	8.9	0.9		0.2	0.08		0.05
T92	0.13	2	0.6	9	1	1.87	0.2	0.05	0.005	0.06

For high temperature and high-pressure resistance, plain 9Cr–1Mo (T9) steel is modified into T91 steel by adding Nb: 0.08 wt%, V: 0.2 wt%, and N: 0.05 wt%, and partly substituting C by N. In addition, T91 steel is modified into T92 steel by alloying with tungsten (1.8 wt%) and boron (0.005 wt%) [37].

Austenitic Steel

High-alloyed steels with an austenitic structure and face-centered cubic (FCC) microstructure are known as austenitic steels or 300-series stainless steels[44]. Due to their austenitic structure, austenitic steels have good high temperature strength and creep resistance due to austenitic microstructure, as well as corrosion resistance due to their high chromium concentration. But the cost is expensive than ferritic steels because of the increment of chromium concentration. It is resisted creep up to 675°C operating temperature. The most well-known austenitic stainless steels are 18-10 and 18-8, which have an official 18 weight percent Cr and 8–10 weight percent Ni content. Steels like TP304H, Super304H, Tempaloy A-1, TP347H, and TP347HFG are examples of this kind. To preserve an austenitic microstructure at room temperature, these steels include the bare minimal number of alloying elements. The austenitic steel may be stabilized against intergranular corrosion with the right amounts of Nb and Ti (sensitization). When copper is added and the right heat treatment is used, the precipitation is strengthened by the fine precipitation of the Cu-rich phase. More nickel or manganese is needed to stabilize the austenitic phase when increased chromium content is desired for improved corrosion resistance.

Table 3.2: Chemical composition (wt.%) of selected Ferritic steels

Steel Grade	Chemical composition, wt.-%										
	C	Si	Mn	Ni	Cr	Mo	Nb	Ti	Cu	B	N
Super 304H	0.1	0.2	0.8	9	18	-	0.4		3		0.1
TP304H	0.08	0.6	1.6	8	18	-	-	-	-	-	-
Tempaloy A-1	0.12	0.6	1.6	10	18	-	0.1	0.08			
TP347H	0.08	0.6	1.6	10	18	-	0.8	-	-	-	-
Tempaloy A-3	0.05	0.4	1.5	15	22	-	0.7	-		0.002	0.15
NF709	0.15	0.5	1	25	20	1.5	0.2	0.1	-	-	-

The material selected in this research to investigate the formation of steam side oxide scale, to analyze the effect of oxide scale in heat transformation of the boiler tube and also to analyze the stress and oxide failure and also to analyze creep behavior and remaining life of boiler tube are Ferritic steel.

From the list of ferritic alloy steel in Table 3.1, T92 steel is a preferred material for applications involving operating temperatures up to 620°C[45,47] as it exhibits higher thermal conductivity and smaller coefficient of thermal expansion than austenitic stainless steels used in high-temperature applications and also has high temperature stability to resist creep deformation. Up to 625 °C, creep strength of T92 steel is 20% more than that of T91 steel and higher or equal to that of 304 austenitic stainless steels[47]. In this thesis select T92 alloy steel to investigate the oxidation mechanics and kinetics of high alloy ferritic steel, to show the effect of variation of flue gas steam temperature for the growth of oxide scale and to show how to calculate the elastic, thermal, and creep stress and strain of oxide scaled boiler tube by deriving the mathematical equation and by finite element simulation at high operating (steam) temperature. The dimension and the geometry of the superheater boiler tube is selected by referring different research papers[8,22,48], based on this the selected dimension and geometry is listed in Table A-1.

Formation of steam side oxidation, the growth of oxide scale and the stress analysis is discussed more extensively in chapter 4.

Table 3.3: Chemical composition (wt.%) of selected Ferritic steel for this research

Steel Grade	Chemical composition, wt.-%									
	C	Si	Mn	Cr	Mo	W	V	Nb	B	N
T92	0.13	2	0.6	9	1	1.87	0.2	0.05	0.004	0.06

3.2 Research methodology

The methodology explains what and how to do, allowing readers to evaluate the reliability and validity of the research. The procedure for attaining the objective of the research is by attending the sequences of the methods and tools by cross-checking with the literature to validate each of the methods and result. This study performed analytically and numerically to achieve the objective of the research.

3.2.1 Selection of Appropriate Approach

Research can be conducted in various ways, whether quantitatively, qualitatively or using a combination of both (mixed method). It is a quantitative study that mathematically models and numerically simulates the growth of oxide scale, elastic, thermal, and creep strains and stresses in oxide-scaled boiler tubes. In addition, it predicts oxide scale failure in oxide-scaled boiler tubes and the creep rupture time. A mathematical model and software package is very appropriate for this type of research.

3.2.2 Tools or Techniques

The most applicable ways to predict the steam side oxide scale growth is the LMP method. Based on this method the oxide scale is a function of time and average temperature. The average temperature can be computed by two methods the first one is by using FEM matrix form and use Python code shown in Appendix B, the second one is by modeling the two-dimensional boiler tube using ABAQUS software and compute the temperature of each surface. For iterative procedure of oxide scale growth, develop Python code to compute at different steam and flue gas temperature. For elastic, thermo-mechanical and creep stress and strain analysis of oxide scaled boiler tube, mathematical model is necessary. For computing the integral constants developing the matrix is the best and simplest way. The analytical analysis is computed by the Python code shown in Appendix B. For validation numerical analysis is important to compare the result with analytical one. The numerical analysis like the 2D modeling of the part, simulation of elastic, thermo-mechanical and creep analysis is computed has done using ABAQUS software package.

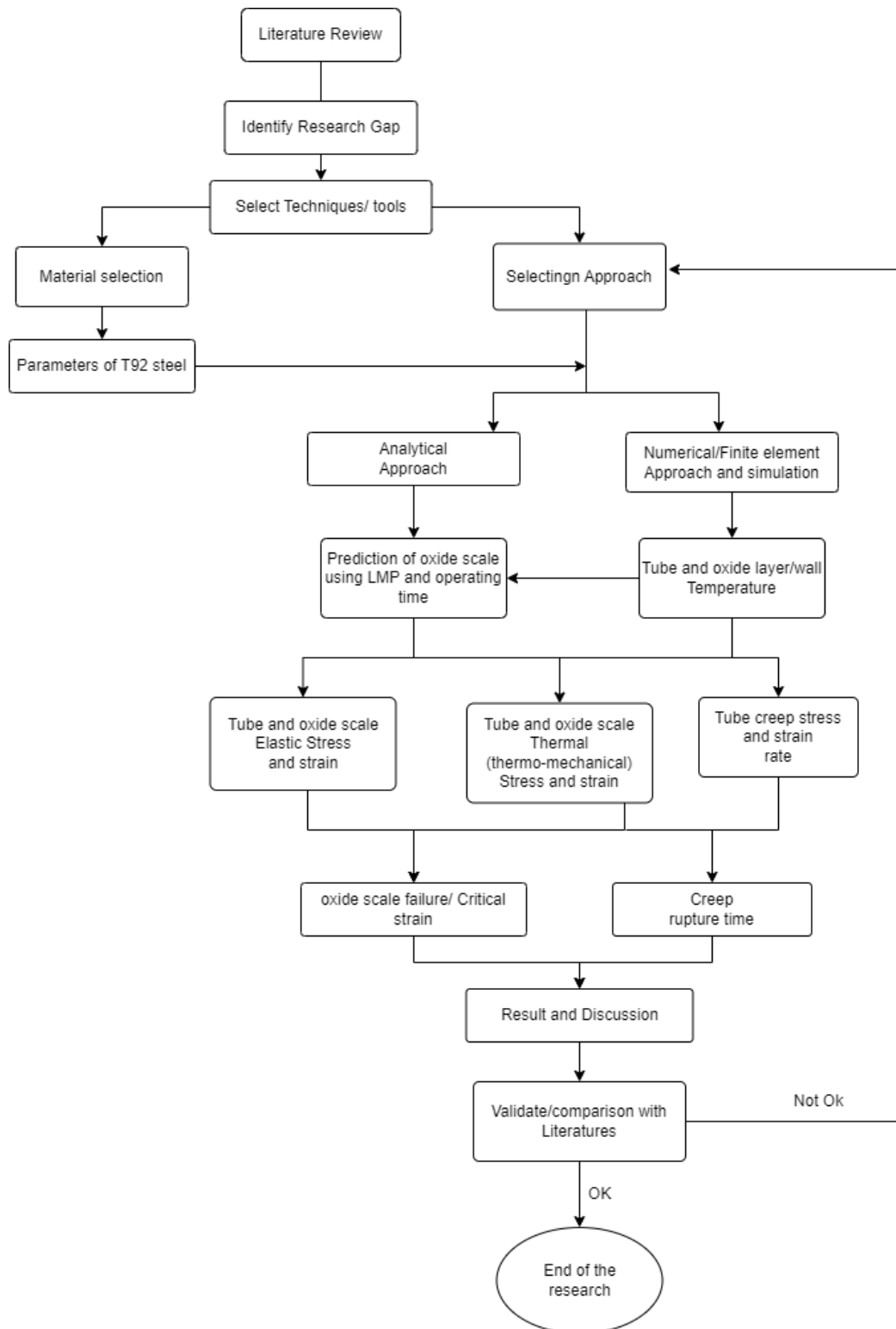


Figure 3.1: Research Methodology

3.2.3 Method of oxide scale growth prediction

The objective of prediction or estimation of steam side oxide thickness at different steam and flue gas temperature are achieved by follow the following iterative procedure.

Step 1: The first model is generated according to the geometry of the tube listed on Table A-1 by using ABAQUS software with the absence of oxide scale. The 2D heat transfer computed by applying, the value of h_s , h_g , T_s , T_g , and thermal conductivity of the material (k).

Step 2: After computation the average temperature of $T_{ave\ 1}$ is the temperature on the inner surface of the tube as determined by the numerical simulation in the absence of scale (δ_x or X_0).

Step 3: Use Equation 4.32 and 4.33 to calculate the scale thickness of X_{1a} for the service hours of 1 hr. and the scale thickness of X_{1b} for the service hours of 100 hr. by using the average temperature of $T_{ave\ 1}$. The increment of oxide thickness is obtained by the difference of the two oxide values.

$$\Delta X_1 = (X_{1b} - X_{1a}), \text{ the new scale become } X_1 = X_0 + \Delta X_1$$

Step 4: Due to new oxide thickness $X_1(\delta_x)$, the value of h_s and r_i is changed, based on Equation 4.26 and 4.27 the h_s value is affected by the value of δ_1 which means half of the total oxide scale thickness ($\delta_1 = X_1/2$), after substituting δ_1 into the equation, new h_{s1} value is obtained for each step. Based on the oxide behavior under T92 alloy steel, it has two layers one is grow into inside the tube and the other one is grown outside from the inner surface of the tube. So, the value of internal radius of the tube r_i is changed, the new $r_{i1} = (r_i + X_1/2)$.

Step 5: Develop the new model by adding the oxide scale thickness (X_1). The new model has two parts, those are the substrate(metal) part with r_0 and r_{i1} dimension and the oxide part with r_{i1} and $(r_{i1} - X_1)$ dimension. The 2D heat transfer computed by applying, the value of h_{s1} , h_g , T_s , T_g , and thermal conductivity of the material and oxide, K_{metal} and K_{ox} respectively.

Step 6: After computation the average temperature of $T_{ave\ 2}$ is obtained from the average of the inner surface and the scale/metal interface temperature.

Step 7: Use Equation 4.32 and 4.32 to calculate the scale thickness of X_{2a} for the service hours of 100 hr. and the scale thickness of X_{2b} for the service hours of 250 hr. by using the average temperature of $T_{ave\ 2}$. The increment of oxide thickness is obtained by the

difference of the two oxide values.

$$\Delta X_2 = (X_{2b} - X_{2a}), \text{ the new scale become } X_2 = X_1 + \Delta X_2$$

Step 8: Repeat the steps from step 4 to 7, up to the maximum step hour of 1000 hr. the steps are shown in Table 4.3.

To estimate the oxide scale thickness at different T_s and T_g value is by following the above iterative procedure or step. The summery of the above iterative procedure can be shown by Figure 3.2.

This iterative procedure is applicable also for analytically analysis using the stiffness matrix. Instead of modeling the tube by using ABAQUS the FEM stiffness matrix help us to get the temperature at each surface of the tube, then the other iterative procedure is the same. The analytical oxide scale growth is computed by Python code and the code is shown in Appendix B.1 (Python code for predicting oxide scale growth)

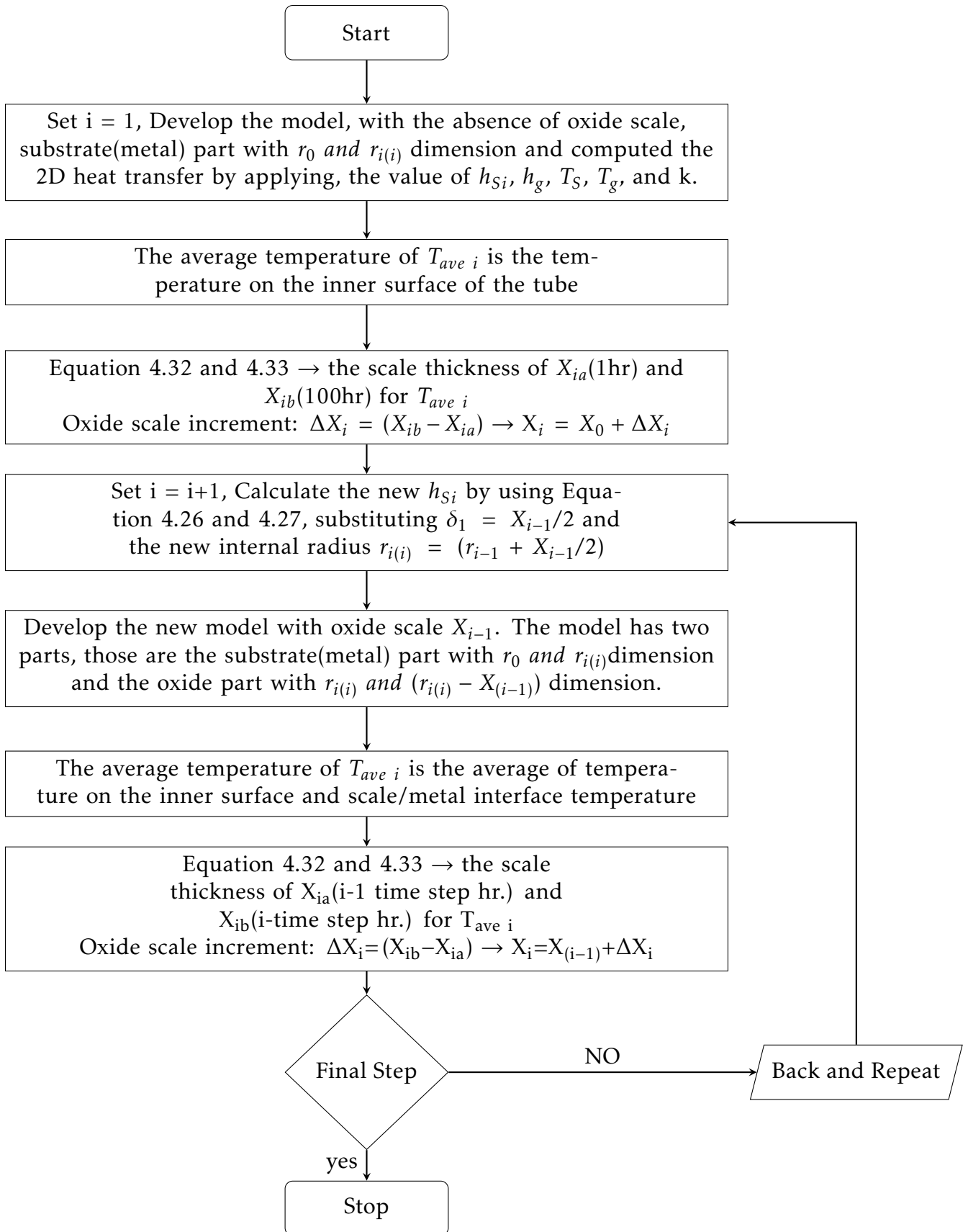


Figure 3.2: Flow chart of the iterative procedure

4. HIGH TEMPERATURE OXIDATION AND MATHEMATICAL MODELING

High temperature oxidation is defined as an interaction between a material that is operating at a high temperature and the environment around it that causes an oxide to form on the substance's surface.

To investigate, oxidation at high temperatures can take many different forms. The oxidation kinetics and oxidation mechanism, or the nature of the oxidation process, are the most popular or interesting ones.

4.1 Steam-side oxidation

The inner part of the superheater tube steel is contact to steam in high temperature and pressure condition over a long period of time oxide is formed this oxide is called steam side oxide. When the steam temperature increases the thermal efficiency of the boiler also increase and the CO_2 emission is reduced but this increase the service time of boiler in high temperature condition then the oxide is increase in the inner tube.

Oxide films build faster as the steam temperature rises, creating different potential problems and failures. The major failures caused by steam side oxide scales are:

- When the thickness of wall or tube reduce because of oxidation may increase the stress in tube walls and cause creep ruptures.
- The increase of oxide layer is inhibiting the heat transfer from flue gas to steam and also reduce the cooling effect of the metal. So, the metal become over heated then the creep accelerated and corrosion processes.
- As the oxide scale on the steam side thickens, it will spall more easily Usually the thicker oxide scales spall more easily, especially when the boiler is cooled down and restarted. It happens when due to differences in coefficients of thermal expansion between the oxide and base metal. The spalled oxide scale particles may become lodged in the steam circulation, clogging tubes, or causing turbine blade erosion if they enter the steam turbine.

4.1.1 Oxidation Mechanics (Formation)

The oxidation of metals may occur by the reaction of a metal and oxygen gas to form an oxide. The first process of oxide formation is the adsorption of oxygen on the surface of a metal[49,50]. The reaction proceeds as oxygen is dissolving in the iron substrate, which serves as a nucleation site for the formation and growth of oxide scale nuclei. As a result, both adsorption and diffusion depend on the metal surface conditions (e.g., rugose and clean) and defects (e.g., crystal defects, cracks, inclusions, and porosity). A sufficiently high oxygen concentration at the surface of the oxide controls the oxidation rate through solid-state diffusion of ions through the scale[51]. Furthermore, the nucleated oxide scale on the surface is thickening with time[49,51]. As oxide scales grow, there may be defects inside the oxide scale, such as micro or macro cracks, cavities, or porosity, leading to an acceleration of the oxidation rate.

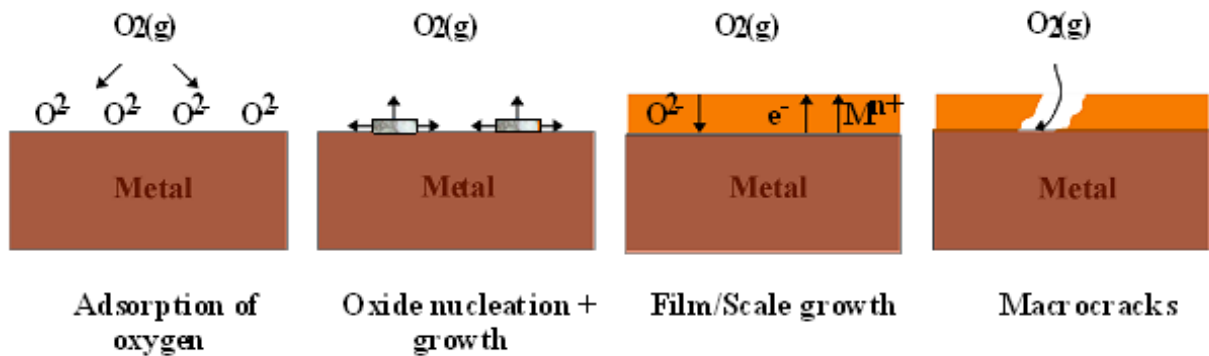


Figure 4.1: Schematic representation of the oxidation process. Adapted from[49,52]

The oxidation process of metal shown by schematic representation of Figure 4.1. Then let define this schematic representation with analytical expression. The metal surface is always oxidized when it exposed to oxygen contained environment.



Where: M is a solid metal atom O is oxygen, and MO is the oxide.

Equation 4.1 is further divided into two steps. Those are oxidation and reduction step reactions.

Oxidation reaction: produces metal ions.



Reduction reaction: produces oxygen ions.



The above equation 4.2 and 4.3 shows the oxidation and reduction reaction and also the formation of metal ions and oxygen ions respectively. Figure 4.2 represents schematically metal-scale-gas system and oxidation and reduction step reactions[50].

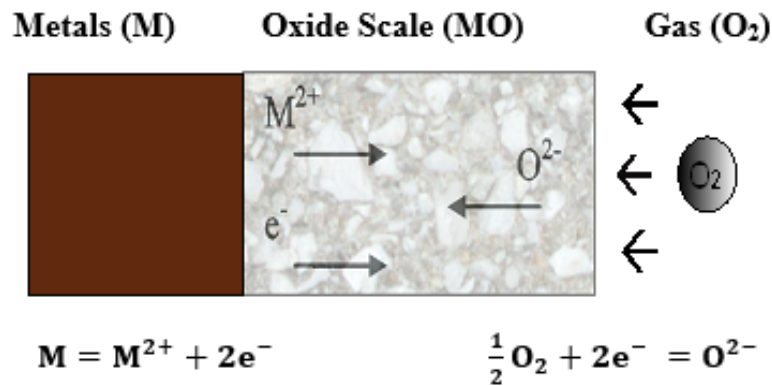


Figure 4.2: Schematic representation of the metal-scale-gas system[50]

During the initial stages of oxidation, the rate of oxidation or diffusion may be rapid, but it will slow down once the metal surface is separated from the gas phase by the oxide layer. Nevertheless, the rate of oxidation or diffusion increases as the temperature rises.

As oxidation progresses, a dense scale forms, separating the bulk materials from the surrounding environment. Thus, the oxidation process will continue through solid state diffusion of the reactants and electrons. Which means the reaction will proceed if either of the reactants can penetrate the oxide scale, defects in the oxide have an important role to transport the ions. There are three types of defects in metals and oxides: point defects (e.g. vacancies and interstitials), linear and planar defects (e.g. dislocations and grain boundaries), and bulk defects (e.g. precipitates and voids)[49,50].

It is possible for the oxide layer to expand outwards or inwards. Metal ions travel through the oxide scale to the scale-gas contact when the scale expands outwards. The scale grows inwards as oxygen ions migrate to the metal-scale interface (internal oxidation). Cation mobile and anion mobile oxidation mechanisms are the two types of oxidation mechanisms[50,51].

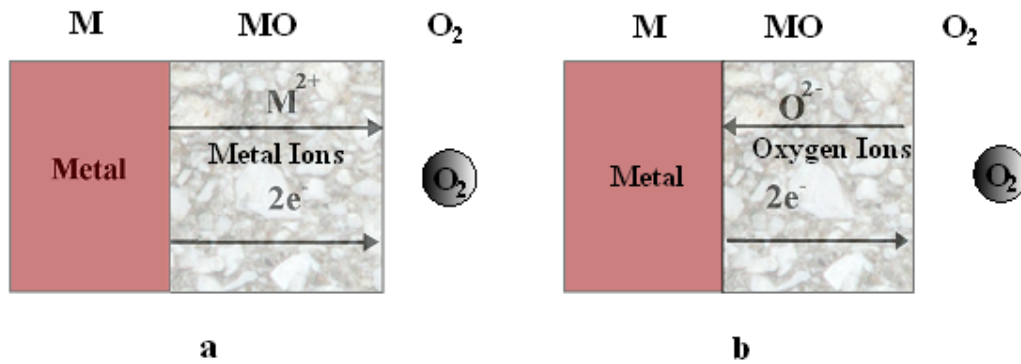


Figure 4.3: Oxidation mechanisms of ions transfer in high temperature. Cation mobile (a) and Anion mobile (b) [50,51]

4.1.2 Oxidation Kinetics

We can estimate the amount of oxide that can form at a certain temperature using Ellingham diagrams and other thermodynamic calculations, but we can't estimate the rate of the reaction. The relevant way to determine the rate of the reaction in the given environment is oxidation kinetics. Kinetics describes how quickly a metal or alloy oxidizes. Therefore, knowing about the kinetics of an oxidation reaction is important when attempting to understand a material's oxidation behavior specially for alloy materials. In order to determine the service life of a tube at a particular temperature, steam oxidation kinetics is crucial.

A mass gain curve is created by plotting a sample's weight change as a function of time. Oxygen intake during oxide production causes this mass gain. To express the oxidation kinetics or the oxide growth of the metal or alloy, there are three basic oxidation rate laws: linear, parabolic, and logarithmic.

1. Linear law:

The oxidation rate of some metals remains constant over time. In such a mechanism, reaction time is proportional to reaction speed[53]. It usually occurs when a protective oxide splits or spalls, allowing gas to enter the metal directly. It means the oxide scale does not prevent diffusion. The law can be expressed by the following equation:

$$\frac{dX}{dt} = K_L \text{ or } X = K_L t \quad (4.4)$$

Where X is the oxide thickness, K_L is the linear rate constant ($\mu\text{m}/\text{h}$), and t is the time.

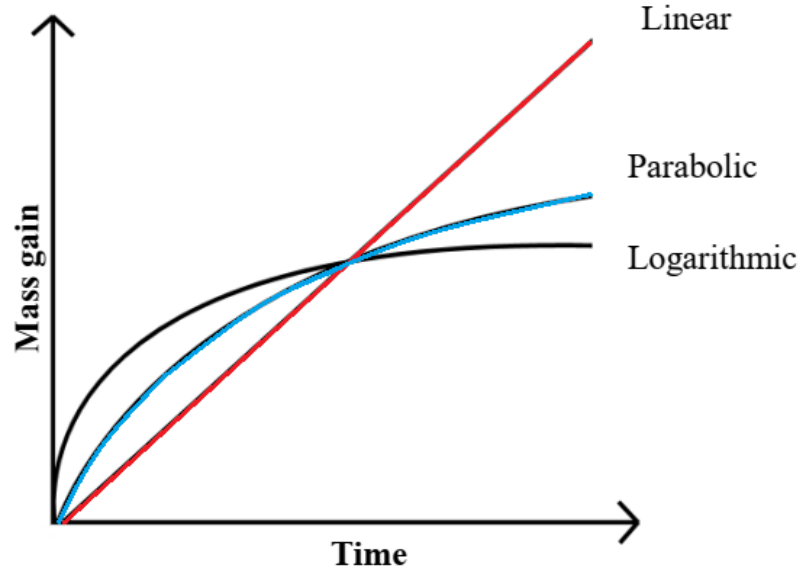


Figure 4.4: Mass gain curve versus time for the three-oxidation kinetics law

2. Logarithmic Law:

The oxidation of thin layers is frequently included in this law. Most metals display logarithmic behavior when exposed to low temperatures, often below 300-400°C. The reaction is fast at the initial stage and it becomes slow after some time[53]. The transfer of electrons or ions from the metal through the oxide to the adsorbed oxygen atoms at the sample surface is thought to be the rate-determining step[49,53]. The law can be expressed by the following equation:

$$X = k_c \log t \quad (4.5)$$

$$\frac{1}{X} = k_c' \log t \quad (4.6)$$

Equation 4.5 and Equation 4.6 is direct logarithmic and inverse logarithmic respectively. where X can be change in the weight as a result of oxidation, thickness of the oxide formed (g or μm), k_c direct logarithmic constant, k_c' inverse logarithmic constant, and t is time.

3. Parabolic law:

It is the most common one law for metals and alloys at high temperature. Ionic diffusion controls the rate of oxide layer formation for a parabolic law when the oxide is nonporous and bonds strongly to the surface. The parabolic law states that when the oxidation rate decreases, the oxide thickness increase. Consequently, the oxidation rate has an inverse relation with the thickness of the oxide. The law can be expressed by the following equation:

$$\frac{dX}{dt} = \frac{K_p}{X} \text{ or } X^2 = 2K_p t \quad (4.7)$$

Where X can be change in the weight gain per unit area or thickness of the oxide formed. In the above-mentioned equation 4.4-4.7, the proportional constant (K) is dependent on temperature. The rate constant k may be calculated by Arrhenius equation[44,54]:

$$K_p = A e^{-Q/RT} \quad (4.8)$$

where A is the Arrhenius constant, Q is the activation energy for the rate controlling process, R is the universal gas constant and T is the absolute (metal) temperature.

Oxidation of Steel Alloys (Cr content)

Oxidation of Pure Iron is simple and it has three different oxide layers, those are Magnetite (Fe_3O_4), Hematite (Fe_2O_3), and Wustite (FeO). But the oxidation mechanisms of steels are more complicated, because the oxidation of alloying elements must be taken into account too. alloy oxidation is much more complex as a result of some, or all, of the following factors:

- Metals in the alloy will have different affinities for oxygen reflected by the different free energies of formation of the oxides.
- Ternary and higher oxides are formed.
- A degree of solid solubility between the oxides may exist.
- The various metal ions will have different mobilities in the oxide phases.
- The various metals will have different diffusivities in the alloy.
- Dissolution of oxygen into the alloy may result in sub-surface precipitation of oxides of one or more alloying elements (internal oxidation).

Chromium oxide Cr_2O_3 is detected as a solid solution with magnetite and in a mixed spinel $Fe(Fe, Cr)_2O_4$. Additionally, if the chromium content of the alloy is sufficient, a continuous layer of pure Cr_2O_3 may be detected. However, in elevated temperatures the chromium content required to form a continuous scale of Cr_2O_3 is relatively high, approximately 25 wt% as seen from Figure 4.5. On lower chromium contents the Cr_2O_3 can be detected, but it does not form a continuous layer and thus does not provide sufficient protection at elevated temperature and pressure levels.

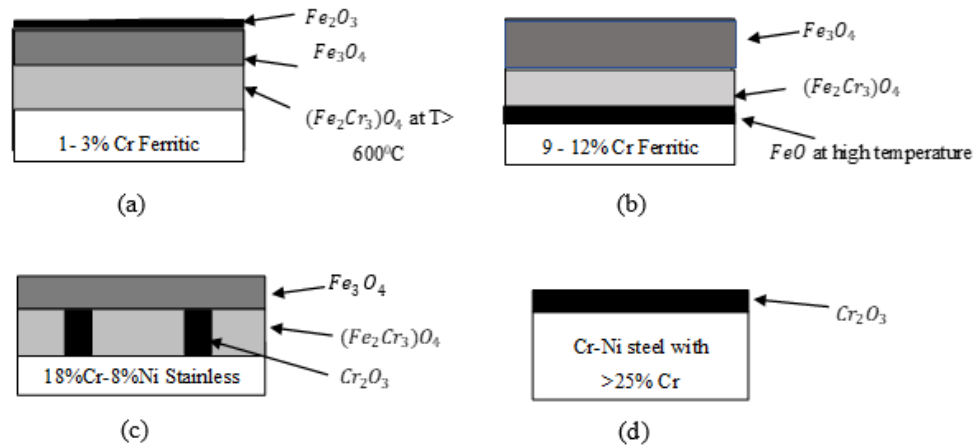


Figure 4.5: Summary of oxide scale morphologies formed on chromium containing steels in high temperature steam.

4.2 Oxidation of Ferritic steel

From open literature, conference proceedings, and reports from various agencies, we gathered the information presented here about alloy oxidation behavior in steam. The data shows that ferritic steel can be divided into two categories based on their Cr content, those with 1-3% Cr content are known as low alloy ferritic steel, and those with 9-12 Cr content are known as high alloy ferritic (martensitic) steel. In the next section, we discuss the oxidation behavior of high alloy ferritic (Martensitic) steel.

4.2.1 Oxidation of high alloy ferritic (Martensitic) steel (T92)

Oxidation Mechanism

An exterior layer (consisting of both haematite and magnetite) grows by outward diffusion of Fe cations beneath the original alloy surface, whereas an inner layer (consisting of Cr-rich spinel, $(Fe, Cr)_3O_4$, and Fe_3O_4) grows by inward diffusion of O anions beneath the original alloy surface. Magnetite makes up the majority of the scale's outer layer on the steam side. Figure 4.6 (c) and Figure 4.7 (a) shows haematite (Fe_2O_3) as a very thin outermost layer that forms during the cooling or at the beginning of the process of the specimen after the experiment is ended. On the steam side, the equilibrium oxygen partial pressure is relatively low, therefore haematite does not occur[55].

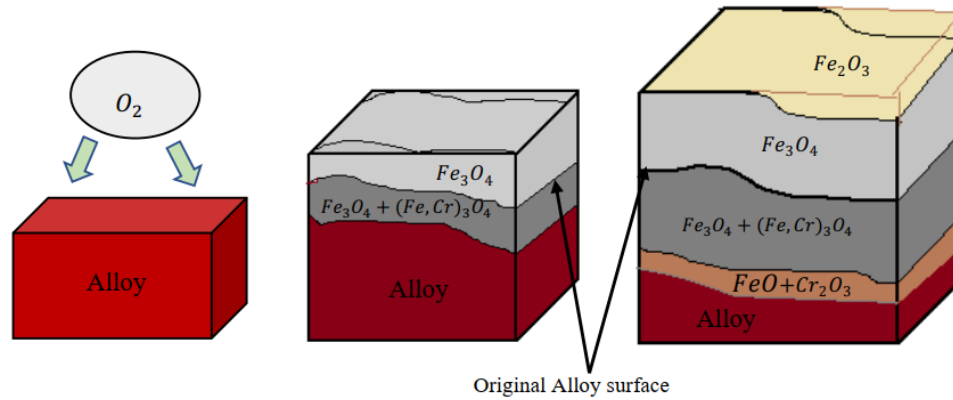


Figure 4.6: Schematic representation of oxidation mechanism of T92 alloy steel

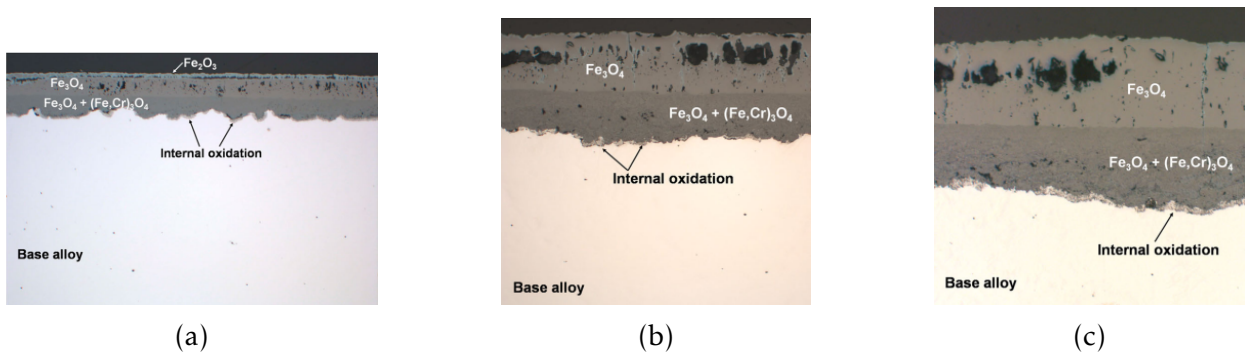


Figure 4.7: Optical micrographs showing oxide scale cross-section of T92 steel on the steam side after exposure at 650°C for (a) 25 h (b) 250 h and (c) 1000 h. [55]

Oxidation kinetics

The approach used to compile the kinetic data was to assume that the oxidation process followed a parabolic rate law and the parabolic rate constants were calculated from plotting the literature data on coordinates of oxide thickness versus square root of time.

For calculating oxide thickness (X) after a given time (t), can be calculated using parabolic law. This law discussed under section 4.1.2 and the equation to calculate the oxide thickness given in equation 4.6 and 4.7.

$$X^2 = 2K_p t \text{ and } K_p = A e^{-Q/RT}$$

Researchers obtain K_p , A, and Q value of T92 steel through experiment. Based on the researcher value, the summarized value of K_p is show in Table 4.1. It is the summarized K_p value based on oxide thickness.

Table 4.1: Value of the parabolic rate constant K_p value for oxide thickness

Alloy	K_p value for different Temperature ($\mu m^2/s$)				References
	600°C	650	700	750	
T92					
A	1.10×10^{-3}	1.34×10^{-2}	1.74×10^{-2}	4.75×10^{-2}	[42]
B	1.71×10^{-3}	9.92×10^{-3}	2.11×10^{-2}	-	[56]
C		5.8×10^{-3}			[55]

The oxide thickness obtained/calculated by substitute K_p value into equation 4.6. The oxide scale thickness of the above literatures after the computation shown in Figure 4.8.

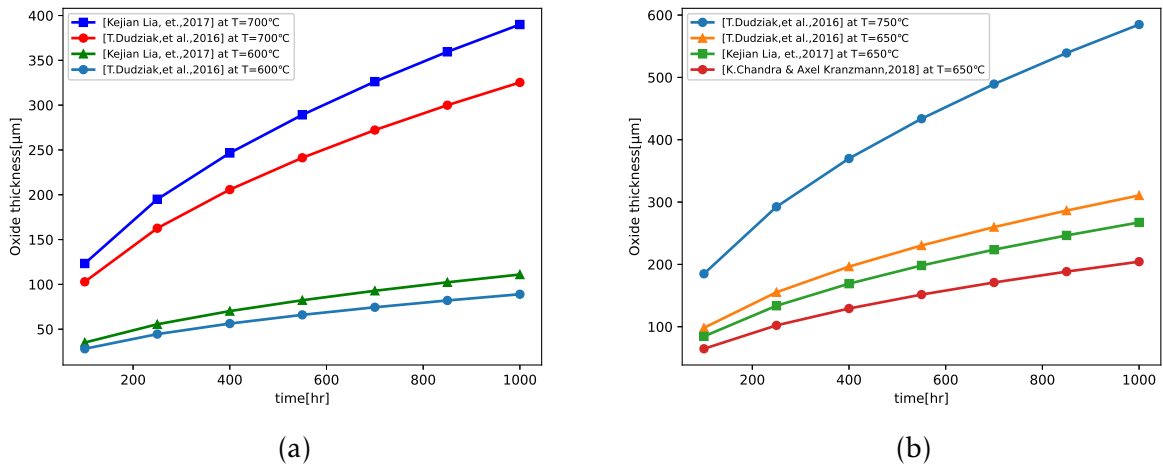


Figure 4.8: Summarized oxide thickness of T92 steels with time in temperature range between 600 and 750 C, based on Table 4.1

Based on Figure 4.8 the increment or growth rate of oxide thickness at 600°C steam temperature is very slow, it looks like linear increment, after 1000hr working time, the thickness is around $89\mu m$ [42] and $110\mu m$ [56] for 650°C the oxide thickness is around $310\mu m$ [42], $260\mu m$ [56], and $208\mu m$ [55] and also for 700°C the thickness is around $325\mu m$ [42] and $380\mu m$ [56] but at 750 °C the rate growth is more significant; it is around $550\mu m$ after 1000hr working time[42].

The researchers conclude the oxide growth rate of T92 steel shows significantly faster growth at the beginning of the process, which reduces with exposure period. The oxide scale thickness growth or increment at 600°C of steam temperature is very slow for 1000 working hour it is also described [57] and but at this temperature even very thin oxide scales can lead to overheating of T92 tube[54]. The oxide scale thickness growth is affected by the variation of steam temperature, when the steam temperature increase it also increase and become thick, these leads overheating of the tube and creep. When the time increase around 10,000hr T92 steel is exposed to creep at 600°C[59].

4.3 Mathematical Modeling

4.3.1 Heat transfer Analysis

Numerical methods, on the other hand, are based on replacing the differential equation by a set of n algebraic equations for the unknown temperatures at n selected points in the medium, and the simultaneous solution of these equations results in the temperature values at those discrete points.

There are several ways of obtaining the numerical formulation of a heat conduction problem, such as the finite difference method, the finite element method, the boundary element method, and the energy balance (or control volume) method[60].

Empirical Finite element method (FEM)

This section outlines the idea of developing mathematical models with 1D heat conduction equation using finite element method. The objective of this mathematical model is to show the variation of temperature due to different radius and it helps to calculate the average metal temperature. The FEM can be computed by two ways, the first one is developing the global stiffness matrix of the metal and oxide element by using Galerkin finite element method, then calculate the temperature at each node by using Excel, Python or by normal calculator, and the next way is by modeling the boiler with oxide scale by using ABAQUS software and analysis the temperature at each node.

In order to develop the mathematical model and simulate the oxide growth of the material during exposure of steam gas and flue gas, the following assumption are made:

1. The oxide formed on T92 steel consists equal dual layer. The outer layer contact with steam, is magnetic layer and the inner layer, in contact with the steel (substrate), is Fe-Cr spinel layer.
2. The two layers of oxide are separated by inner diameter of the steel, it is near-ideally straight line. Which means the magnetic layer grows outside and Fe-Cr spinel grows inside to the substrate.
3. For the sake of simplicity, the magnetite and spinel layers were treated as one, because there is no sufficient data on the growth kinetics of the individual oxide layers. Thus, the thermal conductivity value of the scale was assumed as the average of the two layers.
4. For the sake of simplification consider the heat transfer is steady state 1D heat conduction.

5. The growth or kinetics of oxide scales follows parabolic law.
6. Both the steam-side oxide scale and the metal substrate are isotropic and elastic materials
7. For sake of simplification consider the boiler like composite wall with convection ends.

For this research the superheater tubes are arranged in line shown in Figure 4.9, N_W is the number of tube wide; S_L is tube pitch along the flow direction of flue gas, and S_T is the pitch in the perpendicular direction.

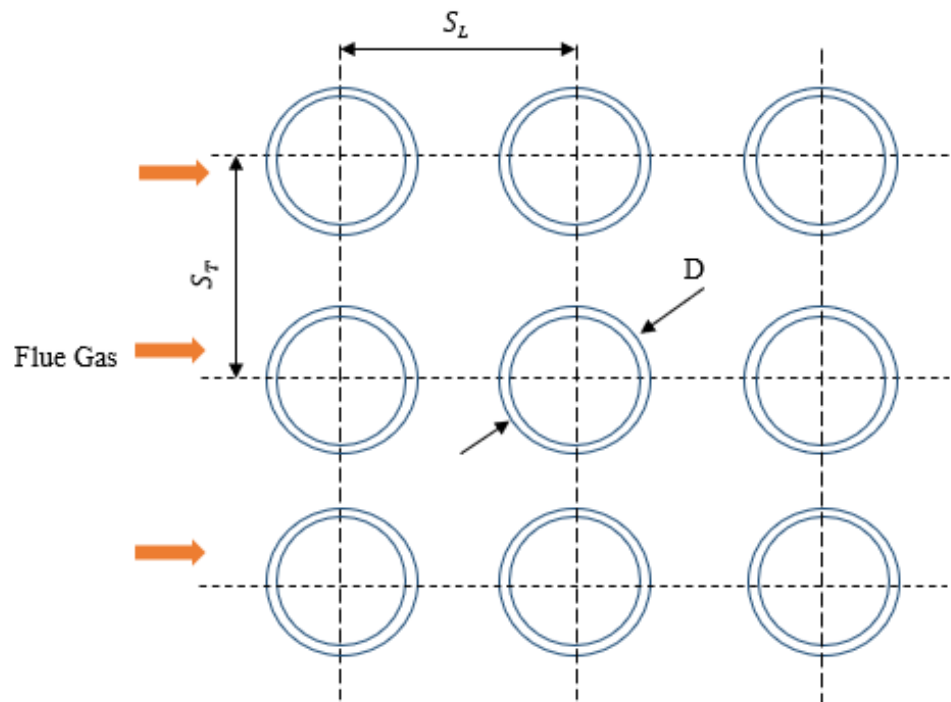


Figure 4.9: Arrangement and geometry of superheater tubes.

D is the outer tube diameter; d is the initial inner tube diameter, i.e., the inner diameter of a new tube without steam-side oxidation, δ_{ox} , δ_1 and δ_2 are total steam side oxide, Fe-Cr spinel oxide and Magnetite oxide respectively.

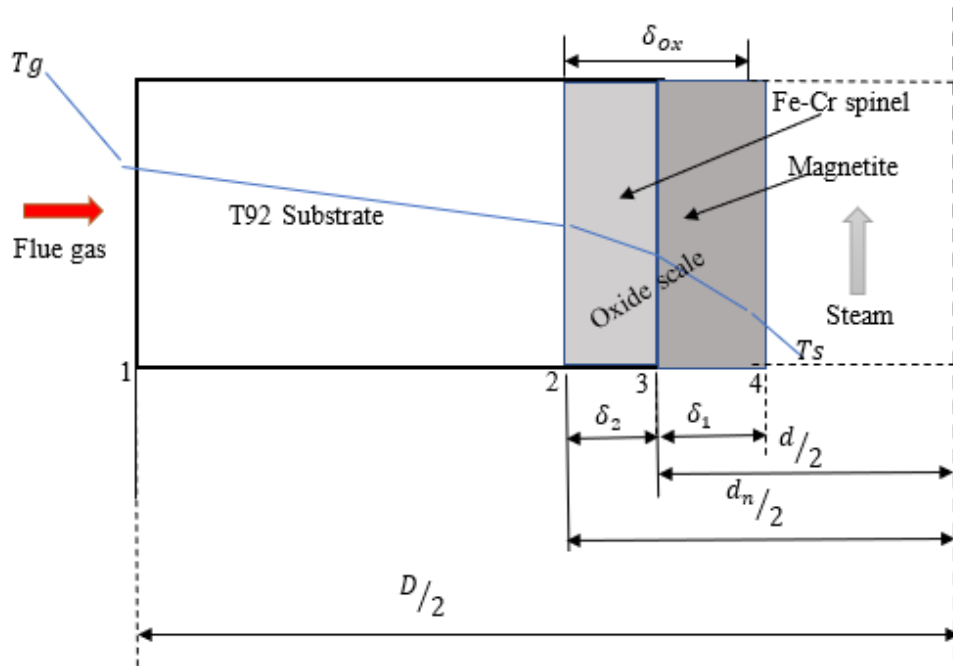


Figure 4.10: Schematic representation of the steam-side oxide scale and the discretization model.

Steady state Heat conduction

The governing equation of steady state equation with no internal generation of thermal energy

$$K \frac{d^2 T}{dr^2} = 0 \text{ or } K \frac{\partial^2 T}{\partial r^2} = 0 \quad (4.9)$$

To calculate the average metal or substrate temperature, discretize the region into finite element regions are the most accurate method. To discretize this second order governing equation, weight residual method, specifically Galerkin finite element method is appropriate.

Galerkin Finite element method

$$\int_0^{L_e} w(r) R(r) dr = 0 \quad (4.10)$$

$$w(r) = N_i(r) \quad (4.11)$$

Where $w(r)$, $R(r)$, $N_i(r)$ and 0 to L_e are weight functions, the governing equation, the shape function and the domain or boundary elements respectively.

Substitute equation 4.13 into 4.14 and the equation become:

$$\int_0^{L_e} K \frac{\partial^2 T}{\partial r^2} w(r) dr = 0 \quad (4.12)$$

Apply integration by part method

$$K \left(w(r) \frac{\partial T}{\partial r} - \int_0^{L_e} \frac{\partial w(r)}{\partial r} \frac{\partial T}{\partial r} dr \right) = 0 \quad (4.13)$$

$$\int_0^{L_e} K \frac{\partial w(r)}{\partial r} \frac{\partial T}{\partial r} dr = K w(r) \frac{\partial T}{\partial r} \quad (4.14)$$

Substitute equation 4.11 into 4.14 and the equation become:

$$\int_0^{L_e} K \frac{\partial N_i(r)}{\partial r} \frac{\partial T}{\partial r} dr = K N_i(r) \frac{\partial T}{\partial r} \quad (4.15)$$

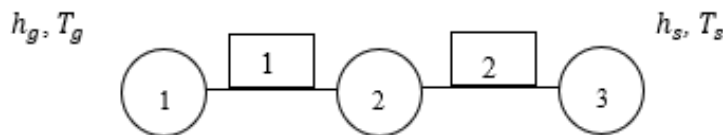
The boundary condition for this system is convection condition, in which the heat flux to/from the surface is proportional to the difference between the surface temperature and gas or steam temperature;

$$K_1 A_1 \frac{\partial T}{\partial r} = h_g A_1 [T_g - T_1] \quad (4.16)$$

$$-K_3 A_3 \frac{\partial T}{\partial r} = h_s A_3 [T_4 - T_s] \quad (4.17)$$

Based on the third assumption, treated the two oxide scales at one. So, the boiler tube can be divided into two elements and it has 3 nodes, the figure above shows the total dimension of the boiler and each element.

Assuming typical linear, heat conduction element



To calculate temperature at each node, assumed that the temperature varies linearly from flue gas to node 1 to node 2, from node 2 to node 3, and from node 3 to steam gas ($T_g > T_1 > T_2 > T_3 > T_s$). The heat transfer process of the boiler tube is:

Convection \Rightarrow Conduction \Rightarrow Conduction \Rightarrow Convection

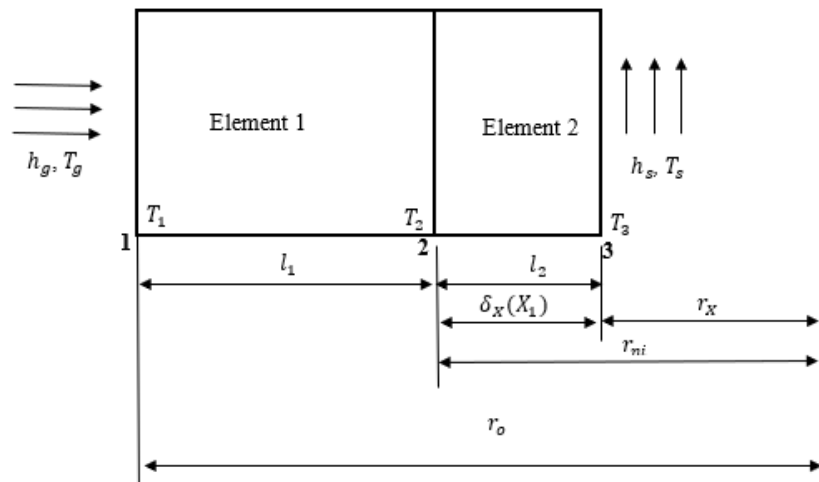
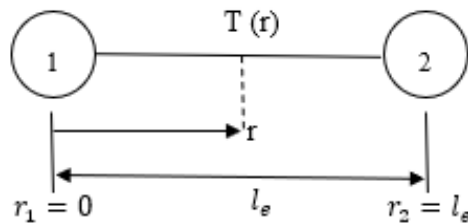


Figure 4.11: Discretize representation of the steam side oxide with dimensional representation.

Based on the heat transfer process of boiler tube node one and node three have the combined equation of conduction and convection and for node two the equation is pure conduction. There are some steps to obtain the element heat conductivity and temperature, those are select element type, choose temperature function, define the temperature and heat flux relation, derive the element conductive matrix and equation, and finally assemble the element equation to obtain the global equation.

Based on the steps select element one with nodes 1 and 2, and also select the linear equation $T(r) = mr + c$ to drive the temperature equation at each node



$$T(r) = \left(1 - \frac{r}{l_e}\right)T_1 + \left(\frac{r}{l_e}\right)T_2$$

$$T(r) = N_1 T_1 + N_2 T_2 \quad (4.18)$$

N_1 and N_2 are shape function, T_1 and T_2 are nodal temperature

Calculating the temperature gradient matrix $\{g\} = \frac{dT}{dr}$ or $\frac{\partial T}{\partial r}$ in the governing equation in terms of element length (l_e) and the nodal temperature venture (T) gives:

$$\frac{dT}{dr} = \frac{1}{l_e}(-T_1, T_2)$$

$$\frac{dT}{dr} = \frac{1}{l_e} \begin{bmatrix} -1 & 1 \end{bmatrix} \begin{Bmatrix} T_1 \\ T_2 \end{Bmatrix} \quad (4.19)$$

Also, it is known that: $w(r) = N_i(r)$, $w_1(r) = N_1(r) = 1 - \frac{r}{l_e}$ and $w_2(r) = N_2(r) = \frac{r}{l_e}$

$$\frac{dw_1}{dr} = -\frac{1}{l_e} \text{ and } \frac{dw_2}{dr} = \frac{1}{l_e}$$

First consider the left-hand side term

$$\text{L.H.S term} = \int_0^{L_e} K_e \frac{\partial w(r)}{\partial r} \frac{\partial T}{\partial r} dr \quad (4.20)$$

By substituting $w_1(r)$ and $w_2(r)$ in to the L.H.S term, can be obtain the simplified form of the equation

When substituting $w_1(r)$ and $w_2(r)$, the L.H.S term become

$$\begin{aligned} &= \frac{K_e A_e}{l_e} \begin{bmatrix} 1 & -1 \\ -1 & 1 \end{bmatrix} \begin{Bmatrix} T_1 \\ T_2 \end{Bmatrix} \\ &= [K]^e [T]^e \end{aligned} \quad (4.21)$$

At node 1, there is heat convection so, the convection stiffness matrix is

$$K_h = h_e A_e \begin{bmatrix} 1 & 0 \\ 0 & 0 \end{bmatrix}$$

The stiffness matrix at element 1 become the submission of conductive and convection stiffness matrix

$$k^1 = \frac{K_1 A_1}{l_1} \begin{bmatrix} 1 & -1 \\ -1 & 1 \end{bmatrix} + h_g A_1 \begin{bmatrix} 1 & 0 \\ 0 & 0 \end{bmatrix}$$

The stiffness matrix at element 2 become the submission of conductive and convection stiffness matrix, because at node 3 there is a convection boundary

$$k^2 = \frac{K_2 A_2}{l_2} \begin{bmatrix} 1 & -1 \\ -1 & 1 \end{bmatrix} + h_2 A_2 \begin{bmatrix} 0 & 0 \\ 0 & 1 \end{bmatrix}$$

The global stiffness matrix is the summation of all element stiffness matrices,

$$\begin{bmatrix} \left(\frac{K_1 A_1}{l_1} + h_g A_1 \right) & -\frac{K_1 A_1}{l_1} & 0 \\ -\frac{K_1 A_1}{l_1} & \left(\frac{K_1 A_1}{l_1} + \frac{K_2 A_2}{l_2} \right) & -\frac{K_2 A_2}{l_2} \\ 0 & -\frac{K_2 A_2}{l_2} & \left(\frac{K_2 A_2}{l_2} + h_s A_2 \right) \end{bmatrix} \begin{Bmatrix} T_1 \\ T_2 \\ T_3 \end{Bmatrix} = \begin{Bmatrix} f_1 \\ f_2 \\ f_3 \end{Bmatrix} \quad (4.22)$$

When come to the right-hand side term, this side is the heat flux which means the force required to drive the fluid.

$$R.H.S \text{ term} = Kw(r) \frac{\partial T}{\partial r}$$

When substituting $w_1(r)$ and $w_2(r)$, the R.H.S term become

$$= \begin{Bmatrix} -q_1 \\ q_2 \end{Bmatrix}$$

When there is convection end, the R.H.S term is change by including the convection force matrix at node 1 and node 3

$$f_C^1 = h_g T_g A_1 \begin{Bmatrix} 1 \\ 0 \end{Bmatrix} \text{ and}$$

$$f_C^2 = h_s T_s A_3 \begin{Bmatrix} 0 \\ 1 \end{Bmatrix}$$

So, the total R.H.S term become

$$\begin{Bmatrix} f_1 \\ f_2 \\ f_3 \end{Bmatrix} = \begin{Bmatrix} -q_1^1 + f_C^1 \\ q_2^1 + q_1^2 \\ q_2^2 + f_C^2 \end{Bmatrix}$$

There is no heat flux on the system. So, the simplified form of the force matrix is:

$$\begin{Bmatrix} f_1 \\ f_2 \\ f_3 \end{Bmatrix} = \begin{Bmatrix} h_g T_g A_1 \\ 0 \\ h_s T_s A_2 \end{Bmatrix}$$

The final global matrix to calculate the temperature at each node is

$$\begin{bmatrix} \left(\frac{K_1 A_1}{l_1} + h_g A_1\right) & -\frac{K_1 A_1}{l_1} & 0 \\ -\frac{k_1 A_1}{l_1} & \left(\frac{K_1 A_1}{l_1} + \frac{K_2 A_2}{l_2}\right) & -\frac{K_2 A_2}{l_2} \\ 0 & -\frac{K_2 A_2}{l_2} & \left(\frac{K_2 A_2}{l_2} + h_s A_2\right) \end{bmatrix} \begin{Bmatrix} T_1 \\ T_2 \\ T_3 \end{Bmatrix} = \begin{Bmatrix} h_g T_g A_1 \\ 0 \\ h_s T_s A_2 \end{Bmatrix} \quad (4.23)$$

The value of l_1 , l_2 , A_1 , A_2 , and h_s is changing in each iterative step because of the formation and growth of oxide scale thickness. So, the general equation needed to include those changes. The notation i represent the steps.

$$\begin{bmatrix} \left(\frac{K_1 A_{1i}}{l_{1i}} + h_g A_{1i}\right) & -\frac{K_1 A_{1i}}{l_{1i}} & 0 \\ -\frac{k_1 A_{1i}}{l_{1i}} & \left(\frac{K_1 A_{1i}}{l_{1i}} + \frac{K_2 A_{2i}}{l_{2i}}\right) & -\frac{K_2 A_{2i}}{l_{2i}} \\ 0 & -\frac{K_2 A_{2i}}{l_{2i}} & \left(\frac{K_2 A_{2i}}{l_{2i}} + h_{s_i} A_{2i}\right) \end{bmatrix} \begin{Bmatrix} T_1 \\ T_2 \\ T_3 \end{Bmatrix} = \begin{Bmatrix} h_g T_g A_{1i} \\ 0 \\ h_{s_i} T_s A_{2i} \end{Bmatrix} \quad (4.24)$$

At the absence of oxide scale, only element one is available. In this case the above equation is changed and simplified to the following equation:

$$\begin{bmatrix} \left(\frac{K_1 A_1}{l_1} + h_g A_1\right) & -\frac{K_1 A_1}{l_1} \\ -\frac{k_1 A_1}{l_1} & \left(\frac{K_1 A_1}{l_1} + h_s A_1\right) \end{bmatrix} \begin{Bmatrix} T_1 \\ T_2 \end{Bmatrix} = \begin{Bmatrix} h_g T_g A_1 \\ h_s T_s A_1 \end{Bmatrix} \quad (4.25)$$

Table 4.2: Parameters of the steady state heat transfer stiffness matrix

Notation	Representation	Source or Equation
k_1	k_{metal}	From Table A-2
k_2	k_{oxide}	From Table A-2
h_g	h_g	From Table 5.1
h_s	h_s	From Table 5.3-5.8
l_1	Thickness of metal	$l_1 = r_0 - r_{ni}$
l_2	Thickness of oxide scale	$l_2 = r_{ni} - r_{xi}$
r_{ni}	Oxide/metal interface radius	$r_{ni} = r_i + \delta_x/2$
r_{xi}	Inner radius of tube due to oxide	$r_{xi} = r_i - \delta_x/2$
A_1	Surface Area of the metal	$A_1 = 2 \times \pi \times r_0$
A_2	Surface Area of the oxide	$A_2 = 2 \times \pi \times r_{xi}$

The material of the seamless ferritic high-alloy steel tube used in this work is T92. The dimension of the superheater boiler tube and thermos-physical properties of the material and the oxide is listed in Table A-1 and Table A-2 respectively.

Convection coefficient of the steam, h_s and its correlation for fully developed turbulent flow in circular tubes can be expressed by heat transfer books[61,62]. The thermo-physical properties of steam are listed in Table A-3

$$h_s = 0.023 \times \frac{k_s}{d-2\delta_1} (Re_s)^{0.8} (Pr_s)^{0.4} \quad (4.26)$$

The Reynolds Number and Prandtl Number can be calculated

$$Re_s = \frac{4m_s}{3600 \times \pi (d-2\delta_1) \mu_s} \quad (4.27)$$

$$Pr_s = \frac{\mu_s C_s}{k_s} \quad (4.28)$$

The dynamics viscosity (μ_s), thermal conductivity (K_s) and specific heat of the steam (C_s), and can be calculated using the equations of IAPWS-IF97 and select from table of properties of water and steam with the specific temperature and pressure[63].

Equation 4.29 provides conservative estimates for the flue gas convection coefficient, h_g , for forced flue gas convection over bare tubes[64].

$$h_g = 0.33 \times 12 \frac{k_g}{D} \times (Re_g)^{0.6} (Pr_g)^{0.33} \quad (4.29)$$

The Reynolds Number and Prandtl Number is calculated

$$Re_g = \frac{m_g D}{3600 N_w H (S_T - D) \mu_g} \quad (4.30)$$

$$Pr_g = \frac{\mu_g C_g}{K_g} \quad (4.31)$$

In this work; H equal to 10 m is the height of the gas flow region; μ_g , K_g and C_g are dynamics viscosity, thermal conductivity and specific heat of the flue gas respectively, and are influenced by various factors such as coal content, gas temperature, excess air coefficient and so on[65] and [66]. The thermos-physical properties of flue gas are listed in Table A-4.

4.3.2 Estimation of oxide scale growth

There are several known techniques for determining metal temperature using oxide scale thickness. The most known technique is a Larson–Miller–type expression.

$$\log X = C + D \left[T (20 + \log t) \times 10^{-3} \right]$$

The data and formula of the LMP versus the scale thickness for martensitic steel of 9–12% chromium is reported by [35].

$$\log X = 0.000564 \times P - 9.934 \quad (4.32)$$

$$P = (T + 273)(20 + \log t) \quad (4.33)$$

Where X is scale thickness in μm , p is the Larson miller parameter as a function of temperature and time, T is average temperature in $^{\circ}\text{C}$, and t is service time in hours.

The increase temperature in superheater boiler tube is calculated by numerical simulation corresponding to the given hours and scale thickness. In this work, the simulations performed for the predictions are made up to the maximum of 1000 h with an increment of time as shown in the below table.

Table 4.3: The time used in the iterative procedure

Steps (i)	hr.
1	100
2	250
3	400
4	550
5	700
6	850
7	1000

4.4 Stress analysis of steam side oxide scaled boiler tube

Many pressure vessels and other engineering constructions like boiler tubes are subjected to stress and high temperatures at the same time. When the pressure inside a cylinder of a diameter D , wall thickness t and length L is larger than the pressure outside, it causes stress around the cylinder (σ_C) and along the cylinder (σ_L) as shown in Figure 4.12 [67].

The term "longitudinal stress" (stress created in the longitudinal direction) and "circumferential stress" (stress acting in the circumferential direction) are interchangeable. Hoop or tangential stress are other names for the latter.

For thick-walled and thin-walled tubes, various stress equations may be used. When a cylinder's wall thickness is less than one-tenth of its radius, it is said to have thin walls. It is considered to be a thick wall if the wall thickness is greater than this.

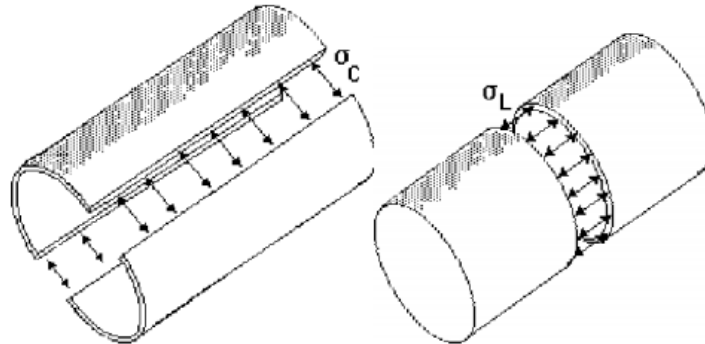


Figure 4.12: Applied stress acting on circumferential and longitudinal direction of the tubes[67]

This section covers the derivative of equilibrium equation, derivative of elastic and thermal stress and strain equation due to steam side oxide scale. For this analysis consider the boiler tube working at long period of time to get a better result, the working times are 2000hr, 4000hr, 6000hr, 8000hr and 10,000hr. The steam side oxide scale for this operating time is calculated by following the procedure under section 4.3.2. For this analysis the radii and temperature of inner, interface and outer tube and also the thickness of oxide scale is listed in Table A-5 and other parameters like E and ν of the oxide and the metal is listed in Table A-2.

Assumptions

1. The length of the cylinder is large as compared to its cross-sectional dimensions, the cylinder is then in a state of plane stress and strain.
2. The material is homogenous and isotropic
3. Consider an axisymmetric compound hollow circular cylinder of inner radii, interface radii of metal and oxide part and outer radii a , b , and c , respectively.
4. The Norton's Law of creep and time-hardening rule is applicable

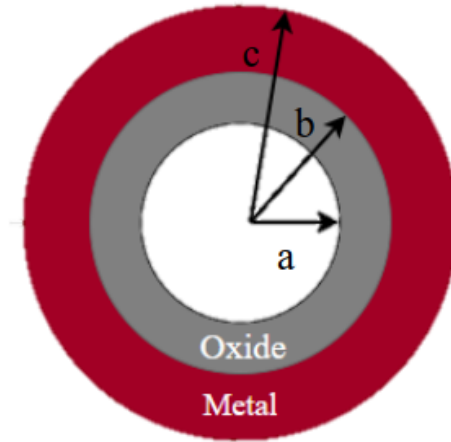


Figure 4.13: Radial representation of oxide scaled boiler tube

4.4.1 Derivative of Equilibrium Equation

Based on the above assumption thick wall compound cylinder subjected to internal and/or external pressure and at different temperature may induced creep. Consider the ends of the boiler tube to be constrained rigidly by end plates. Therefore, we may assume the longitudinal stress and strain is negligible and the tube is in state of plane stress and strain.

Consider the finite dimension stress element and cut an element from the cylinder by two planes perpendicular to the axis and at a unit distance. The equation is derivate based on Lam's equation.

The two stresses develop on the stress element has the hoop stress σ_{θ} and radial stress σ_r . Considering the force equilibrium in a radial direction and summing up the forces gives us the following equilibrium equation

$$\sigma_r r d\theta + 2\sigma_{\theta} dr \frac{\sin d\theta}{2} = (\sigma_r + d\sigma_r)(r + dr) d\theta \quad (4.34)$$

For further simplification take for small angles $\frac{\sin d\theta}{2} = \frac{d\theta}{2}$, cancel out $d\theta$ from each side and assume the multiplication of two small terms equal to zero.

$$\frac{d\sigma_r}{dr} + \frac{\sigma_r - \sigma_{\theta}}{r} = 0 \quad (4.35)$$

4.4.2 Elastic stress and strain

Before proceed to the displacement derivation of the stress element due to applying pressure, let revise Hooke's law plane stress expression in terms of strains are

$$\sigma_r = \frac{E}{(1-\nu^2)} (\varepsilon_r + \nu\varepsilon_\theta) \quad (4.36)$$

$$\sigma_\theta = \frac{E}{(1-\nu^2)} (\varepsilon_\theta + \nu\varepsilon_r) \quad (4.37)$$

The displacement of the stress element is shown in Figure 4.14. Let u denotes the displacement in the radial direction. CDEF is the initial position of stress element; after the applying of pressure the stress element changes the position into $C'D'E'F'$. The amount of displacement from point A to A' is equal to $u(r)$ and the amount of displacement from point B to B' is equal to $u(r) + \frac{\partial u}{\partial r} dr$. The normal strain in the radial direction is then given by the amount of stretch divided by the original length.

$$\varepsilon_r = \frac{u(r) + \frac{\partial u}{\partial r} dr - u(r)}{dr} = \frac{du}{dr} \quad (4.38)$$

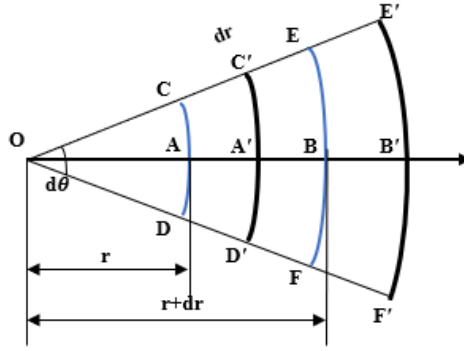


Figure 4.14: Schematic representation of displacement stress element

The tangential displacement is the displacement of the point CD to $C'D'D$. The length of CD is equal to $rd\theta$ and the length of $C'D'$ is equal to $(r + u(r))d\theta$. The tangential strain given by

$$\varepsilon_\theta = \frac{(r + u(r))d\theta - rd\theta}{rd\theta} = \frac{u}{r} \quad (4.39)$$

Substitute the value of ε_r and ε_θ into Equation 4.36 and 4.37 and the Hook's law (Equation 4.36 and 4.37) become into:

$$\sigma_r = \frac{E}{(1-\nu^2)} \left(\frac{du}{dr} + \nu \frac{u}{r} \right) \quad (4.40)$$

$$\sigma_\theta = \frac{E}{(1-\nu^2)} \left(\frac{u}{r} + \nu \frac{du}{dr} \right) \quad (4.41)$$

Substitute equation 4.40 and 4.41 into equation 4.35, then obtain the following second order differential equation for determining u .

$$\frac{d^2u}{dr^2} + \frac{1}{r} \frac{du}{dr} - \frac{u}{r^2} = 0 \quad (4.42)$$

The general solution for this equation is

$$u = C_1 r + \frac{C_2}{r} \quad (4.43)$$

Substituting equation 4.43 into equation 4.40 and 4.41, the stress-strain relation for a plain strain condition in the j th layer (oxide (1st layer) and metal (2nd layer)) become:

$$\sigma_\theta = \frac{E}{(1-\nu^2)} \left(C_{j1}(1+\nu_j) + C_{j2} \left(\frac{(1-\nu_j)}{r^2} \right) \right) \quad (4.44)$$

$$\sigma_r = \frac{E}{(1-\nu^2)} \left(C_{j1}(1+\nu_j) - C_{j2} \left(\frac{(1-\nu_j)}{r^2} \right) \right) \quad (4.45)$$

$$\varepsilon_\theta = C_{j1} + \frac{C_{j2}}{r^2} \quad (4.46)$$

$$\varepsilon_r = C_{j1} - \frac{C_{j2}}{r^2} \quad (4.47)$$

The value of the integration constant of C_{j1} and C_{j2} obtained from boundary conditions. The boundary conditions are:

$$\sigma_{ox,r}(r=a) = -P_i \quad \text{and} \quad \sigma_{met,r}(r=c) = -P_o$$

$$\sigma_{ox,r}(r=b) = \sigma_{met,r}(r=b)$$

$$u_{ox} = u_{met} \text{ at } r = b$$

After substituting the boundary condition, the equations become

$$-P_i = \frac{E_{ox}}{(1-\nu_{ox}^2)} \left[C_{11}(1+\nu_{ox}) - C_{12} \left(\frac{(1-\nu_{ox})}{a^2} \right) \right] \quad (4.48)$$

$$-P_o = \frac{E_{met}}{(1-\nu_{met}^2)} \left[C_{21}(1+\nu_{met}) - C_{22} \left(\frac{(1-\nu_{met})}{c^2} \right) \right] \quad (4.49)$$

$$\frac{E_{ox}}{(1-\nu_{ox}^2)} \left[C_{11}(1+\nu_{ox}) - C_{12} \left(\frac{(1-\nu_{ox})}{b^2} \right) \right] = \frac{E_{met}}{(1-\nu_{met}^2)} \left[C_{21}(1+\nu_{met}) - C_{22} \left(\frac{(1-\nu_{met})}{b^2} \right) \right] \quad (4.50)$$

$$C_{11}b + \frac{C_{12}}{b} = C_{21}b + \frac{C_{22}}{b} \quad (4.51)$$

After applying the boundary condition, the above summarized equation become in matrix form for easy calculation of the integration constant

$$\begin{bmatrix} 1 & k_{12} & 0 & 0 \\ 0 & 0 & 1 & k_{24} \\ 1 & k_{32} & k_{33} & k_{34} \\ 1 & k_{42} & -1 & k_{44} \end{bmatrix} \begin{Bmatrix} C_{11} \\ C_{12} \\ C_{21} \\ C_{22} \end{Bmatrix} = \begin{Bmatrix} B_1 \\ B_2 \\ B_3 \\ B_4 \end{Bmatrix} \quad (4.52)$$

Where

$$k_{12} = -\frac{(1-\nu_{ox})}{(1+\nu_{ox})a^2}, \quad k_{24} = -\frac{(1-\nu_{met})}{(1+\nu_{met})c^2}, \quad k_{42} = \frac{1}{b^2}, \quad k_{44} = \frac{-1}{b^2}$$

$$k_{32} = -\frac{(1-\nu_{ox})}{(1+\nu_{ox})b^2}, \quad k_{33} = -\left[\frac{E_{met}}{E_{ox}} \right] \frac{(1-\nu_{ox})}{(1-\nu_{met})}, \quad k_{34} = \left[\frac{E_{met}}{E_{ox}} \right] \frac{(1-\nu_{ox})}{(1+\nu_{met})b^2}$$

$$B_1 = -\frac{(1-\nu_{ox})}{E_{ox}}P_i, \quad B_2 = -\frac{(1-\nu_{met})}{E_{met}}P_o, \quad B_3 = 0, \quad B_4 = 0$$

After the integration constant is obtained from the inverse of matrix or from Equation 4.52, substitute into equation 4.44 and 4.45 to get the radial and hoop stress respectively, and substitute into equation 4.46 and 4.47 to get the radial and hoop strain in the radial position.

This analytical equation computed by python code, the code is found under Appendix B.2 (Python code for Elastic radial and hoop stress-strain). All the required parameters with their value is listed their.

4.4.3 Thermo-Mechanical (Thermal) stress and strain

Thermal loads have a significant influence on the stress's distributions and displacements of a multilayered composite pressure vessel due to thermal gradients through the thickness and the difference between the thermal expansion coefficients of the used materials[24]. The thermal expansion coefficient of both T92 alloy and oxide scale are shown in Figure A-1 and it clearly shows the thermal expansion influences by temperature[68-70].

The free thermal strain resulting from a temperature variation is calculated in the following integral form

$$\varepsilon_{th,j} = \int_{T_{1,j}}^{T_{2,j}} \alpha_j(T) dT \quad \text{or} \quad \varepsilon_{th,j} = \alpha_j \Delta T \quad (4.53)$$

Where $\varepsilon_{th,j}$ is the free thermal strain of jth layer (oxide and metal), α_j is thermal expansion coefficient of jth layer (oxide and metal), and ΔT is the temperature difference of each layer i.e., metal to oxide/metal interface and oxide/metal interface to oxide layer.

The stress-strain relation for a plain strain condition in the jth layer (oxide and metal) become:

$$\varepsilon_{j,r} = \frac{\sigma_{j,r}}{E_j} - \frac{\nu_j}{E_j} (\sigma_{j,\theta} + \sigma_{j,z}) + \alpha_j \Delta T \quad (4.54)$$

$$\varepsilon_{j,\theta} = \frac{\sigma_{j,\theta}}{E_j} - \frac{\nu_j}{E_j} (\sigma_{j,r} + \sigma_{j,z}) + \alpha_j \Delta T \quad (4.55)$$

$$\varepsilon_{j,z} = \frac{\sigma_{j,z}}{E_j} - \frac{\nu_j}{E_j} (\sigma_{j,r} + \sigma_{j,\theta}) + \alpha_j \Delta T = 0 \quad (4.56)$$

Substituting equation 4.56 into equation 4.54 and 4.55, the stress equation become

$$\sigma_{j,r} = \frac{E_j}{(1 + \nu_j)(1 - 2\nu_j)} \left[(1 - \nu_j) \varepsilon_{j,r} + \nu_j \varepsilon_{j,\theta} \right] \quad (4.57)$$

$$\sigma_{j,\theta} = \frac{E_j}{(1 + \nu_j)(1 - 2\nu_j)} \left[(1 - \nu_j) \varepsilon_{j,\theta} + \nu_j \varepsilon_{j,r} - (1 + \nu_j) \alpha_j \Delta T \right] \quad (4.58)$$

$$\sigma_{j,z} = \nu_j (\sigma_{j,r} + \sigma_{j,\theta}) - E_j \alpha_j \Delta T \quad (4.59)$$

Substitute equation 4.57 and 4.58 into equation 4.35, then the equation become

$$\frac{d^2 u}{dr^2} + \frac{1}{r} \frac{du}{dr} - \frac{u}{r^2} = \frac{(1 + \nu_j)}{(1 - \nu_j)} \alpha_j \frac{\Delta T}{dr} \quad (4.60)$$

The value of u after integration become

$$u_j = \frac{(1+\nu_j)}{(1-\nu_j)} \left(\frac{\alpha_j}{r} \right) \int_{r_{in}}^r \Delta T r dr + p r + \frac{q}{r} \quad (4.61)$$

After substituting the displacement (u_j) value into radial strain and hoop strain equation, the result become,

$$\varepsilon_r = \left(\frac{1+\nu_j}{1-\nu_j} \right) \left[\frac{-\alpha_j}{r^2} \int_{r_{in}}^r \Delta T r dr + \alpha \Delta T \right] + p_{j1} - \frac{q_{j2}}{r^2} \quad (4.62)$$

$$\varepsilon_\theta = \left(\frac{1+\nu_j}{1-\nu_j} \right) \frac{\alpha_j}{r^2} \int_{r_{in}}^r \Delta T r dr + p_{j1} + \frac{q_{j2}}{r^2} \quad (4.63)$$

After computing the value of radial and hoop strain the radial and hoop stress become,

$$\sigma_{j,r} = E_j \left[\frac{-\alpha_j}{(1-\nu_j)r^2} \int_{r_{in}}^r \Delta T r dr + \frac{p_{j1}}{(1+\nu_j)(1-2\nu_j)} - \frac{q_{j2}}{(1+\nu_j)r^2} \right] \quad (4.64)$$

$$\sigma_{j,\theta} = E_j \left[\frac{\alpha_j}{(1-\nu_j)r^2} \int_{r_{in}}^r \Delta T r dr + \frac{p_{j1}}{(1+\nu_j)(1-2\nu_j)} + \frac{q_{j2}}{(1+\nu_j)r^2} - \frac{\alpha_j \Delta T}{1-2\nu_j} \right] \quad (4.65)$$

The integration constant p_{j1} and q_{j1} are calculated by applying the boundary condition, the boundary conditions are:

$$\sigma_{ox,r}(r=a) = -P_i \quad \text{and} \quad \sigma_{met,r}(r=c) = -P_o$$

$$\sigma_{ox,r}(r=b) = \sigma_{met,r}(r=b)$$

$$u_{ox} = u_{met} \text{ at } r = b$$

After applying the boundary condition, the summarized equation become in matrix form for easy calculation of the integration constant

$$\begin{bmatrix} 1 & k_{12} & 0 & 0 \\ 0 & 0 & 1 & k_{24} \\ 1 & k_{32} & -1 & k_{34} \\ 1 & k_{42} & k_{43} & k_{44} \end{bmatrix} \begin{Bmatrix} p_{ox,1} \\ q_{ox,2} \\ p_{met,1} \\ q_{met,2} \end{Bmatrix} = \begin{Bmatrix} B_1 \\ B_2 \\ B_3 \\ B_4 \end{Bmatrix} \quad (4.66)$$

Where

$$\begin{aligned}
k_{12} &= \frac{-(1-2\nu_{ox})}{a^2}, \quad k_{24} = \frac{-(1-2\nu_{met})}{c^2}, \quad k_{32} = \frac{1}{b^2}, \quad k_{34} = \frac{-1}{b^2} \\
k_{42} &= \frac{-(1-2\nu_{ox})}{b^2}, \quad k_{43} = -\left[\frac{E_{met}}{E_{ox}}\right] \frac{(1+\nu_{ox})(1-2\nu_{ox})}{(1+\nu_{met})[1-2\nu_{met}]} \\
k_{44} &= \left[\frac{E_{met}}{E_{ox}}\right] \frac{(1+\nu_{ox})(1-2\nu_{ox})}{(1+\nu_{met})b^2}, \quad B_1 = -\frac{(1+\nu_{ox})(1-2\nu_{ox})}{E_{ox}} P_i \\
B_2 &= \alpha_{met} \left(\frac{1+\nu_{met}}{1-\nu_{met}}\right) \left(\frac{1-2\nu_{met}}{c^2}\right) \int_b^c (T_c - T_b) r dr - \frac{(1+\nu_{met})(1-2\nu_{met})}{E_{met}} P_o \\
B_3 &= -\frac{\alpha_{ox}}{b^2} \left(\frac{1+\nu_{ox}}{1-\nu_{ox}}\right) \int_a^b (T_b - T_a) r dr, \quad B_4 = \frac{\alpha_{ox}(1-2\nu_{ox})}{b^2} \left(\frac{1+\nu_{ox}}{1-\nu_{ox}}\right) \int_a^b (T_b - T_a) r dr
\end{aligned}$$

After the integration constant is obtained from the inverse of matrix or from equation 4.66, substitute into equation (4.64 and 4.65) and equation (4.62 and 4.63) give the stress and strain in the radial position respectively.

This analytical equation computed by python code, the code is found under Appendix B.3 (Python code for Thermo-Mechanical radial and hoop stress-strain). All the required parameters with their value is listed their.

4.4.4 Failure of oxide scale

Scale exfoliation on the steam side of the superheater tube is reducing flow, obstructing tube bends, eroding the nozzle, and eroding the first stage of the turbine's blades. Scale exfoliation becomes an issue between five and fifty kilometers into service. The most important factor for calculating the remaining life of a boiler tube and for the safe and effective operation of a power plant is the study or examination of the failure of steam side oxide scale.

Mechanical failure of oxide scales can result if critical compressive and/or tensile stresses or strains are reached in the oxide/metal system. A significant number of publications exist modelling the different failure mechanisms and reporting about measurements of critical failure stresses and strains. Figure 4.15 shows the critical strain rate of oxide failure at different oxide scale due to tension and compression. The elastic and thermal strain can be compared to the critical strains (ϵ_c) which the scales can tolerate before through-scale cracking, delamination, spalling, etc. can occur to predict whether and when failure will occur for a particular failure mechanism. Due to the lack of sufficient data of the parameters like radius of detached part of oxide scale, interfacial amplitude

and interfacial energy need for scale separation, the oxide scale spallation, buckling and delamination is not calculated. In this study only check the oxide scale crack initiation due to tension and compression using equation 4.67 and Figure 4.15 respectively. The equation for all types of oxide scale failures are discussed by[25].

$$\varepsilon_c = \frac{K_{Ic} \times \left(\frac{c_0}{c}\right)^{0.5}}{f \times E(\pi \times c)^{1/2}} \quad (4.67)$$

The parameters for this equation (scale cracking in tension) are:

K_{Ic} : fracture toughness (mode I) of oxide scale, take $1.35 \text{MPa m}^{0.5}$

f : geometrical parameter ($f = 1$ for this work)

c, c_0 : size of a physical scale defect (pore, flaw, etc. in μm) with c_0 as a value for normalizing the defect size (c/c_0 dimensionless), c_0 equal to $1 \mu\text{m}$ is for normalized defect size c .

E : Young's modulus of the oxide scale (MPa)

Take the ratio of c/δ_{ox} equal to 0.1 based on Figure 4.15.

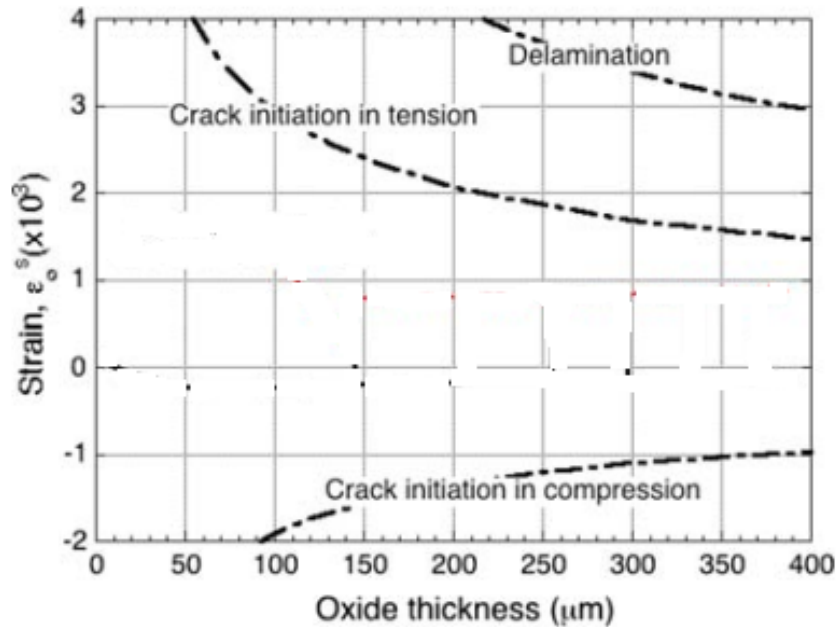


Figure 4.15: Representation of criteria for oxide failure in an Exfoliation Diagram[12]

4.5 Creep stress and Strain rate of Metal

In this study consider viscoelastic creep in secondary steady state stage in which the deformation is plastic. In this stage the creep rate reaches a minimum and remains

constant as the effect of strain hardening is counter balanced by an annealing influence. Here the creep rate is a function of stress level and temperature[12,23].

$$\dot{\varepsilon}_{cr} = f(\sigma_e)g(T) \quad (4.68)$$

The stress dependence follows the Norton's law (power creep law), which assumes a power law, gives creep strain components a relationship between equivalent stress and equivalent strain. The relationship is given by the following equation:

$$f(\sigma_e) = \varepsilon_{cr,\sigma_e} = K\sigma_e^n t^q \quad (4.69)$$

Where q, n, and K are the material constants, and σ_e and t are the stress and time parameters, correspondingly. The value of stress constant n and K is suggested by many researchers due to the working pressure, temperature, and material. The value of n is suggested by different researchers the most common is the range of 3 and 5 [71,72]. Creep parameter of T92 steel at temperature of 600°C of steam is listed in Table A-6.

To analysis creep under combined stress take some assumption[73,74]

1. The volume(density) of the material remains constant, so that for small deformations

$$\varepsilon_\theta + \varepsilon_r + \varepsilon_z = 0 \sim \dot{\varepsilon}_\theta + \dot{\varepsilon}_r + \dot{\varepsilon}_z \quad (4.70)$$

2. During creep and plastic deformation, the direction of the principal stresses, σ_θ , σ_r and σ_z , coincide with the direction of the principal strains ε_θ , ε_r and ε_z
3. The ratios of principal shear-strain rates to principal shear stresses are constant and take the following form

$$\frac{\dot{\varepsilon}_\theta - \dot{\varepsilon}_r}{\sigma_\theta - \sigma_r} = \frac{\dot{\varepsilon}_r - \dot{\varepsilon}_z}{\sigma_r - \sigma_z} = \frac{\dot{\varepsilon}_z - \dot{\varepsilon}_\theta}{\sigma_z - \sigma_\theta} = \frac{3}{2\psi} \quad (4.71)$$

The principal creep rates obtained by Computing equation 4.70 and 4.71. The principal creep rates denote by $\dot{\varepsilon}_\theta$, $\dot{\varepsilon}_r$ and $\dot{\varepsilon}_z$. The equation become:

$$\dot{\varepsilon}_\theta = \frac{1}{\psi} \left[\sigma_\theta - \frac{1}{2}(\sigma_r + \sigma_z) \right] \quad (4.72)$$

$$\dot{\varepsilon}_r = \frac{1}{\psi} \left[\sigma_r - \frac{1}{2}(\sigma_\theta + \sigma_z) \right] \quad (4.73)$$

$$\dot{\varepsilon}_z = \frac{1}{\psi} \left[\sigma_z - \frac{1}{2} (\sigma_r + \sigma_\theta) \right] \quad (4.74)$$

For simple tension model, where $\sigma_\theta = \sigma_e$ and $\sigma_r = \sigma_z = 0$, the strain become

$$\dot{\varepsilon}_e = \frac{\sigma_e}{\psi} \quad (4.75)$$

For steady state creep rate, the Norton's law (power creep rate) become

$$\dot{\varepsilon}_e = K \sigma_e^n \quad (4.76)$$

To bring equation 4.75 and equation 4.76 into agreement, we must take

$$\psi = K^{-1} \sigma_e^{1-n} \quad (4.77)$$

After substituting the function of ψ to the general creep equation (4.72,4.73 and 4.74)

$$\dot{\varepsilon}_\theta = K \sigma_e^{n-1} \left[\sigma_\theta - \frac{1}{2} (\sigma_r + \sigma_z) \right] \quad (4.78)$$

$$\dot{\varepsilon}_r = K \sigma_e^{n-1} \left[\sigma_r - \frac{1}{2} (\sigma_\theta + \sigma_z) \right] \quad (4.79)$$

$$\dot{\varepsilon}_z = K \sigma_e^{n-1} \left[\sigma_z - \frac{1}{2} (\sigma_r + \sigma_\theta) \right] \quad (4.80)$$

To calculate the value of equivalent stress, use the Von Mises yielding condition for a three-dimensional stress system

$$\sigma_e = \frac{1}{\sqrt{2}} \sqrt{(\sigma_\theta - \sigma_r)^2 + (\sigma_r - \sigma_z)^2 + (\sigma_z - \sigma_\theta)^2} \quad (4.81)$$

When assume the tube is in a plane strain condition, $\dot{\varepsilon}_z = 0$, and equation 4.80 become:

$$\sigma_z = \frac{1}{2} (\sigma_r + \sigma_\theta) \quad (4.82)$$

Substituting equation 4.82 into equation 4.81, then the equivalent stress become:

$$\sigma_e = \frac{\sqrt{3}}{2} (\sigma_\theta - \sigma_r) \quad (4.83)$$

After substituting equation 4.82 and 4.83 into equation 4.78 and 4.79

$$\dot{\varepsilon}_\theta = -\dot{\varepsilon}_r = K \left[\frac{\sqrt{3}}{2} \right]^{n+1} (\sigma_\theta - \sigma_r)^n \quad (4.84)$$

Equation 4.84 is the radial and hoop strain rate, to find the radial and hoop strain multiply the equation with time. The equation become:

$$\dot{\varepsilon}_\theta = -\dot{\varepsilon}_r = K \left[\frac{\sqrt{3}}{2} \right]^{n+1} (\sigma_\theta - \sigma_r)^n \times t \quad (4.85)$$

To determine the magnitude of σ_θ and σ_r , consider equation 4.85 and assumption ii, which says the direction of principal stress is the same as strain, based on this consideration substituting equation 4.85 in to equation 4.35, the equation in the jth layer (oxide and metal) become:

$$u = \frac{C_{j1}}{r}, \quad (\sigma_\theta - \sigma_r)^n = \frac{C_{j1}^n}{r^2} \quad \text{and} \quad \sigma_r = -\frac{n}{2} C_{j1} r^{-2/n} + C_{j2} \quad (4.86)$$

The constant value of C_1 and C_2 determined from the boundary conditions. Due to the increase of steam side oxide scale the thickness of the metal tube decreases through time.

$$\sigma_{ox,r}(r = a) = -P_i \quad \text{and} \quad \sigma_{met,r}(r = c) = -P_o$$

$$\sigma_{ox,r}(r = b) = \sigma_{met,r}(r = b)$$

$$u_{ox} = u_{met} \text{ at } r = b$$

After substituting the boundary conditions into radial stress of creep, the equation become:

$$-P_i = -\frac{n_{ox}}{2} C_{11} a^{-2/n_{ox}} + C_{12}$$

$$-P_o = -\frac{n_{met}}{2} C_{21} c^{-2/n_{met}} + C_{22}$$

$$-\frac{n_{ox}}{2} C_{11} b^{-2/n_{ox}} + C_{12} = -\frac{n_{met}}{2} C_{21} b^{-2/n_{met}} + C_{22}$$

$$\frac{C_{12}}{b} = \frac{C_{21}}{b}$$

After applying the boundary condition, the above summarized equation become in matrix form for easy calculation of the integration constant

$$\begin{bmatrix} k_{11} & 1 & 0 & 0 \\ 0 & 0 & k_{23} & 1 \\ k_{31} & 1 & k_{33} & -1 \\ 0 & k_{42} & k_{43} & 0 \end{bmatrix} \begin{Bmatrix} C_{11} \\ C_{12} \\ C_{21} \\ C_{22} \end{Bmatrix} = \begin{bmatrix} B_1 \\ B_2 \\ B_3 \\ B_4 \end{bmatrix} \quad (4.87)$$

Where

$$k_{11} = -\frac{n_{ox}}{2} a^{-2/n_{ox}}, \quad k_{23} = -\frac{n_{met}}{2} c^{-2/n_{met}}, \quad k_{31} = -\frac{n_{ox}}{2} b^{-2/n_{ox}}$$

$$k_{33} = \frac{n_{met}}{2} b^{-2/n_{met}}, \quad k_{42} = \frac{1}{b}, \quad k_{43} = \frac{-1}{b}$$

$$B_1 = -25000, B_2 = -100000, \quad B_3 = 0, \quad B_4 = 0$$

After the integration constant is obtained from the inverse of matrix or from equation 4.87, substitute into equation 4.86 to get the creep stress.

Based on the time-hardening rule, the creep rate is primarily governed by how long the material has been exposed time at the particular temperature involved, regardless of stress history. The creep strain formula become:

$$\dot{\varepsilon}_r^c = \frac{3}{4} K \sigma_e^{n-1} (\sigma_r - \sigma_\theta) t^{1-q} \quad (4.88)$$

$$\dot{\varepsilon}_\theta^c = \frac{3}{4} K \sigma_e^{n-1} (\sigma_\theta - \sigma_r) t^{1-q} \quad (4.89)$$

The creep properties and other important parameters for creep analysis is listed in Table A-6.

This analytical equation computed by python code, the code is found under Appendix B.4 (Python code for Creep stress and strain rate). All the required parameters with their value is listed their.

4.5.1 Predict creep rupture time

As a result, the boiler tube's remaining life needs to be frequently evaluated for safer and better boiler performance because the superheater material of T92 alloy steel susceptible to creep when it operates at high temperature and pressure for a long period of time. Therefore, it is important to evaluate the progressing of creep. There is a lot of techniques available for life prediction or evaluate the creep progress of superheater tubes. The most commons are estimate creep life based on the history of temperature and stress operating

on the tubes, extrapolation of parameters, microstructural studies, Distractive and Non-Destructive Oxide scale thickness measurements or test, and hardness measurement[75].

The Larson–Miller parameter method based on creep damage life evaluation is a time–temperature parameter (TTP) method. The method comprehensively considers the stress and temperature during the operation of the boiler superheater tube.

The Larson-Miller parameter of T92 alloy refers to the following equation[76]:

$$P(\sigma) = T(28.48 + \log t_r) \quad (4.90)$$

$$P(\sigma) = a + b \log \sigma + c(\log \sigma)^2 + d(\log \sigma)^3 \quad (4.91)$$

where T is the average tube temperature in Kelvin, t_r is the fracture time, $P(\sigma)$ is a stress function, and (a, b, c and d) are constants.

From the fitting result of LMP principal curve equation of T92 steel the constant values and equation 4.91 become[76,77]:

$$P(\sigma) = 70022.3 - 54631.2 \log \sigma + 28747.6(\log \sigma)^2 - 5585.2(\log \sigma)^3 \quad (4.92)$$

Selecting the appropriate stress equation of the boiler tube under a given operating condition is the crucial part to predict the creep rupture life. There are different equation and consideration to calculate the stress of the tube, some of them are maximum elastic hoop stress, minimum diameter stress and Tresca reference stress[31]. The most common and widely used representative stress of tubes under the given operating condition is maximum elastic hoop stress[31,78,79].

Based on different researches the maximum elastic stress of the tube due to oxide scale is calculated by considering only the thickness of metal tube, which means removing the oxide scale thickness and apply the internal pressure on the inner metal tube surface[78]. This stress value is greater than the stress value calculated in section 4.4.2 because in that section the thickness of oxide scale is included for elastic hoop stress calculation. The reason for selecting equation (4.93) for Elastic hoop stress calculation is to calculate the creep rupture time at worst condition or at high stress condition.

$$\sigma_{\theta,i} = P_s \left(\frac{r_O^2 + r_{ni}^2}{r_O^2 - r_{ni}^2} \right) - P_g \left(\frac{2r_O^2}{r_O^2 - r_{ni}^2} \right) \quad (4.93)$$

where P_s and P_g are steam pressure and gas pressure (MPa) respectively, r_O is outside radius (m), r_i initial inner tube radius (at oxide free condition) and r_{ni} is the variable

radius of oxide/metal substrate interface (m) shown in Figure 4.10 and 4.11 and the value of r_o is equal to the value of **c** and the value of r_{ni} is equal to the value of **b** on Table A-5. The value of r_{ni} calculated as follows:

$$r_{ni} = r_i + \delta_2 = r_i + \delta_x/2$$

The second way to calculate the creep rupture time or modeling of the creep life of the tube material is based on steady state creep rates with the Norton's Law of minimum creep strain rate relation, the rupture life expression can be written as[72]

$$t_r = \frac{1}{nK\sigma_e^n} \quad (4.94)$$

The value of inner, outer and oxide/metal interface radii is listed in Table A-5 and the value of n and K is listed in Table A-6.

4.6 Numerical (Finite Element) Method Simulation

The most popular technique for resolving issues with mathematics and engineering models is the numerical method. Numerous numerical approaches, including the finite difference method, finite element method, and boundary integral methods, have been almost solely used to solve solid mechanics-related problems. A complex system can be broken down into incredibly tiny units called elements using a numerical technique called finite element analysis.

By using the numerical analysis program ABAQUS/CAE, the finite element analysis is carried out. The Abaqus program suite implements finite element methods to unravel a range of engineering issues, from generally simple linear problems to the most challenging nonlinear situations. In addition to static and dynamic analysis, ABAQUS can simulate thermal and electrical problems, as well as acoustics, soil mechanics, piezoelectric analysis, fluid dynamics, and electromagnetic analysis.

4.6.1 Finite Element Simulation/Modeling Procedure

Step-by-step, the analysis proceeds from the part modeling to Visualization of the results is discussed in this section. Abaqus software allows any procedure or module to be performed without retaining its consequences. Heat transfer analysis and stress analysis are computed separately in this study. Therefore, each analysis has a different method for obtaining the final result. This section discusses each analysis' procedures.

1. Part Modeling

For heat transfer analysis the two-dimensional circular shell geometry is modeled for oxide part and metal part separately based on their dimensions. The dimensions are listed on Table A-1. The next step is created surfaces for both oxide and metal parts and name the surface inside and outside of metal and oxide. These surfaces use to connect the two parts shown in Figure 4.16(a). For thermo-mechanical stress and creep analysis Modeled arc (1/4 of the full circle), with the dimension of outer radius of the metal tube and inner radius of oxide part. After creating the model, create partition the face with the dimension of the oxide/metal interface. The model is shown in Figure 4.16(b). The dimensions needed for numerical simulation is listed under Table A-1 and A-5.

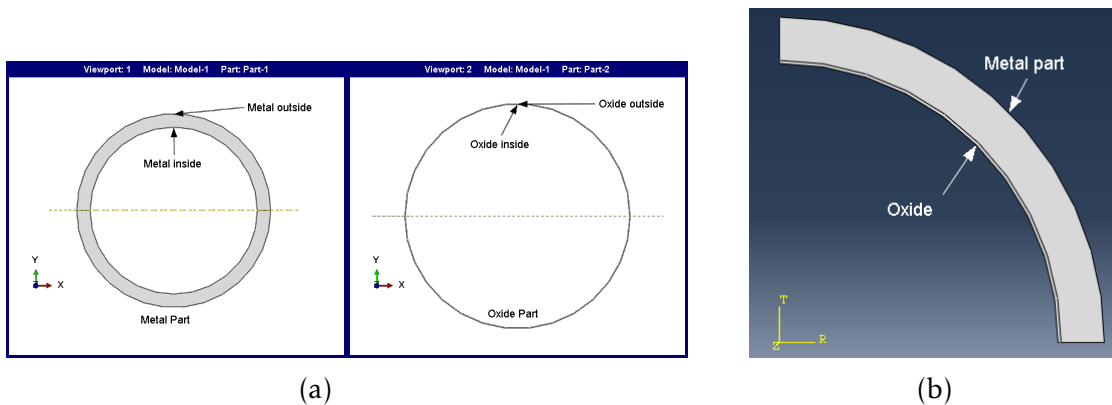


Figure 4.16: Two-dimensional part model boiler tube

2. Assign Material Property

From property module create two materials for both oxide and metal part. Then set the thermal conductivity value of both parts at different temperatures to analysis the heat transfer of boiler tube. After create the material property the next step is create Solid, Homogeneous section for each material. The final step in property module is assign those sections for each part. For stress analysis remove thermal conductivity and add the Elastic property (young's modulus and Poisson's ratio) for elastic stress analysis and when for thermal stress the thermal expansion coefficient is added for both parts beside to elastic property and when come to creep the plastic properties of creep those listed in Table A-6 is added. The material properties like thermal conductivity, young's modulus and Poisson's ratio are found under Table A-2, and the thermal expansion coefficient obtained from Figure A.1.

3. Assemble Module

The assembly module merges the modeled parts from the part module to form instances of parts and to position them properly based on the analysis type.

4. Step Module

The software's analysis types are ordered and selected in this section. A variety of procedures are available, such as heat transfer analysis, mechanical stress analysis, electrical analysis, or the combination of the listed procedures either jointly or separately.

For Heat Transfer Analysis, create the first step of heat transfer procedure at steady state condition, which means the increment size is doesn't affect the output result. For Stress Analysis, for this analysis create the general, static procedure to analysis, the stress and the strain of the tube and for creep analysis create the Visco procedure for the first step and adjust the working hour of the boiler tube.

5. Interaction Module

Tie contact constrain is used for heat transfer analysis to connect the oxide and metal surface/part, in Tie contact the master type is inside surface of metal part and the slave type is outside surface of the oxide part. For Surface Film Condition: select the surface film condition for the steam side and the convection coefficient of steam and its sink temperature then do the same on flue gas side, select the outer surface of metal part and put the convection coefficient of gas and its sink temperature.

6. Load Module

For heat transfer we assume there is no internal load and for stress analysis first create displacement/rotation type boundary condition for initial step based on plane stress assumption. The next step is applied internal and external pressure load 25MPa and 0.1Mpa respectively on the inner surface of oxide part and the outside surface of metal part respectively. For thermal stress analysis, beside the first two load module procedures, the last one is creating predefined field, which changes the temperature value of the oxide and metal parts.

7. Mesh Module

For Heat Transfer: The mesh size for metal part is 1mm and the mesh size for oxide part is 0.5mm. For heat transfer analysis this mesh size gave better result and close to the analytical result.

For Stress and creep Analysis: Based on plane strain assumption of the tube, select the plane strain element type and quadrilateral element shape is selected. The size of the mesh in Finite Element Analysis affects how accurate the results are. When compared to modals with large element sizes, finite modals with small element sizes produce excellent accuracy. Selection of the appropriate element size is crucial to increase the accuracy of the result. The model of oxide scaled boiler tube with 242.82 μm oxide scale thickness is taken as a sample. The value of Elastic von Mises is the value to compare the mesh

global size between 0.2mm, 0.1mm, 0.05mm, and 0.025mm. The value of Von Mises stress, computational time taken, number of node and element at different element size is listed/summarized in Table 4.4.

Table 4.4: Mesh convergency result

	0.2mm	0.1mm	0.05mm	0.025mm
No nodes	3458	13394	53576	211554
No elements	3258	12996	52779	209960
Computational time (sec)	46	100	225	324
Von Mises stress (MPa)	161.5	161.9	162.1	162.1

When the value of mesh size become smaller the value of von Mises stress converges or become the constant value. The von mises stress at 0.05mm and 0.025 mm global size become the same but the computational time is higher compare to other global mesh sizes. The maximum analytical von mises stress is 174MPa from the above four different mesh element size, the value of von mises stress is closer to the analytical value at mesh size of 0.025mm. Based on the above result 0.025mm mesh size is selected for this research.

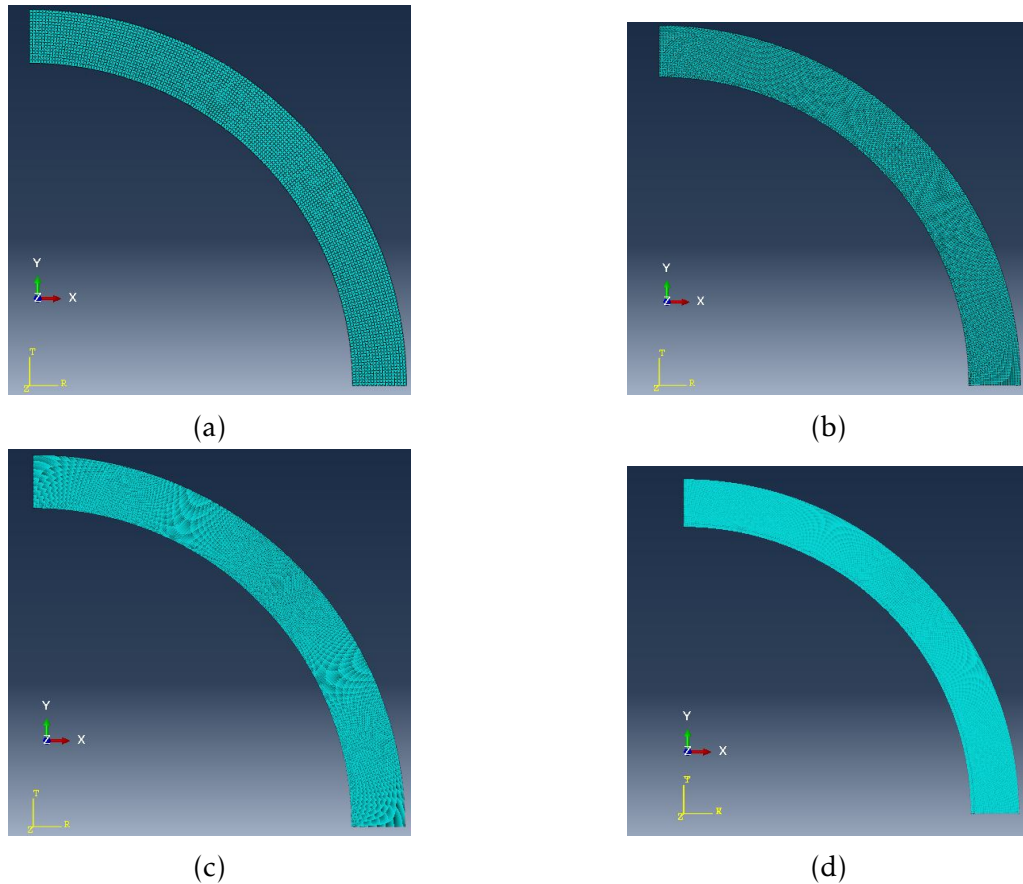


Figure 4.17: Quadrilateral mesh surface of the oxide scale boiler tube at $242.82 \mu\text{m}$ of oxide scale thickness at different mesh size (a) 0.2 mm, (b) 0.1mm, (c) 0.05mm, and (d) 0.025mm

8. Post Processing/ Job module

Part modeling, property modules, meshing, etc. are inputs for the analysis and lead to the analysis being processed. In the job module, all data is checked and submitted for analysis so that the results can be visualized in the real arena. By using the job module, you can analyze the part, submit it, and monitor progress.

Following the completion of the work, the Abaqus Standard allows visualization of the results logged in the history output request module and the field output request module. Thus, in field output requests, parameters are visualized using contours, lines, graphs, un-deformed and deformed shapes, etc., which allows extracting results in any field of the module for each parameter requested previously.

5. RESULT AND DISCUSSION

This chapter classified into three categories based on the result obtained from analytical and numerical analysis, those are estimation/prediction of oxide growth, stress analysis due to oxide scale and creep analysis at different oxide scale thickness from the prediction.

5.1 Oxidation kinetics

The result of the oxidation kinetics which means the oxide thickness is calculated by analytical calculation using Larson miller parameter.

5.1.1 Estimation of oxide scale growth at different temperature

The value of h_g at different temperature obtained by using the given data in Table A-4 and computing the data by using Equation 4.29-4.31. The value of h_g is shown below in tabulated form.

Table 5.1: The value of h_g at different temperature

Temperature (°C)	800	900	1000
h_g (W/m ² K)	220.03	227.78	234.64

The value of h_s at different temperature obtained by using the given data in Table A-3 and computing the data by using Equation 4.26-4.28. The value of h_s at pure oxide condition, when δ_1 equal to zero is shown below in tabulated form.

Table 5.2: The value of h_s at different temperature and free from oxide scale condition

Temperature (°C)	500	550	600	650	700
h_s (W/m ² K)	3338.48	3072.58	2952.53	2901.45	2887.18

The value of h_s is changed when the value of δ_1 is changed in each iterative or step at different steam and flue gas temperature. The new value of h_s is shown in Table 5.3-5.8.

Numerical simulation Result

The numerical simulation result of heat transfer is computed by ABAQUS software, by following the finite element simulation/ modeling procedure under section 4.6.1. To obtain the temperature value of inner, outer and oxide/metal interface layer of the boiler

tube at different steam and flue gas temperature 42 models is needed. To show all the simulation/visualization is take a lot of pages so, take one as sample and the rest of the result is listed in table. Figure 5.1 shows the simulation result of temperature distribution of boiler tube at step 6 in Table5.5.

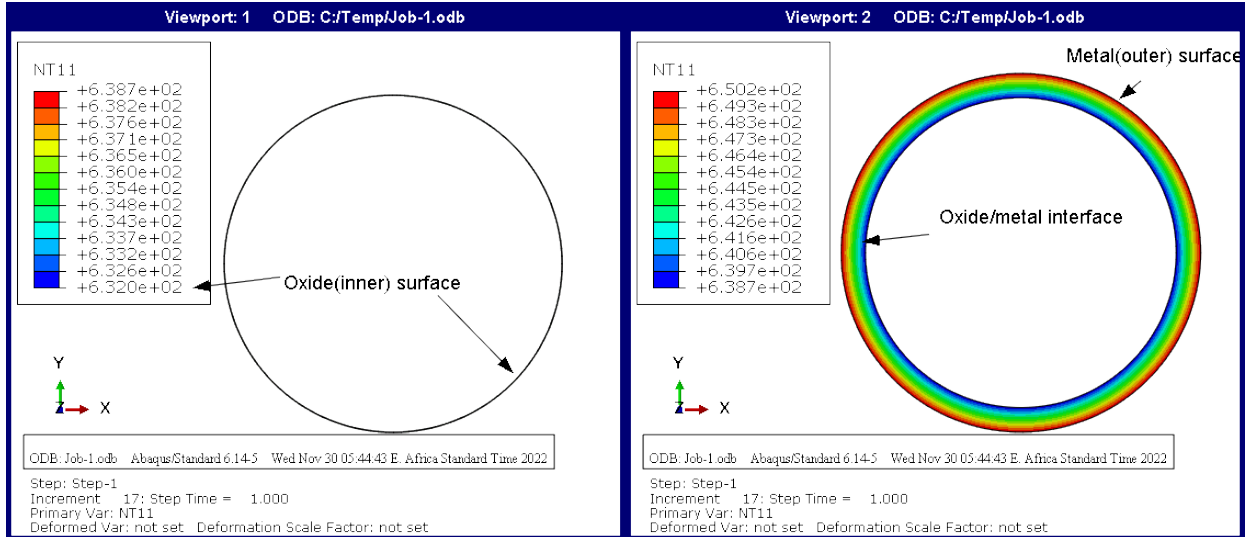


Figure 5.1: Simulation result of Temperature distribution at 60.0686 μm of oxide scale thickness

The prediction of steam side oxide scale thickness at different flue gas and steam temperature over a service hour are calculated by following the iterative procedure described in Figure 3.2. The value (result) of $h_s, r_i, r_x, \delta_x,$ and T_{ave} in each iterative steps is listed in Table 5.3-5.8.

Table 5.3: Oxide growth at each iterative step when $h_g = 220.03, T_s = 600^\circ\text{C}$ and $T_g = 800^\circ\text{C}$

Step	$r_o(m)$	$r_{ni}(m)$	$r_x(m)$	$\delta_x(\mu\text{m})$	h_s	$T_1(^{\circ}\text{C})$	$T_3(^{\circ}\text{C})$	$T_2(^{\circ}\text{C})$	$T_{ave}(^{\circ}\text{C})$
Initial	0.0254	0.0219	-	0	2952.532	621	615.5	-	615.5
1	0.0254	0.021906	0.021894	11.0917	2953.879	621.5	615.3	615.9	615.6
2	0.0254	0.021909	0.021891	18.2911	2954.753	621.8	615.3	616.2	615.75
3	0.0254	0.021912	0.021888	23.5078	2955.387	622	615.2	616.5	615.85
4	0.0254	0.021914	0.021886	27.8225	2955.911	622.2	615.2	616.7	615.95
5	0.0254	0.021916	0.021884	31.5919	2956.369	622.4	615.2	616.9	616.05
6	0.0254	0.021917	0.021883	34.9862	2956.782	622.5	615.2	617	616.1
7	0.0254	0.021919	0.021881	38.0977	2957.16				

Table 5.4: Oxide growth at each iterative step when $h_g = 227.78, T_s = 600^\circ\text{C}$ and $T_g = 900^\circ\text{C}$

Step	$r_o(m)$	$r_{ni}(m)$	$r_x(m)$	$\delta_x(\mu m)$	h_s	$T_1(^{\circ}\text{C})$	$T_3(^{\circ}\text{C})$	$T_2(^{\circ}\text{C})$	$T_{ave}(^{\circ}\text{C})$
Initial	0.0254	0.0219	-	0	2952.532	632.5	623.9	-	623.9
1	0.0254	0.021907	0.021893	14.1338	2954.248	633.4	623.7	624.8	624.25
2	0.0254	0.021912	0.021888	23.4637	2955.381	634.1	623.6	625.6	624.6
3	0.0254	0.021915	0.021885	30.2876	2956.211	634.7	623.6	626.2	624.9
4	0.0254	0.021918	0.021882	35.9771	2956.903	634.9	623.6	626.4	625
5	0.0254	0.02192	0.02188	40.9547	2957.508	635.3	623.5	626.8	625.15
6	0.0254	0.021923	0.021877	45.4488	2958.055	635.7	623.5	627.3	625.4
7	0.0254	0.021925	0.021875	49.5977	2958.560				

Table 5.5: Oxide growth at each iterative step when $h_g = 234.64, T_s = 600^\circ\text{C}$ and $T_g = 1000^\circ\text{C}$

Step	$r_o(m)$	$r_{ni}(m)$	$r_x(m)$	$\delta_x(\mu m)$	h_s	$T_1(^{\circ}\text{C})$	$T_3(^{\circ}\text{C})$	$T_2(^{\circ}\text{C})$	$T_{ave}(^{\circ}\text{C})$
Initial	0.0254	0.0219	-	0	2952.53	644.5	632.8	-	632.8
1	0.0254	0.021909	0.021891	18.2709	2954.75	646.1	632.4	634.4	633.4
2	0.0254	0.021915	0.021885	30.5430	2956.24	647.3	632.3	635.7	634
3	0.0254	0.02192	0.02188	39.6184	2957.32	648.3	632.2	636.7	634.45
4	0.0254	0.021924	0.021876	47.2356	2958.27	649	632.1	637.5	634.8
5	0.0254	0.021927	0.021873	53.9609	2959.09	649.6	632.1	638.1	635.1
6	0.0254	0.02193	0.02187	60.0686	2959.83	650.2	632	638.7	635.35
7	0.0254	0.021933	0.021867	65.7127	2960.52	650.7	631.9	639.3	635.6

Figure 5.2 shows the oxide scale thickness at three different flue gas temperatures at 600°C of steam temperature. After 1000 working hour of boiler tube the oxide scale thickness become $38.1 \mu\text{m}$, $49.6 \mu\text{m}$, and $65.7 \mu\text{m}$ at 800°C , 900°C , and 1000°C respectively. The oxide scale thickness at 900°C is more than by 30.2% of the oxide scale thickness of 800°C and the oxide scale thickness at 1000°C is more than by 32.46% of the oxide scale thickness of 900°C .

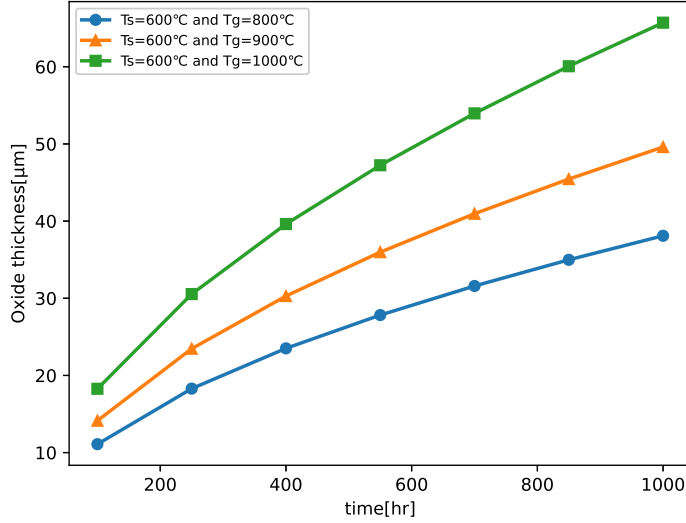


Figure 5.2: Summary of oxide scale thickness as a function of time with the steam temperature of 600°C for different flue gas temperature

Table 5.6: Oxide growth at each iterative step when $h_g = 220.03$, $T_s = 650^\circ\text{C}$ and $T_g = 800^\circ\text{C}$

Step	$r_o(m)$	$r_{ni}(m)$	$r_x(m)$	$\delta_x(\mu m)$	h_s	$T_1(^\circ\text{C})$	$T_3(^\circ\text{C})$	$T_2(^\circ\text{C})$	$T_{ave}(^\circ\text{C})$
Initial	0.0254	0.0219	-	0	2901.45	666	661.8	-	661.8
1	0.0254	0.021921	0.021879	42.15902	2906.48	667.3	661.6	663.2	662.4
2	0.0254	0.021936	0.021864	71.3967	2909.98	668.3	661.5	664.2	662.85
3	0.0254	0.021947	0.021853	93.1556	2912.59	669	661.4	665	663.2
4	0.0254	0.021956	0.021844	111.4781	2914.79	669.6	661.4	665.6	663.5
5	0.0254	0.021964	0.021836	127.7033	2916.74	670.1	661.4	666.1	663.75
6	0.0254	0.021971	0.021829	142.4672	2918.51	670.6	661.3	666.6	663.95
7	0.0254	0.021978	0.021822	156.1288	2920.16				

Table 5.7: Oxide growth at each iterative step when $h_g = 227.78$, $T_s = 650^\circ\text{C}$ and $T_g = 900^\circ\text{C}$

Step	$r_o(m)$	$r_{ni}(m)$	$r_x(m)$	$\delta_x(\mu m)$	h_s	$T_1(^\circ\text{C})$	$T_3(^\circ\text{C})$	$T_2(^\circ\text{C})$	$T_{ave}(^\circ\text{C})$
Initial	0.0254	0.0219	-	0	2901.45	677.5	670.3	-	670.3
1	0.0254	0.021927	0.021873	53.8611	2907.88	680.4	669.8	673.4	671.6
2	0.0254	0.021946	0.021854	92.3613	2912.49	682.5	669.7	675.6	672.65
3	0.0254	0.021961	0.021839	121.6396	2916.01	684.2	669.5	677.4	673.45
4	0.0254	0.021973	0.021827	146.6885	2919.02	685.5	669.4	678.7	674.05
5	0.0254	0.021985	0.021815	169.1109	2921.72	686.9	669.3	680.1	674.7
6	0.0254	0.021995	0.021805	189.7933	2924.22	687.9	669.2	681.2	675.2
7	0.0254	0.022005	0.021795	209.1306	2926.55				

Table 5.8: Oxide growth at each iterative step when $h_g = 234.64$, $T_s = 650^\circ\text{C}$ and $T_g = 1000^\circ\text{C}$

Step	$r_o(m)$	$r_{ni}(m)$	$r_x(m)$	$\delta_x(\mu m)$	h_s	$T_1(^{\circ}\text{C})$	$T_3(^{\circ}\text{C})$	$T_2(^{\circ}\text{C})$	$T_{ave}(^{\circ}\text{C})$
Initial	0.0254	0.0219	-	0	2901.45	689.5	679.1	-	679.1
1	0.0254	0.021935	0.021865	69.4051	2909.74	695	678.4	684.9	681.65
2	0.0254	0.021961	0.021839	121.4022	2915.98	699.1	678	689.3	683.65
3	0.0254	0.021981	0.021819	162.2515	2920.89	702.2	677.8	692.6	685.2
4	0.0254	0.021999	0.021801	198.0944	2925.22	705	677.5	695.5	686.5
5	0.0254	0.022015	0.021785	230.9348	2929.19	707.4	677.3	698	687.65
6	0.0254	0.022031	0.021769	261.7428	2932.92	709.7	677.1	700.5	688.8
7	0.0254	0.022046	0.021754	291.1690	2936.49				

Figure 5.3 shows the summary of oxide scale thickness growth at different flue gas temperature, based on the figure the increment of oxide scale is direct relation to the increment of flue gas temperature. After 1000 working hour of boiler tube with 650°C of steam temperature the oxide scale thickness become $156.1\mu\text{m}$, $209.1\mu\text{m}$, and $291.2\mu\text{m}$ at 800°C , 900°C , and 1000°C respectively. The oxide scale thickness at 900°C is more than by 33.9% of the oxide scale thickness of 800°C and the oxide scale thickness at 1000°C is more than by 39.3% of the oxide scale thickness of 900°C .

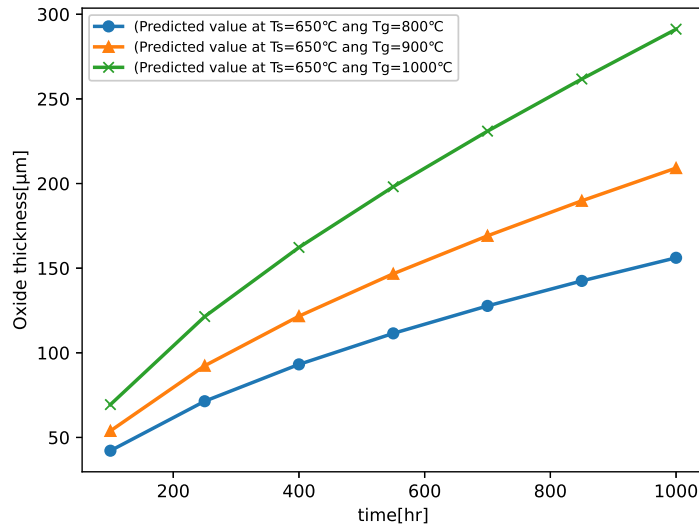


Figure 5.3: Summary of oxide scale thickness as a function of time with the steam temperature of 650°C for different flue gas temperature

5.1.2 Compare the effect of steam and flue gas temperature

To analyze the effect of change of the temperatures for the growth of oxide scale thickness, the crucial step is summarizing the result in tabular form.

Table 5.9: summary of the effect of different temperature for the growth of oxide scale thickness

Step	$\delta_x (\mu\text{m})$ at $T_g = 800^\circ\text{C}$		$\delta_x (\mu\text{m})$ at $T_g = 900^\circ\text{C}$		$\delta_x (\mu\text{m})$ at $T_g = 1000^\circ\text{C}$	
	$T_s = 600^\circ\text{C}$	$T_s = 650^\circ\text{C}$	$T_s = 600^\circ\text{C}$	$T_s = 650^\circ\text{C}$	$T_s = 600^\circ\text{C}$	$T_s = 650^\circ\text{C}$
1	11.0917	42.15902	14.1338	53.8611	18.2709	69.4051
2	18.2911	71.3967	23.4637	92.3613	30.5430	121.4022
3	23.5078	93.1556	30.2876	121.6396	39.6184	162.2515
4	27.8225	111.4781	35.9771	146.6885	47.2356	198.0944
5	31.5919	127.7033	40.9547	169.1109	53.9609	230.9348
6	34.9862	142.4672	45.4488	189.7933	60.0686	261.7428
7	38.0977	156.1288	49.5977	209.1306	65.7127	291.1690

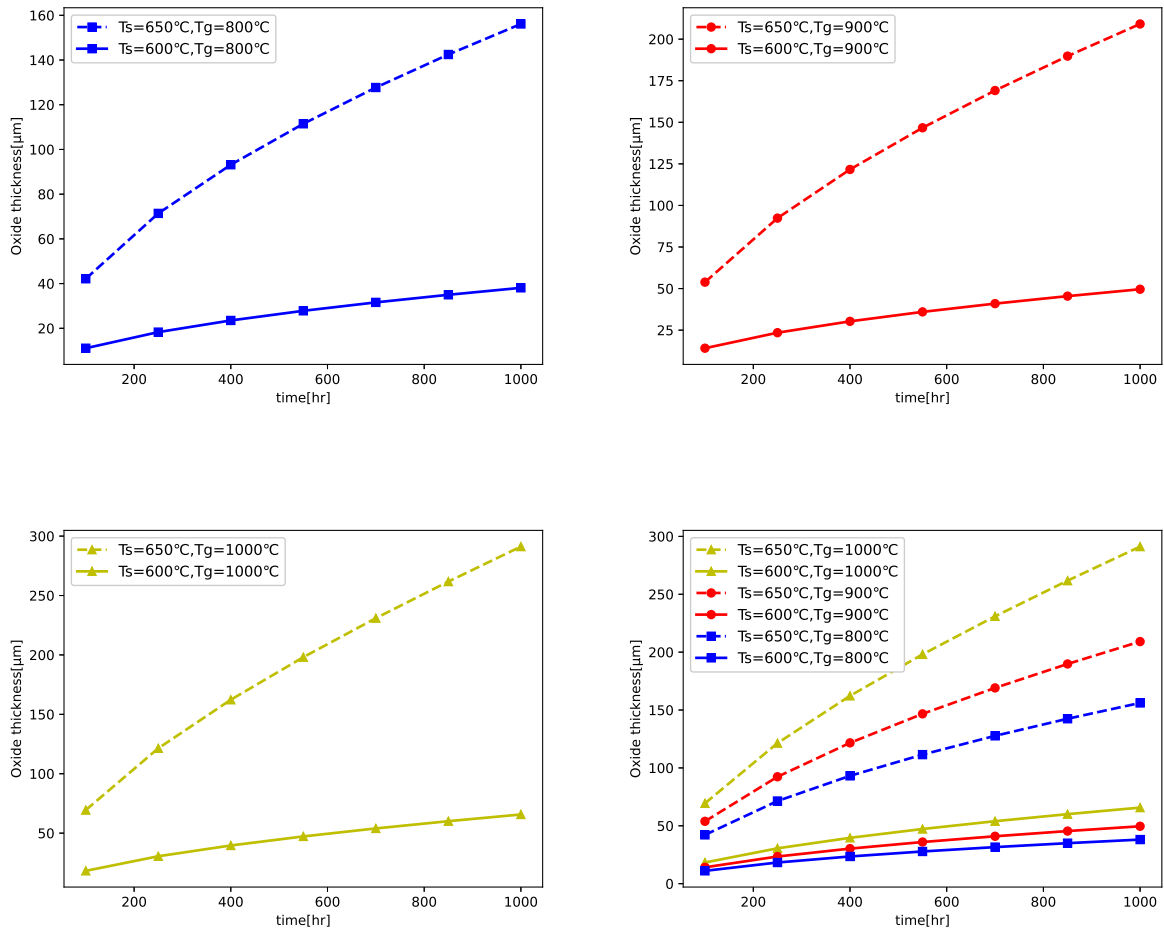


Figure 5.4: Comparison the effect of flue gas and steam temperature for the growth of oxide scale

The difference between the oxide scale thickness after 1000 working hour of the boiler

tube at 600°C and 650°C of steam temperature become around 118 μm , 159.5 μm , and 225.4 μm at 800°C, 900°C, and 1000°C of flue gas temperature respectively. The change of flue gas temperature from 800°C to 900°C at 600°C and 650°C of steam temperature increase the oxide scale thickness with 11.5 μm and 53 μm respectively, and the change from 900°C to 1000°C at 600°C and 650°C of steam temperature increase the oxide scale thickness with 16.1 μm and 82 μm respectively.

The oxide scale growth is more affected by the increase of steam side temperature than flue gas temperature. The small change of steam temperature rapid the growth of oxide scale thickness than the big change of flue gas temperature.

Overheating of the boiler tube

Due to the increase of oxide scale the temperature difference between metal tube outer surface and metal-oxide interface surface decreased. This shows the metal tube become hot due to increasing of oxide scale. Figure 5.5 shows the relevant surface temperature value of boiler tube at different oxide scale. The data of the figure obtained from the operation of boiler tube at 600°C of steam temperature and 1000°C of flue gas temperature for operating hour of 2000, 4000, 6000, 8000 and 10,000 hrs. Based on this figure the difference between the temperature of metal tube surface and oxide-metal surface is decreasing due to increasing of oxide scale. At 96.1 μm the changing temperature is 11.3°C and at 241.82 μm the changing temperature is 10.6°C. It means due to the increasing of oxide scale the metal tube become over heated. The change of temperature between oxide-metal interface and inner oxide surface is increasing due to increasing of oxide scale. At 96.1 μm the changing temperature is 10.6°C and at 241.82 μm the changing temperature is 25.8°C. It explains the transfer rate of the temperature from oxide-metal surface to oxide surface is decreased because of increasing of oxide scale, and the steam is not well heated due to the blockage of oxide scale. This reduces the efficiency and life of boiler tube.

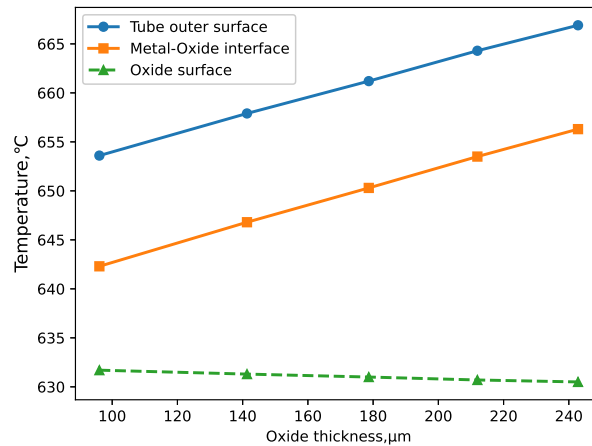


Figure 5.5: Temperature at relevant surfaces

Validation/verification with literature data

In this study the predicted steam side oxide scale due to different steam and flue gas temperature is validated by comparing to the literature data. Based on the literature and experimental data the oxide scale thickness at 600°C is around 80-110 μm it can be seen from Figure 5.6. The specimen for steam oxidation test experiment is used 15mm \times 15mm, with 6mm thickness of T92 machined steel, the oxide scale thickness is measured up to 1000hr[42]. Based on the experimental data the oxide scale is around 89 μm . The estimated/calculated oxide scale thickness with steam temperature of 600°C and flue gas temperature of 1000°C lower by the value of 23.3 μm from the experimented value respectively.

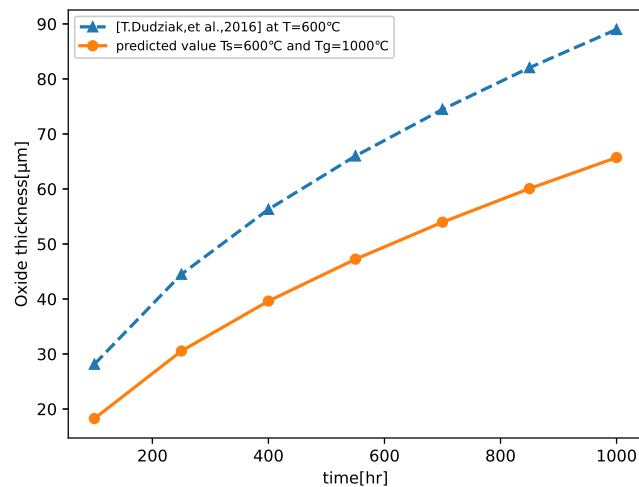


Figure 5.6: The experimental and calculated value of oxide scale thickness at 600°C of steam temperature after 1000hr exposure

The calculated/predicted value of oxide scale at 650°C of steam temperature and at 1000°C flue gas temperature is more approximate to the experimental value. After 1000 working hour the oxide scale become around 267 μm [56]. At this working time the calculated/predicted value is greater than the literature (experimental) value only by 8%. The tube used for oxide scale thickness have the outer diameter and tube thickness of 51 and 11.8mm, respectively and the tube exposed to 650°C of steam temperature and oxyfuel flue gas for 1000hr[55]. The experimental result shows the oxide scale become around 208 μm . The predicted/calculated value of oxide scale thickness at 650°C of steam temperature and 900°C of flue gas temperature become 209 μm . The two results have close value and only having deviation of 1 μm , it shows in Figure 5.7.

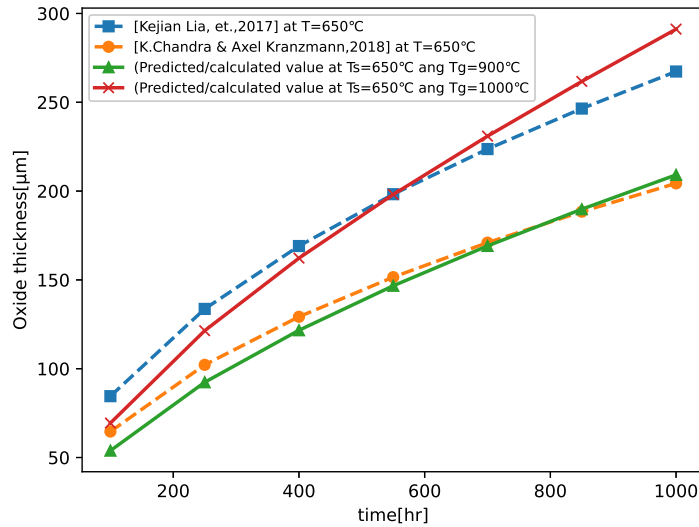


Figure 5.7: The experimental and calculated value of oxide scale thickness at 650°C of steam temperature after 1000hr exposure

The different factors employed, such as the dimension, mass flow rate, steam pressure, flue gas temperature, and other parameters, may be the cause of the discrepancy between the experimental and calculated/predicted value of oxide scale thickness. The experimental data's and the calculated/predicted value of oxide scale thickness have identical parabolic shape graph, and they both comply with the parabolic equation of oxide kinetics.

5.2 Result of stress and strain

Analytical and numerical methods are used to compute the stress and strain on the boiler tube with oxide scale. The analytical stress equation of an oxide-scaled boiler tube is

explored in Chapter 4.4, where in this section the numerical (Finite Element Simulation) and analytical results are presented and analyzed.

Simulation Result

The process of building a model of an existing or projected system in order to pinpoint and comprehend the variables that affect it and forecast its behavior is referred to as simulation. The simulation comes from ABAQUS software. The elastic and thermal stress and strain of oxide scale boiler tube for different oxide scale is simulated and the simulation result is summarized in tabular form in next section. Only the simulation results and visualization of the elastic stress and strain on the metal and oxide parts at $242.82 \mu\text{m}$ oxide scale thickness are shown in this section as an example or sample.

Before plots the contours of the deformable shape, creating the cylindrical coordinate is necessary part to obtain the accurate value of the stress and the strain, otherwise the result is different. After selecting a cylindrical coordinate, the next step is from result option and user specified select the created cylindrical coordinate. After that the deformation result become meaningful.

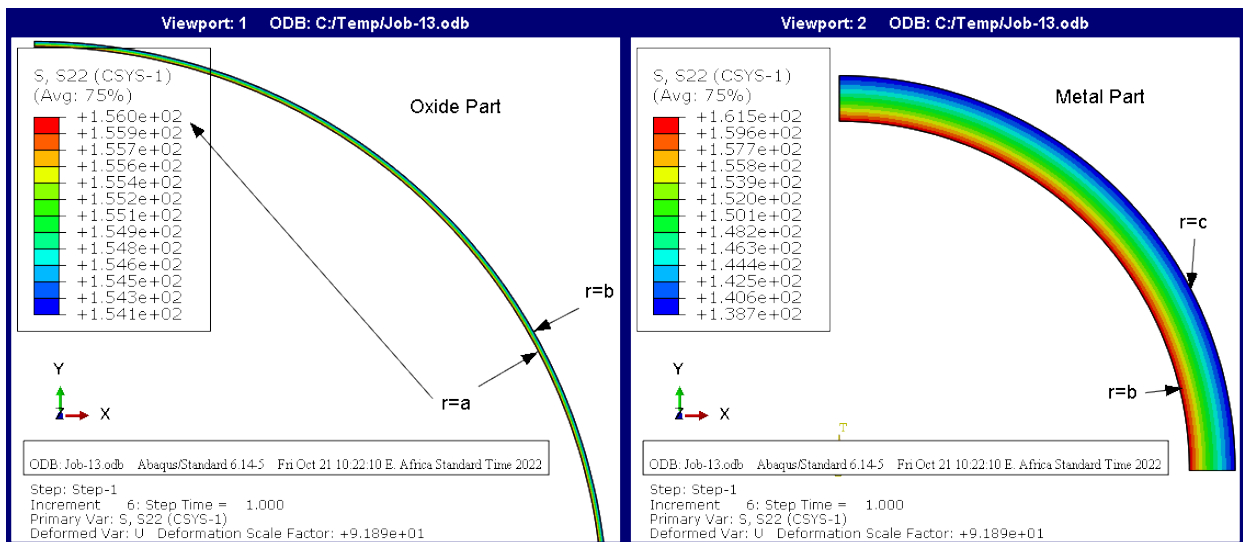


Figure 5.8: Simulation result of Elastic hoop stress at $242.82 \mu\text{m}$ of oxide scale thickness

The simulation output for the oxide and metal parts of the hoop stress created at 25 MPa and 0.1 MPa steam side and gas side pressure load, respectively, is shown in Figure 5.8. The place where stress is greatest is on the opposite side of the radial stress. In accordance with the diagram, the maximum hoop stress for the oxide part occurred at $r=a$, which refers to the inner part of the oxide or the surface that comes into contact with the steam pressure and temperature, and the maximum hoop stress for the metal part occurred at $r=b$, which refers to the surface that comes into contact with the oxide/metal part. The maximum hoop stress, determined by the modeling results, is 161.5MPa.

The simulation result for hoop strain, also known as tensile strain, of an oxide-scaled boiler tube is shown in Figure 5.9. The greatest hoop strain, which occurred at the inside surface or at the surface in contact with steam pressure and temperature, is 1.269×10^{-3} .

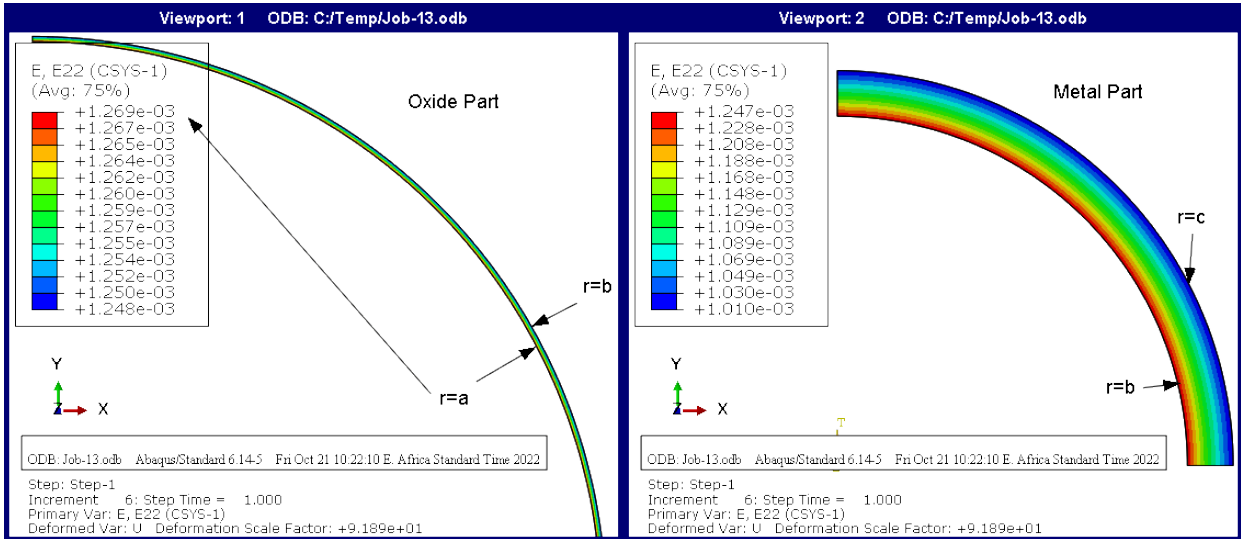


Figure 5.9: Simulation result of Elastic hoop strain at 242.82 μm of oxide scale thickness

5.2.1 Result of Elastic stress and strain at different oxide scale

Analytical and numerical methods are used to determine the radial and hoop stress of an oxide scale boiler tube at various steam side oxide scales. The result is listed separately in oxide and metal parts at each radial distance.

Table 5.10: Summary of analytical and numerical result of elastic radial stress at different oxide scale

Oxide thickness (μm)	Elastic Radial stress (MPa)					
	Oxide part			Metal part		
	Position	Analytical	Numerical	Position	Analytical	Numerical
96.0690	r=a	-25	-24.95	r=b	-24.192	-24.14
	r=b	-24.192	-24.25	r=c	-0.1	-0.2344
141.3280	r=a	-25	-24.90	r=b	-23.814	-23.71
	r=b	-23.814	-23.92	r=c	-0.1	-0.1684
178.6649	r=a	-25	-24.89	r=b	-23.522	-23.42
	r=b	-23.522	-23.63	r=c	-0.1	-0.1681
211.9621	r=a	-25	-24.95	r=b	-23.249	-23.21
	r=b	-23.249	-23.31	r=c	-0.1	-0.1347
242.8193	r=a	-25	-24.95	r=b	-23.011	-22.97
	r=b	-23.011	-23.07	r=c	-0.1	-0.134

Table 5.11: Summary of analytical and numerical result of elastic hoop stress at different oxide scale

Elastic Hoop stress (MPa)						
Oxide thickness (μm)	Oxide part			Metal part		
	Position	Analytical	Numerical	Position	Analytical	Numerical
96.0690	r=a	160.122	159.1	r=b	166.003	166
	r=b	159.314	158.4	r=c	141.911	142
141.3280	r=a	159.116	158.1	r=b	164.559	164.5
	r=b	157.929	157.1	r=c	140.846	140.95
178.6649	r=a	158.336	157.3	r=b	163.433	163.4
	r=b	156.858	156.1	r=c	140.021	140.1
211.9621	r=a	157.607	156.7	r=b	162.398	162.4
	r=b	155.856	155	r=c	139.249	139.3
242.8193	r=a	156.97	156	r=b	161.485	161.5
	r=b	154.979	154.1	r=c	138.574	138.7

Figure 5.10 shows the Elastic radial and hoop stress through the radial position (through the total thickness including the tube and oxide thickness) at different oxide scale thickness. Figure 5.10(a) is a plot of radial stress through the thickness, the radial stress is increase from the inside of the oxide part to outer surface of the tube wall. Based on the calculation and the simulation result the outer surface of the tube has maximum elastic radial stress (compression stress) around -0.13MPa. Figure 5.10(b) is a plot of Elastic hoop stress through the thickness (radial position), the hoop stress (Tensile stress) in both oxide and metal parts decrease through the radial position. The maximum elastic hoop stress is found at the metal/oxide interface surface. In this surface the stress of metal part is greater than the stress of oxide part, the maximum stress is around 160MPa.

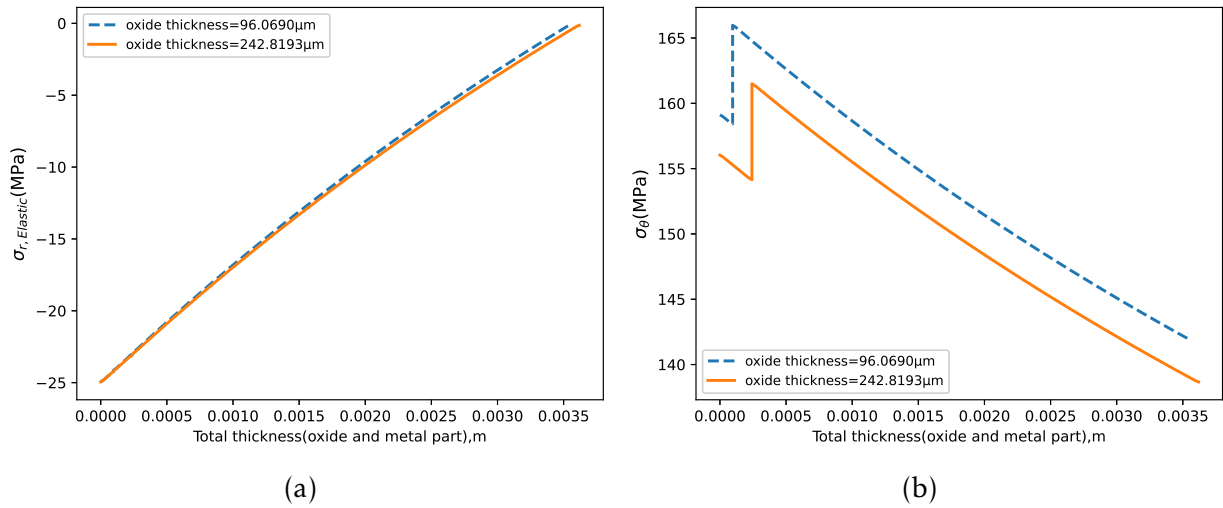


Figure 5.10: Numerical results of elastic radial and hoop stress vs total thickness of tube

Table 5.12: Summary of analytical and numerical result of elastic radial strain at different oxide scale

Elastic Radial Strain (10^{-4})						
Oxide thickness (μm)	Oxide part			Metal part		
	Position	Analytical	Numerical	Position	Analytical	Numerical
96.0690	r=a	-5.953	-6.865	r=b	-6.006	-6.936
	r=b	-5.866	-6.789	r=c	-3.413	-4.439
141.3280	r=a	-5.928	-6.829	r=b	-5.982	-6.859
	r=b	-5.801	-6.723	r=c	-3.388	-4.410
178.6649	r=a	-5.909	-6.804	r=b	-5.964	-6.803
	r=b	-5.751	-6.669	r=c	-3.369	-4.384
211.9621	r=a	-5.892	-6.788	r=b	-5.946	-6.756
	r=b	-5.704	-6.612	r=c	-3.35	-4.357
242.8193	r=a	-5.877	-6.769	r=b	-5.931	-6.711
	r=b	-5.663	-6.566	r=c	-3.334	-4.336

Table 5.13: Summary of analytical and numerical result of elastic hoop strain at different oxide scale

Oxide thickness (μm)	Elastic Hoop Strain (10^{-3})					
	Oxide part			Metal part		
	Position	Analytical	Numerical	Position	Analytical	Numerical
96.0690	r=a	1.395	1.292	r=b	1.395	1.284
	r=b	1.386	1.285	r=c	1.136	1.034
141.3280	r=a	1.386	1.284	r=b	1.386	1.272
	r=b	1.373	1.274	r=c	1.127	1.027
178.6649	r=a	1.379	1.278	r=b	1.379	1.263
	r=b	1.364	1.265	r=c	1.120	1.021
211.9621	r=a	1.373	1.273	r=b	1.374	1.255
	r=b	1.355	1.256	r=c	1.114	1.015
242.8193	r=a	1.368	1.269	r=b	1.368	1.247
	r=b	1.347	1.248	r=c	1.108	1.010

Figure 5.11(a) shows the radial strain increased through the thickness, but the radial strain of oxide is greater than the radial strain of metal at oxide/metal interface. Based on the calculation and the simulation result the outer surface of the tube has maximum elastic radial strain (compression strain) around -4.336×10^{-3} . Figure 5.11(b) is a plot of Elastic hoop strain through the thickness radial position, the hoop strain (Tensile strain) in both oxide and metal parts decrease through the radial position. The maximum elastic hoop strain is found at the internal surface of oxide part. In this surface the maximum strain is around 1.3×10^{-3} .

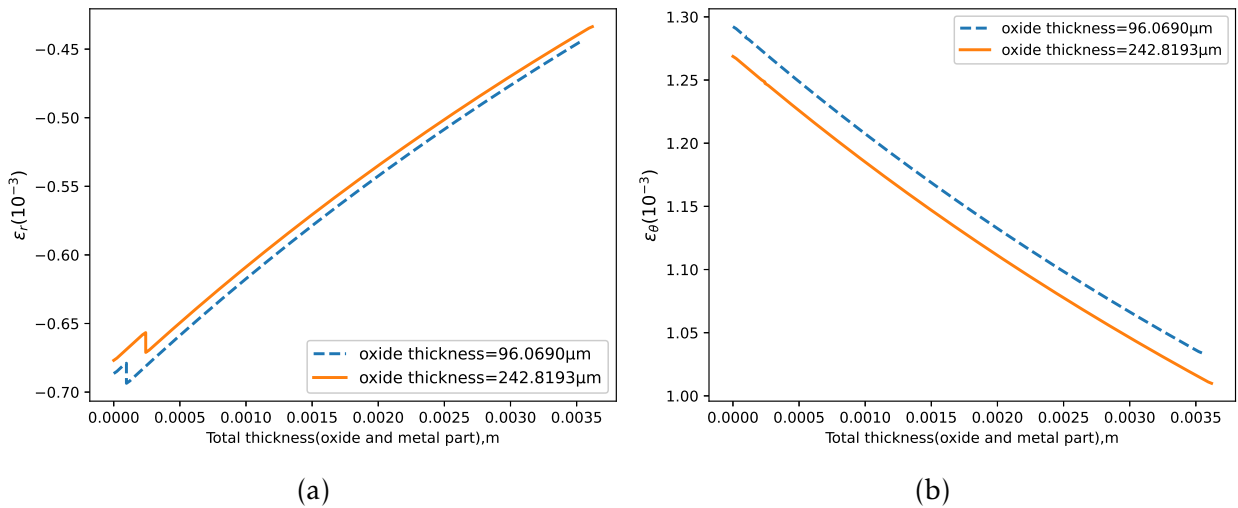


Figure 5.11: Numerical results of elastic radial and hoop strain vs total thickness of tube

Figure 5.12 is a plot of evolution of maximum radial and hoop strain in the increment of oxide scale. Under given load of boiler operation, the calculated and simulated result of metal and oxide part of radial strain is small and increasing with a small amount, but didn't change significantly with increasing oxide thickness. The radial strain of oxide and metal part at 242.82 μm oxide scale is increased by 4.36% and 2.32% from 96.1 μm of oxide scale respectively. For hoop strain the value is decreased with increasing of oxide scale thickness. The hoop strain of metal and oxide part at 242.82 μm oxide scale is decreased by 21.34 % and 3.52% from 96.1 μm of oxide scale respectively.

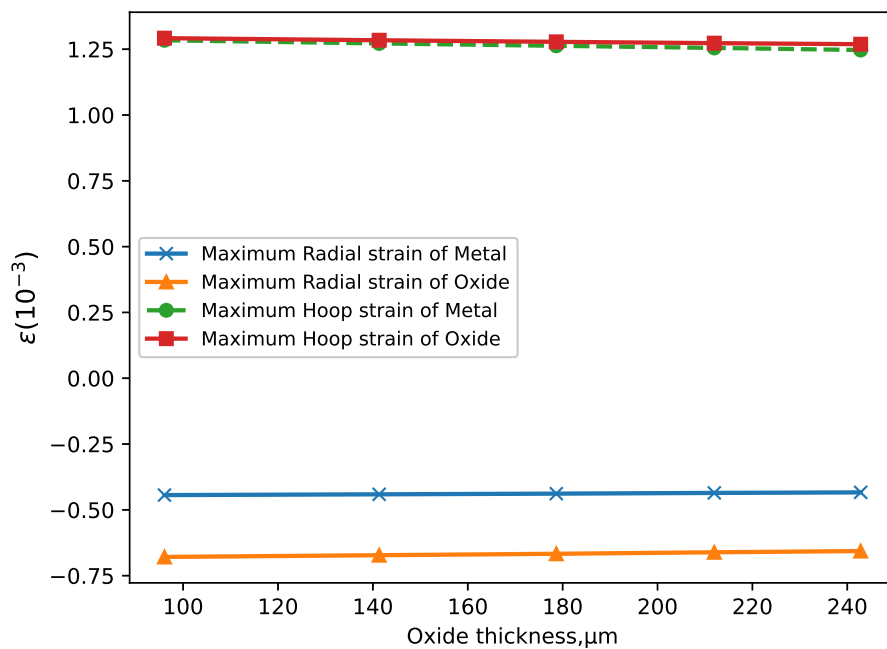


Figure 5.12: Maximum of elastic radial and hoop strain at different oxide scale thickness

Figure 5.13 is a plot of evolution of maximum radial and hoop stress in the increment of oxide scale. Under given load of boiler operation, the calculated and simulated result of metal and oxide part of radial strain is increasing with increasing of oxide thickness. The radial stress of oxide and metal part at 242.82 μm oxide scale is increased by 4.87% and 42.83% from 96.1 μm of oxide scale respectively. For hoop stress the value is decreased with increasing of oxide scale thickness. The hoop strain of metal and oxide part at 242.82 μm oxide scale is decreased by 2.71 % and 3.14% from 96.1 μm of oxide scale respectively.

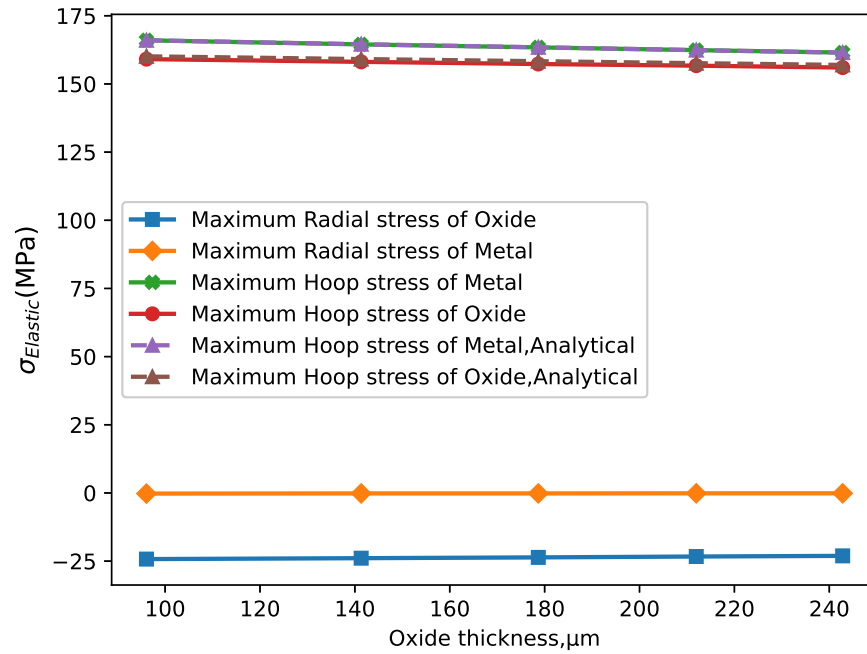


Figure 5.13: Maximum of elastic radial and hoop stress at different oxide scale thickness

5.2.2 Result of Thermal stress and strain at different oxide scale

Analytical and numerical result of thermo-mechanical stress-strain is listed separately in oxide and metal parts at each radial distance.

Table 5.14: Analytical and numerical result of thermal radial stress at different oxide scale

Thermal Radial stress (MPa)						
Oxide thickness (μm)	Oxide part			Metal part		
	Position	Analytical	Numerical	Position	Analytical	Numerical
96.0690	r=a	-25	-24.95	r=b	-24.2	-24.16
	r=b	-24.22	-24.26	r=c	-0.1	-0.135
141.3280	r=a	-25	-24.96	r=b	-23.95	-23.90
	r=b	-23.95	-23.99	r=c	-0.1	-0.134
178.6649	r=a	-25	-24.96	r=b	-23.78	-23.73
	r=b	-23.78	-23.82	r=c	-0.1	-0.134
211.9621	r=a	-25	-24.96	r=b	-23.66	-23.61
	r=b	-23.66	-23.7	r=c	-0.1	-0.134
242.8193	r=a	-25	-24.96	r=b	-23.58	-23.53
	r=b	-23.58	-23.61	r=c	-0.1	-0.134

Table 5.15: Summary of analytical and numerical result of thermal hoop stress at different oxide scale

Thermal Hoop stress (MPa)						
Oxide thickness (μm)	Oxide part			Metal part		
	Position	Analytical	Numerical	Position	Analytical	Numerical
96.0690	r=a	131.88	154.5	r=b	144.12	167
	r=b	131.09	153.8	r=c	120	142.1
141.3280	r=a	105.24	138.4	r=b	143.78	165.1
	r=b	104.19	137.5	r=c	119.93	141.7
178.6649	r=a	84.64	126.1	r=b	143.92	164.9
	r=b	83.42	124.9	r=c	120.24	141.6
211.9621	r=a	65.97	115	r=b	144.11	165
	r=b	64.62	113.7	r=c	120.55	141.8
242.8193	r=a	49.85	105.4	r=b	144.66	165.3
	r=b	48.42	104.1	r=c	121.19	142.1

Figure 5.14(a) shows thermal radial stress increase through the thickness from the inside of the oxide part to outer surface of the tube wall. Based on the calculation and the simulation result the outer surface of the tube has maximum thermal radial stress (compression stress) around -0.13MPa. Figure 5.14(b) is a plot of Elastic hoop stress through the thickness (radial position), the hoop stress (Tensile stress) in both oxide and metal parts decrease through the radial position. The maximum thermal hoop stress is found at the oxide/metal interface surface. In this surface the stress of metal part is greater than the stress of oxide part, the maximum stress is around 165MPa.

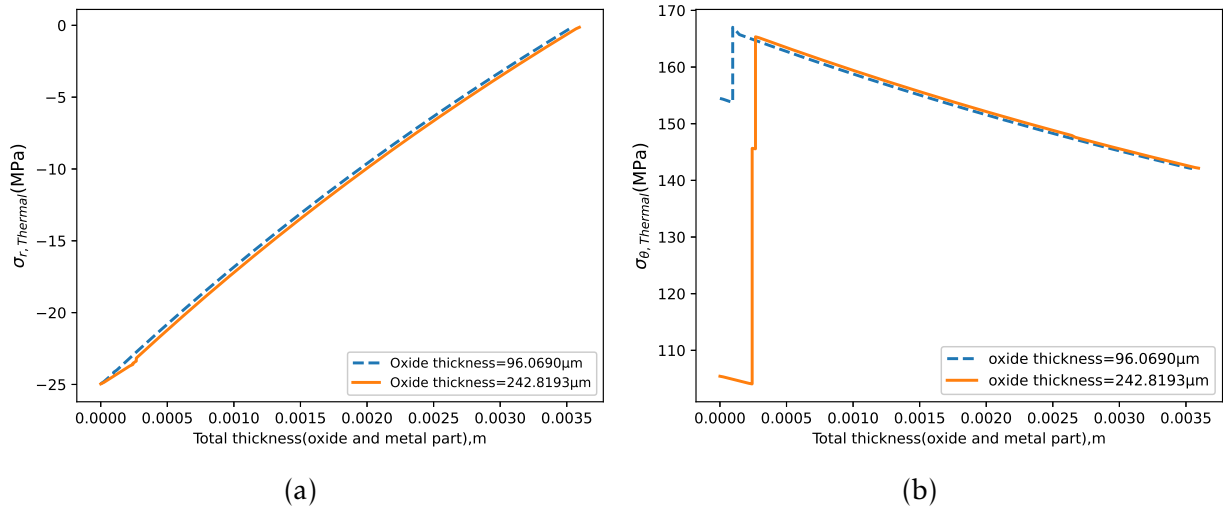


Figure 5.14: Numerical results of thermo- radial and hoop stress vs total thickness of tube

Table 5.16: Summary of analytical and numerical result of thermo-mechanical radial strain at different oxide scale

Thermal Radial Strain (10^{-3})						
Oxide thickness (μm)	Oxide part			Metal part		
	Position	Analytical	Numerical	Position	Analytical	Numerical
96.0690	r=a	-0.421	-0.422	r=b	-0.481	-0.489
	r=b	-0.413	-0.414	r=c	-0.229	-0.230
141.3280	r=a	-0.259	-0.255	r=b	-0.479	-0.476
	r=b	-0.244	-0.245	r=c	-0.231	-0.232
178.6649	r=a	-0.125	-0.126	r=b	-0.481	-0.477
	r=b	-0.113	-0.114	r=c	-0.235	-0.236
211.9621	r=a	-0.077	-0.0076	r=b	-0.482	-0.479
	r=b	0.0067	0.0059	r=c	-0.237	-0.238
242.8193	r=a	0.0941	0.0942	r=b	-0.486	-0.484
	r=b	0.109	0.109	r=c	-0.241	-0.243

Table 5.17: Summary of analytical and numerical result of thermo-mechanical hoop strain at different oxide scale

Thermal Hoop Strain (10^{-3})						
Oxide thickness (μm)	Oxide part			Metal part		
	Position	Analytical	Numerical	Position	Analytical	Numerical
96.0690	r=a	1.508	1.507	r=b	1.499	1.499
	r=b	1.499	1.500	r=c	1.248	1.249
141.3280	r=a	1.502	1.501	r=b	1.490	1.490
	r=b	1.490	1.491	r=c	1.242	1.243
178.6649	r=a	1.498	1.498	r=b	1.484	1.484
	r=b	1.484	1.485	r=c	1.238	1.239
211.9621	r=a	1.496	1.497	r=b	1.482	1.483
	r=b	1.482	1.484	r=c	1.237	1.238
242.8193	r=a	1.495	1.496	r=b	1.480	1.480
	r=b	1.480	1.481	r=c	1.236	1.237

Figure 5.15(a) the thermal radial strain increased through the thickness, but the radial strain of oxide part is greater than the radial strain of metal part at oxide/metal interface. Based on the calculation and the simulation result the maximum thermal radial strain (compression strain) around 0.109×10^{-3} at the oxide/metal interface. Figure 5.15(b) is a plot of thermal hoop strain through the thickness (radial position), the hoop strain (Tensile strain) in both oxide and metal parts decrease through the radial position. The maximum thermal hoop strain is found at the internal surface of oxide part. In this surface the maximum strain is around 1.5×10^{-3} .

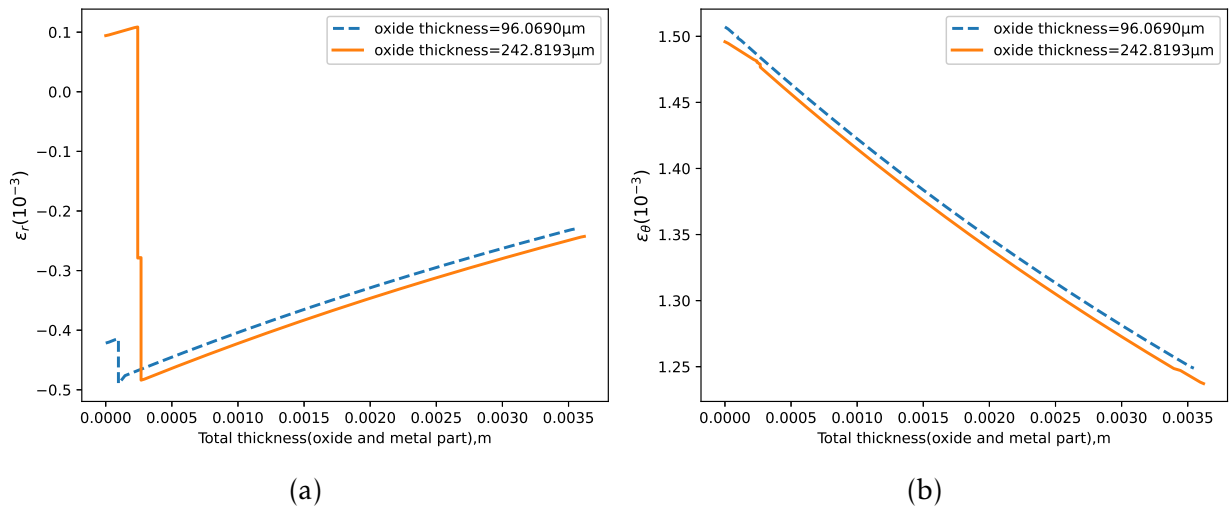


Figure 5.15: Numerical results of thermo-mechanical radial and hoop strain vs total thickness of tube

Figure 5.16 is a plot of evolution of maximum radial and hoop strain in the increment of oxide scale. Under given load of boiler operation, the calculated and simulated result of oxide part of radial strain increasing with a high amount with increasing oxide thickness, but the metal part is decreasing with a small amount. The radial strain of oxide part at $242.82 \mu\text{m}$ oxide scale is increased by 126.32% and the metal part decreased 5.65% from $96.1 \mu\text{m}$ of oxide scale. For hoop strain the value is decreased with increasing of oxide scale thickness. The hoop strain of metal and oxide part at $242.82 \mu\text{m}$ oxide scale is decreased by 1.27 % and 0.73% from $96.1 \mu\text{m}$ of oxide scale respectively.

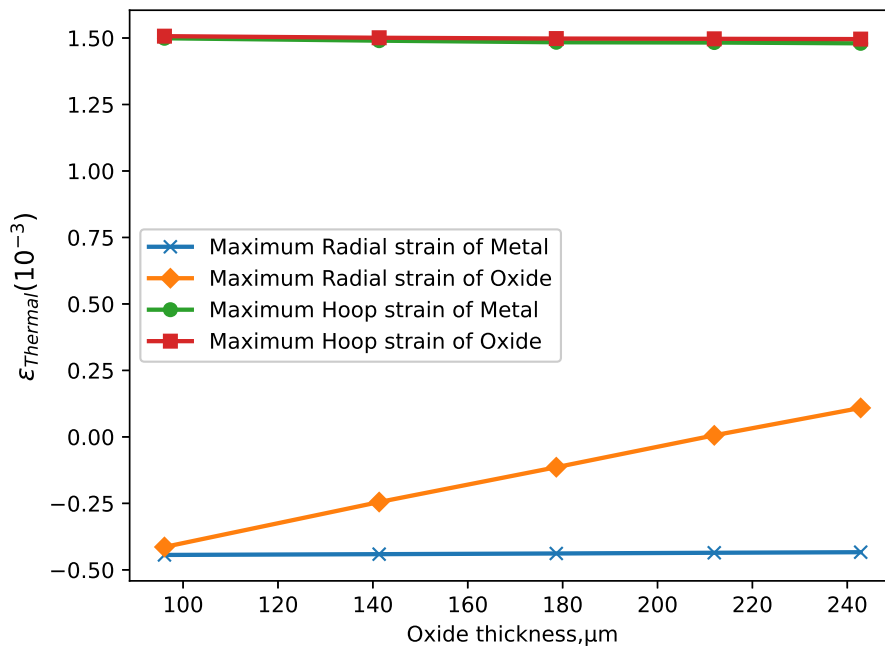


Figure 5.16: Maximum of thermal radial and hoop strain at different oxide scale thickness

Figure 5.17 is a plot of evolution of maximum thermal radial and hoop stress in the increment of oxide scale. Under given load of boiler operation, the calculated and simulated result of metal and oxide part of radial strain is increasing with increasing of oxide thickness. The radial stress of oxide and metal part at $242.82 \mu\text{m}$ oxide scale is increased by 2.67% and 0.74% from $96.1 \mu\text{m}$ of oxide scale respectively. For hoop stress the value is decreased with increasing of oxide scale thickness. The hoop strain of metal and oxide part at $242.82 \mu\text{m}$ oxide scale is decreased by 1.02 % and 31.78% from $96.1 \mu\text{m}$ of oxide scale respectively.

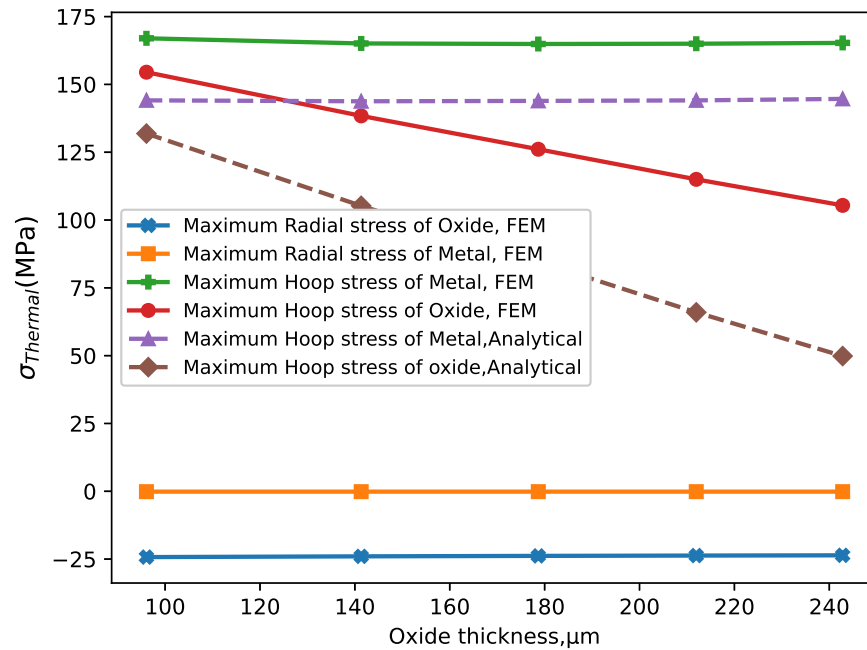
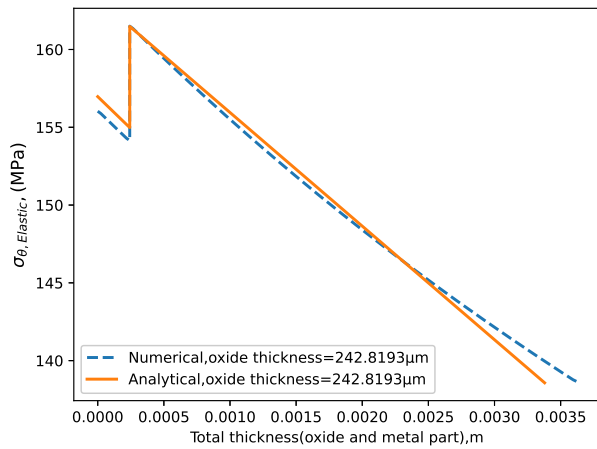


Figure 5.17: Maximum of thermal radial and hoop stress at different oxide scale thickness

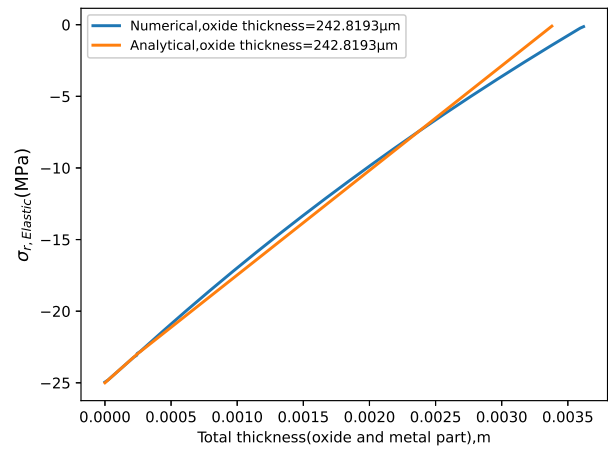
One way of validating the result is by comparing the analytical and numerical result each other and finally compare with literature (Experimental) value. In this research the value of elastic and thermal hoop stress and strain decreasing with small amount due to increasing of oxide scale shown on Figure 5.12, 5.13, 5.16 and 5.17. The validation of the analytical and numerical result of this research is by checking how the elastic and thermal hoop stress and strain are behave due to increasing of oxide scale. On literature[21] at full load operating condition of the superheater boiler tube the oxide hoop stress and strain is decreasing due to increasing of oxide. So, the result of this research has the same decreasing way to the literature.

The analytical solutions will be used to validate our numerical model. Figure 5.18(a), (b), (c) and (d) shows the comparison between analytical and numerical value of elastic hoop stress, elastic radial stress, thermal hoop stress and thermal radial stress respectively at $242.8 \mu\text{m}$ of oxide scale and it take as a sample of other oxide scales. On Figure 5.18 (a) the two results have close value and only having deviation of under 2Mpa. It means the result is accurate. Additional to comparing the analytical and numerical value the more appropriate way of validation is comparing the result to literature/experimental result. Figure 6 (b) and (c) of literature [23] shows the radial and hoop stress with respect to radial position/direction respectively. Based on the Figure 6(b) the radial stress at full

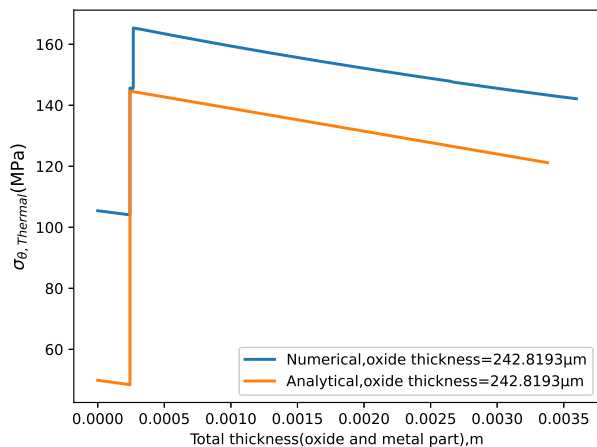
load condition increasing in the radial direction, the peak value is at outer surface of metal tube. It has the same graphical or diagrammatical result as Figure 5.18 (b) and (d). The hoop stress at full load condition the oxide stress value is decreasing when radially goes from the inner surface to oxide/metal interface, and for metal part the peak value is at oxide/metal interface and the value reduced goes to the radial direction, this shows on Figure 6(c). The literature has the same graphical representation or result to Figure 5.18 (a) and (c). Based on this the analytical equations and numerical models of this research is acceptable.



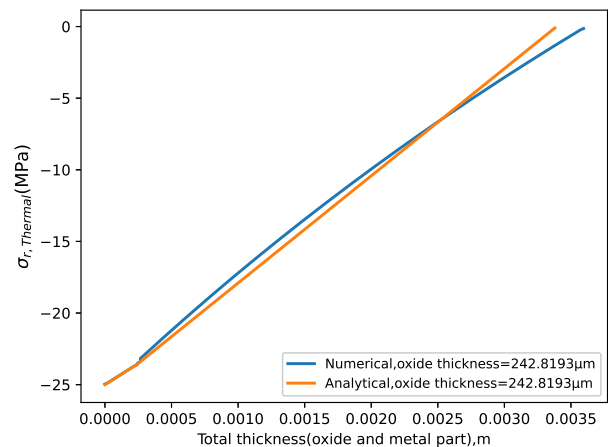
(a)



(b)



(c)



(d)

Figure 5.18: Comparison between analytical and numerical value of stress

5.2.3 Result of Failure of Oxide scale

Figure 5.19 shows the evolution of elastic hoop and radial strain due to the increase of oxide scale and it predict or show the crack initiation of oxide scale due to tension (hoop) and compression (radial) strain. Based on the figure when the oxide scale exceeds 240 μm the crack initiates due to tension but the oxide scale is safe due to compression.

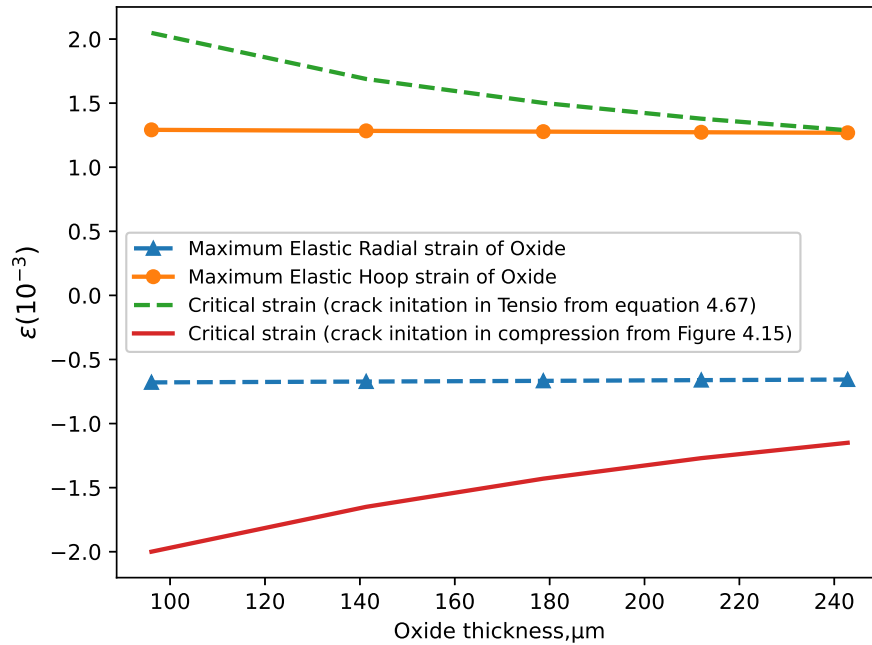


Figure 5.19: Damage map showing critical strains and maximum elastic strains of oxide scale

As shown in Figure 5.20 the strain is sufficient to intersect the oxide failure criteria for crack initiation in tension at times equivalent to an oxide thickness of 178 μm . This oxide thickness reached after 6000hr.

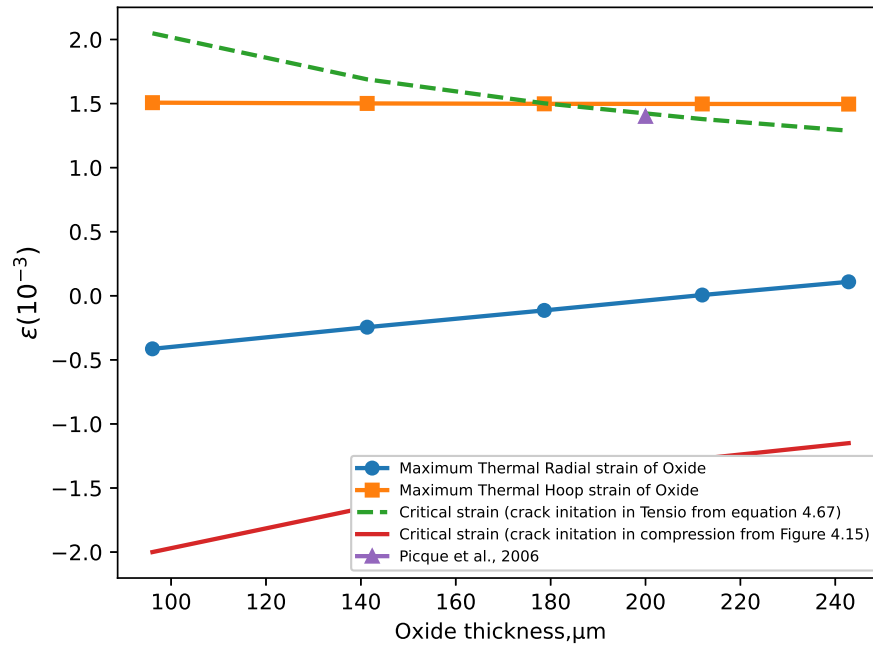


Figure 5.20: Damage map showing critical strains and maximum thermal strains of oxide scale

The experimental value of [80] used to validate the crack initiation of oxide scale. Based on the experiment the cracks are found at 200 μm and the critical strain is around 1.410×10^{-3} . The analytical and experimental critical strain value is almost the same, so the analytical value of the critical strain is acceptable.

5.3 Result of Creep Analysis

Analytical and numerical methods are used to compute the Creep stress and strain rate of boiler tube with oxide scale. The analytical Creep stress and strain rate equation of an oxide-scaled boiler tube is explored in Chapter 4.5, where in this section the numerical (Finite Element Simulation) and analytical results are presented and interpreted.

Table 5.18: Summary of analytical and numerical result of creep radial, hoop and von mises stress at different oxide scale thickness

Creep Stress of Metal (MPa)							
Oxide thickness (μm)	Radial Stress			Hoop Stress		Von Mises Stress	
	Position	Analytical	Numerical	Analytical	Numerical	Analytical	Numerical
96.0690	r=c	-0.1	-0.4247	164.21	165.2	142.29	143.5
	r=b	-24.82	-24.62	149.38	150.7	150.85	151.8
141.3280	r=c	-0.1	-0.4165	164.84	166.4	142.84	144.5
	r=b	-24.73	-24.62	150.06	152	151.37	153
178.6649	r=c	-0.1	-0.4147	165.34	167.4	143.27	145.3
	r=b	-24.66	-24.62	150.61	153	151.78	153.8
211.9621	r=c	-0.1	-0.4095	165.81	168.3	143.68	146.1
	r=b	-24.59	-24.62	151.12	153.9	152.17	154.6
242.8193	r=c	-0.1	-0.4050	166.2	169.2	144.05	146.8
	r=b	-24.54	-24.53	151.6	154.7	152.57	155.3

Table 5.19: Summary of analytical and numerical result of creep radial and hoop strain at different oxide scale thickness

Creep Strain of Metal (10^{-1})						
Oxide thickness (μm)	Radial Strain			Hoop Strain		
	Position	Analytical	Numerical	Position	Analytical	Numerical
96.0690	Max (r=c)	-1.1114	-1.156	Max (r=b)	1.4885	1.545
	Min (r=b)	-1.4885	-1.539	Min (r=c)	1.1114	1.164
141.3280	Max (r=c)	-2.2658	-2.396	Max (r=b)	3.0283	3.199
	Min (r=b)	-3.0283	-3.193	Min (r=c)	2.2658	2.404
178.6649	Max (r=c)	-3.450	-3.702	Max (r=b)	4.604	4.928
	Min (r=b)	-4.604	-4.922	Min (r=c)	3.450	3.710
211.9621	Max (r=c)	-4.667	-5.075	Max (r=b)	6.217	6.742
	Min (r=b)	-6.217	-6.736	Min (r=c)	4.667	5.083
242.8193	Max (r=c)	-5.907	-6.502	Max (r=b)	7.859	8.624
	Min (r=b)	-7.859	-8.617	Min (r=c)	5.907	6.510

Table 5.20: Summary of analytical and numerical result of radial and hoop creep strain rate at different working time

Creep Strain rate of Metal $\dot{\epsilon}_{cr}(10^{-1})$						
Time (hr.)	Radial Strain rate			Hoop Strain rate		
	Position	Analytical	Numerical	Position	Analytical	Numerical
2000	Max (r=c)	-1.1116	-1.150	Max (r=b)	1.4886	1.533
	Min (r=b)	-1.4886	-1.531	Min (r=c)	1.1116	1.153
4000	Max (r=c)	-2.2266	-2.390	Max (r=b)	3.0284	3.188
	Min (r=b)	-3.0284	-3.185	Min (r=c)	2.2266	2.393
6000	Max (r=c)	-3.501	-3.699	Max (r=b)	4.663	4.997
	Min (r=b)	-4.663	-4.915	Min (r=c)	3.501	3.699
8000	Max (r=c)	-4.6668	-5.069	Max (r=b)	6.2174	6.731
	Min (r=b)	-6.2174	-6.729	Min (r=c)	4.6668	5.072
10000	Max (r=c)	-5.907	-6.496	Max (r=b)	7.859	8.612
	Min (r=b)	-7.859	-8.610	Min (r=c)	5.907	6.498

Figure 5.21 (a) shows the creep radial, hoop and vonmises stress of metal tube at the radial position or direction of the tube at 242 μm . Based on the result the Vonmises stress at inner surface of the tube is higher and slightly reduce goes to the outer tube. The maximum vonmises stress of numerical (finite element) method is estimated to 155.3 MPa and the analytical value is 152.57 MPa. These two results have close value and only having deviation of below 10% from eachother.

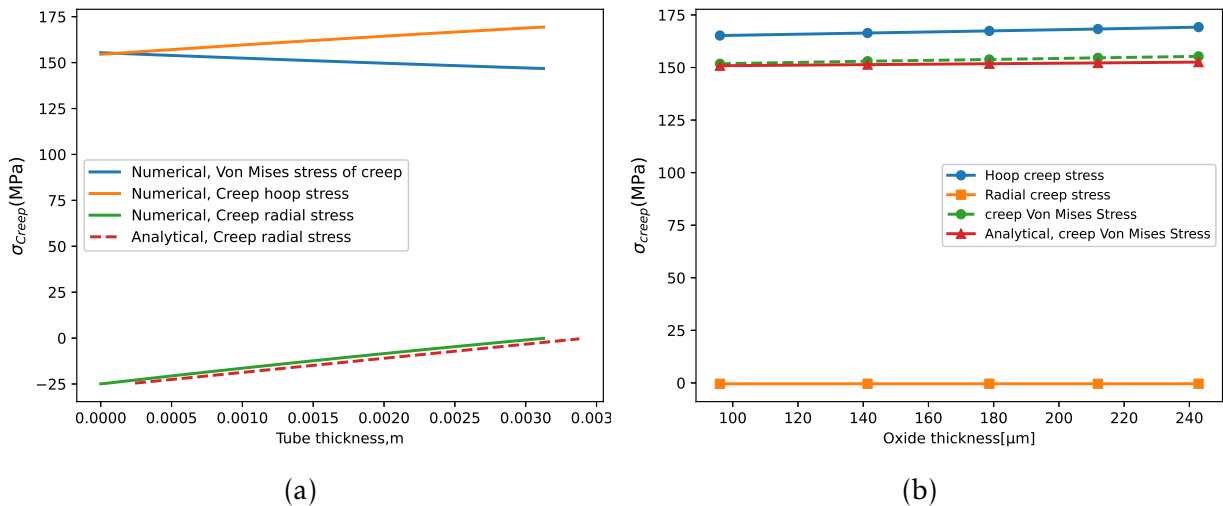


Figure 5.21: creep stress of metal versus radial direction of tube (a) and at different oxide scale (b)

Figure 5.21 (b) shows the effect of oxide scale growth on the creep stress of metal part. The creep radial, hoop and von mises stress of the metal is increasing due to the growth of oxide scale. The increase of creep stress reduces the remaining life of boiler tube. In the Norton's law of minimum creep strain rate relation, the rupture life expression has inversely relation between Von Mises stress and rupture time[72]. So, the increase of Von Mises stress reduces the remaining or creep rupture life of boiler tube.

As time pass the total strain of the boiler tube is become higher due to gradual increase of creep strain because the elastic and thermal strain is remained constant until pressure and temperature change is occurs. So, the creep strain takes the larger contribution to the total strain. Figure 5.22 shows the increase of hoop strain rate due to increase of operating time. The maximum hoop creep strain rate of the tube after 10,000 working hours become $8.612 \times 10^{-1} h^{-1}$ and $7.859 \times 10^{-1} h^{-1}$ numerically and analytically respectively. The results found from both analytical approach and finite element method (FEM) have close value and only having deviation of below 10% from eachother. Thus, those results are valid, since the values are in acceptable range.

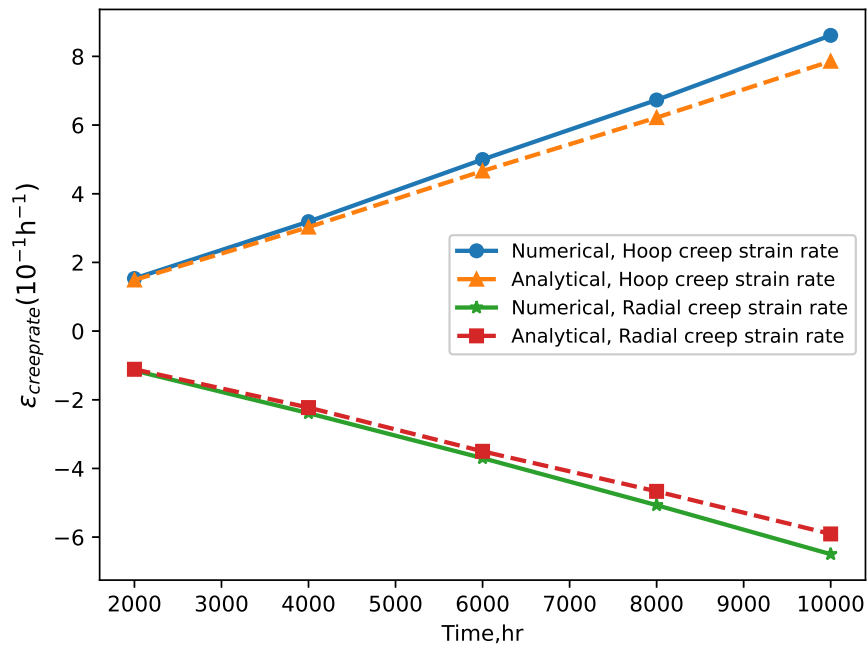


Figure 5.22: Creep strain rate vs working time

The creep deformation property or behavior is investigated by different researchers, to validate the result of this thesis let us compare to the literatures. The creep rate (strain rate) vs time of T/P 92 alloy steel at $650^{\circ}C$ is investigated by [81]. Based on the experimental result of the work the value of creep strain rate is around 10^{-1} , when the time

$10^3 hr$ and the stress exceed $150 MPa$. The strain rate is increasing rapidly when then the time increasing this shown by the experimental value of [81], [82]. When compare the result shown in Figure 5.22 to the experimental result describe in literature, the strain rate is in the same range so the analytical and the numerical analysis of this work is acceptable.

5.3.1 Result of creep rupture time

Table 5.21: Summary of creep rupture time due to growth of oxide scale thickness using LMP

Creep rupture time using LMP				
Working Time (t)(hr)	Average metal Temperature ($^{\circ}C$)	Oxide scale (μm)	Maximum Elastic Hoop Stress (MPa)	Rupture time (t_r)(hr)
2000	647.95	96.0690	171.57	1573.38628
4000	652.35	141.3280	172.79	1031.51473
6000	655.75	178.6649	173.76	745.2241184
8000	658.9	211.9621	174.68	551.9027812
10000	661.6	242.8193	175.51	426.2826763

Table 5.22: Summary of creep rupture time due to growth of oxide scale thickness using power law rupture

Working Time (t)(hr)	Oxide scale (μm)	Von Mises stress (MPa)	Rupture time (t_r)(hr)
2000	96.0690	151.8	2255.68
4000	141.3280	153	2168.60
6000	178.6649	153.8	2112.78
8000	211.9621	154.6	2058.68
10000	242.8193	155.3	2012.70

The above tables shows increased in oxide scale thickness is increase the maximum elastic stress and creep von mises stress. Figure 5.23(a) shows the maximum elastic stress vs the creep rupture time based on LMP method. The result shows that a 73% reduction of creep strength when the boiler tube has $242\mu m$ oxide scale thickness as compared to the oxide scale of $96\mu m$. Figure 5.23(b) shows the maximum Von Mises stress vs the creep rupture time based on Norton's Law of minimum creep strain rate equation. The

result shows that a 10.8% reduction of creep strength when the boiler tube has $242\mu m$ oxide scale thickness as compared to the oxide scale $96\mu m$. This finding shows the creep strength and rupture life in the T92 superheater tube is reduces as oxide scale layer thickening.

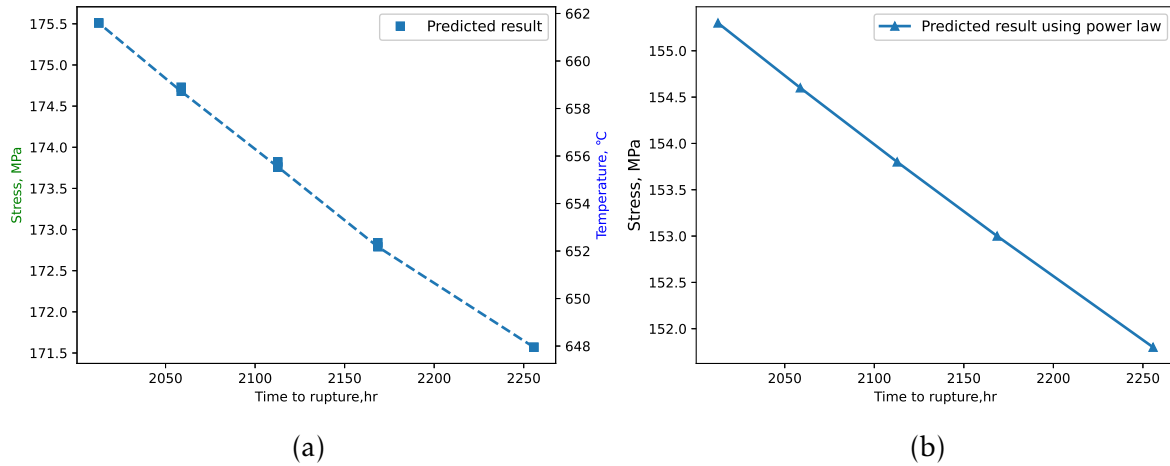


Figure 5.23: Stress vs rupture time

The above figure result shows that a creep rupture time at $96\mu m$ of oxide scale is 30% reduction of creep strength when using Norton power law compared to LMP. Based on different literatures and experimental values the LMP is more accurate to predict the creep rupture time.

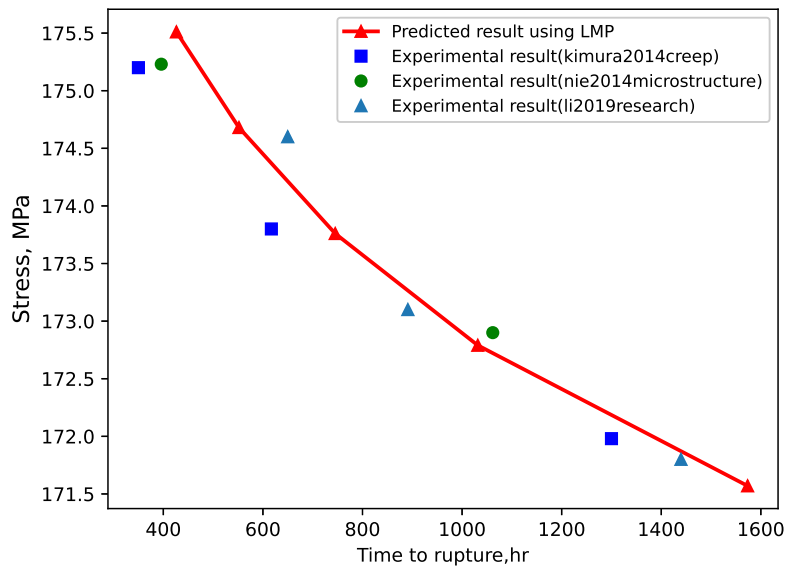


Figure 5.24: Comparison between predicted and experimental value of rupture time

Figure 5.24 shows the comparison of predicted result and experimental data (other literature). The experimental creep rupture life curves in the high-stress regime of T92 steels predicted by the LMP presented by [82]. Based on the experimental value when the stress reached around 171.98MPa the rupture time is around 1300hr, for 173.8MPa the rupture time become 617hr and for 175.2MPa stress the rupture time become 350hr. The other creep test of T92 alloy steel is at different temperature range is computed by [83]. Based on the experimental value when the stress reached around 172.9MPa and 175.23MPa the creep rupture time become 1061.6hr and 395.89hr respectively. Other researcher also try to investigate the creep rupture life of T92 alloy steel by taking different LMP constant C experimental data [76]. Based on the experimental value when the stress reached around 173.1MPa, 174.6 and 171.8MPa the creep rupture time become 891.1hr, 649.8hr and 1439.6hr respectively. The experimental and the predicted results have good agreement to each other with small deviation in acceptable range.

6. CONCLUSION AND RECOMMENDATION

6.1 Conclusion

This study addressed about oxide scale growth, elastic and thermal (thermo-mechanical) stress and creep stress and strain rate of superheater boiler tube of T92 alloy steel. The conclusion derived from this work are presented below:

The prediction of oxide scale growth at different flue and steam gas temperature is computed by using analytical and numerical method and validate with the experimental data. The Larson-Miller parameter is used to predict the oxide scale growth of T92 alloy steel superheater boiler tube. The iterative procedure is developed to predict the growth of oxide scale. The temperature of each surface computed by developing the 2D model of the boiler tube using ABAQUS software and also it calculated by developing the stiffness matrix of the heat transfer and calculated temperature at each node using Python code. The increment of steam gas temperature is more affected the growth of oxide scale than the increment of flue gas temperature. The scale growth estimation obtained by the proposed technique is verified or validated with the experimental value from published literatures. Based on this i conclude that the proposed method of prediction of oxide scale is acceptable.

The elastic and thermal (thermo-mechanical) stress and strain of oxide scaled boiler tube is computed by using analytical and numerical method. For the analytical method develop the governing equation based on Lam's equation and Hooke's law of plane stress and strain expression. To simplify the analytical equation the matrix is developed to compute the integration constants obtained from boundary condition. The analytical stress and strain value is computed by using Python. The analytical elastic and thermo-mechanical stress and strain of oxide scale and metal part were compared and verified with those by the finite element analysis software of ABAQUS. The elastic and thermo-mechanical stress and strain of oxide scaled boiler tube is slightly decreasing due to the increase of oxide scale and the elastic and thermo-mechanical hoop stress and strain at the inner surface of oxide and at the oxide/metal interface layer become higher and decrease through the radial direction. As compared to other works reported in literature

the analytical and numerical solutions proposed in the present work were shown to be more accurate.

The failure or scale exfoliation of steam side oxide scale is proposed by different researchers in different literatures. The exfoliation diagram is developed based on Advanced -oxide scale failure diagram shown in the literatures. From different failure types of oxide scale in this work only consider the crack initiation due to tensile and compressive strain. The determination of the failure or the crack initiation of steam side oxide scale is computed by comparing the elastic and thermo- mechanical (thermal) radial (compressive) and hoop (tension) strain to the critical strain value. Based on this thermal (thermo-mechanical) hoop strain has a great impact on the crack initiation of oxide scale than the elastic value. When the oxide scale increase and reached around $170\mu m$ the thermal (thermo-mechanical) strain crosses the graph of critical oxide scale crack initiation due to tension. The estimated crack initiation or failure is validated with the experimental value from published literatures.

Due to increasing of oxide scale the temperature of the metal is become hotter and hotter. When the boiler operating for a long period of time with high metal temperature leads to creep failure. So, the creep analysis of oxide scaled boiler tube is crucial to know the behavior of the boiler tube due to creep. The creep analysis of the metal is computed by using analytical and numerical method. For the analytical method derive the equation for oxide scaled boiler tube based on Norton's (power) Law of creep and time-hardening rule. The method is used and capable to determine secondary creep. The analytical equation helps to determine the creep behavior of oxide scale boiler tube. As time pass the total strain of the boiler tube is become higher due to gradual increase of creep strain because the elastic and thermal strain is remained constant until pressure and temperature change is occurs. So, the creep strain takes the larger contribution to the total strain. The analytical creep stress, strain and strain rate metal tube of T92 alloy steel were compared and verified with those by the finite element analysis software of ABAQUS and literatures. Due to increase of oxide scale the creep rupture time is decreasing. The effect of oxide scale growth on creep rupture time is calculated by using LMP and power rupture (Norton's) law. The stress calculation is crucial for creep rupture time prediction. So, the equation for maximum elastic stress is take from literatures for LMP and the von mises stress for power rupture is taken from creep stress calculation. The result is validated with literatures.

6.2 Recommendation

During this study there are areas where further work is needed. The first area is oxide creep interaction of cracked superheater boiler tubes. In this research only predict when the oxide scale initiate crack. But the growth of crack and the effect of crack on creep behavior needs detail study. Develop the creep oxide interaction damage model is help to know the cumulative damage of the boiler tube due to oxide and creep.

The second major area of further study maybe the case of corrosion beside to oxide scale. In this research only studied the growth of steam side oxide scale and its effect on thermo-mechanical and creep behavior. But the corrosion part is not considered. In real world the superheater boiler tube faces both steam side oxide scale growth and corrosion together. So, the combined effect needs detail study.

In this research the failure of oxide scale only checks the oxide scale crack initiation due to tension and compression. But the oxide scales failed due to spalling, buckling, deflection towards to the surface and delamination. The scale maybe failed due to these types. So, study of oxide scale failure will be an interesting area.

REFERENCES

- [1] M. Montgomery, S. A. Jensen, F. Rasmussen, and T. Vilhelmsen, "Fireside corrosion and steamside oxidation of 9-i2%Cr martensitic steels exposed for long term testing," *Corros. Eng. Sci. Technol.*, vol. 44, no. 3, pp. 196–210, 2009, doi: 10.1179/174327809X419168.
- [2] C. A. Duarte, E. Espejo, and J. C. Martinez, "Failure analysis of the wall tubes of a water-tube boiler," *Eng. Fail. Anal.*, vol. 79, no. May, pp. 704–713, 2017, doi: 10.1016/j.engfailanal.2017.05.032.
- [3] D. Nandwana and S. Periaswamy, "Tube Failure Analysis and Residual Life Assessment in Water Tube Boiler," no. 25 August, pp. 1–7, 2018.
- [4] R. K. Hosseini and S. Yareiee, "Failure analysis of boiler tube at a petrochemical plant," *Eng. Fail. Anal.*, vol. 106, no. August, p. 104146, 2019, doi: 10.1016/j.engfailanal.2019.104146.
- [5] H. Zhang, "The University of New South Wales ADVANCED BOILER TUBE LIFE," 1997.
- [6] M. Ananda Rao, R. Sekhar Babu, and M. V. Pavan Kumar, "Stress corrosion cracking failure of a SS 316L high pressure heater tube," *Eng. Fail. Anal.*, vol. 90, no. March, pp. 14–22, 2018, doi: 10.1016/j.engfailanal.2018.03.013.
- [7] M. M. Kumar, K. Joshna, R. Markendeya, and M. S. Rawat, "Effect of steamside oxidation and fireside corrosion degradation processes on creep life of service exposed boiler tubes," *Int. J. Press. Vessel. Pip.*, vol. 144, pp. 45–48, 2016, doi: 10.1016/j.ijpvp.2016.05.001.
- [8] H. C. Guo, D. M. Ji, J. Z. Tang, Q. Sun, C. Dai, and J. xing Ren, "Numerical simulation and life prediction on T22 boiler tubes with steam-side and fire-side oxide scale," *Mater. High Temp.*, vol. 36, no. 2, pp. 125–131, 2019, doi: 10.1080/09603409.2018.1471186.
- [9] M. Nad', T. Létal, J. Buzík, and P. Lošák, "Influence of steam-side oxide scales on the creep life of a boiler superheater tube," *Mater. Tehnol.*, vol. 52, no. 1, pp. 43–46, 2018, doi: 10.17222/mit.2017.106.
- [10] M. Alemu, H. Altenbach, and G. Shunki, "Modeling creep-fatigue interaction

- damage and H13 tool steel material response for rolling die under hot milling ?," *Eng. Fract. Mech.*, vol. 223, no. November 2019, p. 106770, 2020, doi: 10.1016/j.engfracmech.2019.106770.
- [11] T. Mushiri, M. Pleasant, and P. O. Box, "MECHANICAL THERMAL STRESSES AND CREEP ANALYSIS," 2006.
- [12] A. S. Sabau and I. G. Wright, "Influence of oxide growth and metal creep on strain development in the steam-side oxide in boiler tubes," *Oxid. Met.*, vol. 73, no. 5–6, pp. 467–492, 2010, doi: 10.1007/s11085-009-9188-4.
- [13] M. S. Haque, C. M. Stewart, and E. Paso, "Comparative analysis of the sin-hyperbolic and kachanov-rabotnov creep-damage models," pp. 1–27, 2019.
- [14] R. E. Of, N. I. B. S. Ingle, and R. S. Uperalloys, "P HENOMENOLOGICAL M ODELING OF THE E FFECT OF O XIDATION ON THE C REEP," pp. 1–22, 2020.
- [15] F. V. Tahami and I. Houshyar, "E ff ect of sediment thickness on the remaining creep lifetime of 9Cr1Mo re fi nery furnace tubes," vol. 105, no. January, pp. 1306–1318, 2019, doi: 10.1016/j.engfailanal.2019.06.081.
- [16] H. Jing, D. Su, L. Xu, L. Zhao, Y. Han, and R. Sun, "Finite element simulation of creep-fatigue crack growth behavior for P91 steel at 625 °C considering creep-fatigue interaction," *Int. J. Fatigue*, vol. 98, pp. 41–52, 2017, doi: 10.1016/j.ijfatigue.2017.01.004.
- [17] S. Ebrahim, M. Torshizi, and A. Jahangiri, "Analysis of Fatigue – Creep Crack Growth in the Superheater Header of a Power Plant Boilers and Estimation of Its Remaining Lifetime," *J. Fail. Anal. Prev.*, 2018, doi: 10.1007/s11668-018-0400-1.
- [18] V. N. Shlyannikov, "Creep – fatigue crack growth rate prediction based on fracture damage zone models," *Eng. Fract. Mech.*, vol. 214, no. April, pp. 449–463, 2019, doi: 10.1016/j.engfracmech.2019.04.017.
- [19] K. Nikbin, "A unified multiscale ductility exhaustion based approach to predict uniaxial, multiaxial creep rupture and crack growth," *Eng. Fract. Mech.*, vol. 179, pp. 240–259, 2017, doi: 10.1016/j.engfracmech.2017.04.046.
- [20] N. A. Alang and K. Nikbin, "An analytical and numerical approach to multiscale ductility constraint based model to predict uniaxial/multiaxial creep rupture and cracking rates," *Int. J. Mech. Sci.*, vol. 135, pp. 342–352, 2018, doi: 10.1016/j.ijmecsci.2017.11.030.
- [21] A. S. Sabau and I. G. Wright, "On the estimation of thermal strains developed

- during oxide growth,” *J. Appl. Phys.*, vol. 106, no. 2, 2009, doi: 10.1063/1.3157199.
- [22] J. L. Huang, K. Y. Zhou, J. Q. Xu, and C. X. Bian, “On the failure of steam-side oxide scales in high temperature components of boilers during unsteady thermal processes,” *J. Loss Prev. Process Ind.*, vol. 26, no. 1, pp. 22–31, 2013, doi: 10.1016/j.jlp.2012.08.004.
- [23] F. Xue, T. Le Cheng, and Y. H. Wen, “Stress Analysis of the Steam-Side Oxide of Boiler Tubes: Contributions from Thermal Strain, Interface Roughness, Creep, and Oxide Growth,” *Oxid. Met.*, vol. 93, no. 5–6, pp. 515–543, 2020, doi: 10.1007/s11085-020-09969-4.
- [24] K. Bahoum, M. Diany, and M. Mabrouki, “Stress analysis of compound cylinders subjected to thermo-mechanical loads,” *J. Mech. Sci. Technol.*, vol. 31, no. 4, pp. 1805–1811, 2017, doi: 10.1007/s12206-017-0328-5.
- [25] M. Schütze, P. F. Tortorelli, and I. G. Wright, “Development of a comprehensive oxide scale failure diagram,” *Oxid. Met.*, vol. 73, no. 3–4, pp. 389–418, 2010, doi: 10.1007/s11085-009-9185-7.
- [26] A. Ahmadi, M. shayegani Akmal, A. Pasha, and S. Yareie, “Failure analysis of cracked 2.25Cr–1.0Mo steel tubes of an oil refinery boiler,” *Eng. Fail. Anal.*, vol. 110, no. February, p. 104435, 2020, doi: 10.1016/j.engfailanal.2020.104435.
- [27] J. Purbolaksono, A. Khinani, A. Z. Rashid, A. A. Ali, and N. F. Nordin, “Prediction of oxide scale growth in superheater and reheater tubes,” *Corros. Sci.*, vol. 51, no. 5, pp. 1022–1029, 2009, doi: 10.1016/j.corsci.2009.02.025.
- [28] A. Firouzeh, K. Ranjbar, S. M. Lari Baghal, A. Heidari Kaidan, and E. Mohemi, “Failure assessment of ASTM A213-T12 superheater boiler tubes in a natural gas liquid plant,” *Eng. Fail. Anal.*, vol. 89, pp. 15–27, 2018, doi: 10.1016/j.engfailanal.2018.03.005..
- [29] T. T. Nguyen, T. M. Jeong, D. T. Erten, and K. B. Yoon, “Creep deformation and rupture behaviour of service-exposed Super304H steel boiler tubes,” *Mater. High Temp.*, vol. 38, no. 1, pp. 61–72, 2021, doi: 10.1080/09603409.2020.1830609.
- [30] J. M. Garcia et al., “Experimental creep behavior and life prediction through observation and numerical analysis for AISI 310,” *J. Mater. Res. Technol.*, vol. 9, no. 1, pp. 222–229, 2020, doi: 10.1016/j.jmrt.2019.10.047.
- [31] U. K. Sahu and R. Shankar, “Residual life estimation of super heater tubes based on oxide scale thickness measurement-A Case Study,” pp. 2497–2505, 2016.

- [32] M. Hong, H. Chae, W. C. Kim, J. G. Kim, H. Kim, and S. Y. Lee, "Failure Analysis of a Water Wall Boiler Tube for Power Generation in a District Heating System," *Met. Mater. Int.*, vol. 25, no. 5, pp. 1191–1201, 2019, doi: 10.1007/s12540-019-00267-6.
- [33] S. Senthur Prabu, A. Choudhary, N. Mittal, S. Gupta, D. Ramkumar, and A. Natarajan, "Failure evaluation of SA 210C riffle water wall tubes in 70MW CFBC boiler," *Eng. Fail. Anal.*, vol. 95, no. September 2018, pp. 239–247, 2019, doi: 10.1016/j.engfailanal.2018.09.028.
- [34] M. Z. Hamzah, W. H. Yeo, A. T. Fry, J. I. Inayat-Hussain, S. Ramesh, and J. Purbolaksono, "Estimation of oxide scale growth and temperature increase of high (9-12%) chromium martensitic steels of superheater tubes," *Eng. Fail. Anal.*, vol. 35, pp. 380–386, 2013, doi: 10.1016/j.engfailanal.2013.03.014.
- [35] B. H. Salman, M. Z. Hamzah, J. Purbolaksono, J. I. Inayat-Hussain, H. A. Mohammed, and M. W. Muhieldeen, "Determination of correlation functions of the oxide scale growth and the temperature increase," *Eng. Fail. Anal.*, vol. 18, no. 8, pp. 2260–2271, 2011, doi: 10.1016/j.engfailanal.2011.08.001.
- [36] J. Qi, H. Xu, and K. Zhou, "Creep rupture life assessment of superheater tube with oxide formation in power plant," no. April, 2020, doi: 10.1002/maco.202011728..
- [37] D. Zhang, J. Liu, Z. Xue, and X. Mao, "Oxidation behavior of T92 steel with NiCoCrAlY coating by EB-PVD," *Surf. Coatings Technol.*, vol. 252, pp. 179–185, 2014, doi: 10.1016/j.surfcoat.2014.04.064.
- [38] Z. Liang and Q. Zhao, "Steam oxidation of austenitic heat-resistant steels TP347H and TP347HFG at 650-800 °C," *Materials (Basel)*, vol. 12, no. 4, 2019, doi: 10.3390/ma12040577.
- [39] N. S. Drastiwati, H. Zakiyya, F. Y. Utama, and W. D. Kurniawan, "Preliminary Study of Failure Analysis on Tube Material Boiler Based on Pressure Aspect," *IOP Conf. Ser. Mater. Sci. Eng.*, vol. 288, no. 1, 2018, doi: 10.1088/1757-899X/288/1/012110.
- [40] F. Dehnavi, A. Eslami, and F. Ashrafizadeh, "A case study on failure of superheater tubes in an industrial power plant," *Eng. Fail. Anal.*, vol. 80, pp. 368–377, 2017, doi: 10.1016/j.engfailanal.2017.07.007.
- [41] M. Morales, J. M. Chimenos, A. I. Fernández, and M. Segarra, "Materials selection for superheater tubes in municipal solid waste incineration plants," *J. Mater. Eng. Perform.*, vol. 23, no. 9, pp. 3207–3214, 2014, doi: 10.1007/s11665-014-1100-y.
- [42] T. Dudziak, M. Łukaszewicz, N. Simms, and J. Nicholls, "Analysis of High

- Temperature Steam Oxidation of Superheater Steels Used in Coal Fired Boilers,” *Oxid. Met.*, vol. 85, no. 1–2, pp. 171–187, 2016, doi: 10.1007/s11085-015-9593-9.
- [43] J. Qi, K. Y. Zhou, J. L. Huang, and X. D. Si, “Numerical simulation of the failure behavior of steam-side oxide scale considering oxide creep and physical defects,” *Mater. Corros.*, vol. 69, no. 2, pp. 215–226, 2018, doi: 10.1002/maco.201709465.
- [44] S. T. Examiner, T. Lepist, M. Engineering, and F. Council, “Steam-Side Oxidation of Materials for,” no. March, 2010.
- [45] T. Zhang, X. Zhang, N. Bayar, and Z. Zhao, “Review of oxide scale on high temperature heating surface in boiler,” *IOP Conf. Ser. Earth Environ. Sci.*, vol. 692, no. 2, 2021, doi: 10.1088/1755-1315/692/2/022049.
- [46] P. J. Ennis, *Ferritic and martensitic steels for power plants*. 2014. doi: 10.1533/9780857097552.2.188.
- [47] P. R. Kannan, V. Muthupandi, B. Arivazhagan, and K. Devakumaran, “Microstructure and Mechanical Properties of Heat-treated T92 Martensitic Heat Resistant Steel,” *High Temp. Mater. Process.*, vol. 36, no. 8, pp. 771–778, 2017, doi: 10.1515/htmp-2016-0030.
- [48] K. Chandra, A. Kranzmann, R. S. Neumann, and F. Rizzo, “Comparative Study on High Temperature Oxidation of T92 Steel in Dry and Wet Oxyfuel Environments,” *Oxid. Met.*, vol. 84, no. 3–4, pp. 463–490, 2015, doi: 10.1007/s11085-015-9565-0.
- [49] P. Kofstad, *High Temperature Corrosion*. 1988.
- [50] N. Birks, G. H. Meier, and F. S. Pettit, *Introduction to the high temperature oxidation of metals*, Second edition, Second Edi., vol. 9780521480. 2006. doi: 10.1017/CBO9781139163903.
- [51] D. J. Young, *High Temperature Oxidation and Corrosion of Metals: Second Edition*, Second. Elsevier, 2016. doi: 10.1016/C2014-0-00259-6.
- [52] R. M. P. Huitron, P. E. R. López, E. Vuorinen, P. N. Jalali, L. Pelcastre, and M. Kärkkäinen, “Scale formation on HSLA steel during continuous casting part I: The effect of temperature–time on oxidation kinetics,” *Metals (Basel)*, vol. 10, no. 9, pp. 1–22, 2020, doi: 10.3390/met10091243.
- [53] A. S. Khanna, *Introduction to high temperature oxidation and corrosion*. Materials Park, OH: ASM International, 2002.
- [54] I. G. Wright, R. B. Dooley, I. G. Wright, and R. B. Dooley, “A review of the oxidation behaviour of structural alloys in steam A review of the oxidation behaviour of structural

- alloys in steam,” vol. 6608, no. July, 2017, doi: 10.1179/095066010X12646898728165.
- [55] K. Chandra and A. Kranzmann, “High temperature oxidation of 9–12% Cr ferritic/martensitic steels under dual-environment conditions,” *Corros. Eng. Sci. Technol.*, vol. 53, pp. 27–33, 2018, doi: 10.1080/1478422X.2017.1374049.
- [56] K. Li, H. Ma, Y. He, J. Chang, S. yeon Bae, and K. Shin, “Microstructural evolution and oxidation resistance of T92 boiler tube steel upon long-term supercritical steam test,” *Fusion Eng. Des.*, vol. 125, pp. 361–366, 2017, doi: 10.1016/j.fusengdes.2017.04.133.
- [57] P. J. Ennis and W. J. Quadackers, “Implications of steam oxidation for the service life of high-strength martensitic steel components in high-temperature plant,” *Int. J. Press. Vessel. Pip.*, vol. 84, no. 1–2, pp. 82–87, 2007, doi: 10.1016/j.ijpvp.2006.09.008.
- [58] C. X. Bian, K. Y. Zhou, J. Q. Xu, and X. W. Ping, “Influence of steam-side oxide scales on heat transfer of T92 tube in power plants,” *Asia-Pacific Power Energy Eng. Conf. APPEEC*, 2009, doi: 10.1109/APPEEC.2009.4918434.
- [59] C. Panait et al., “Long term aging effect on the creep strength of the T92 steel To cite this version: HAL Id: hal-00592020,” 2011.
- [60] Y. A. Cengel, *HEAT TRANSFER A Practical Approach*, Second Edi.
- [61] C. P. Kothandaraman, *Fundamentals of heat and mass transfer*. New Delhi, India: New Age International Limited, 2006.
- [62] L. Incropera, Dewit, Bergman, *Fundamentals of Heat and Mass Transfer*, 6th editio.
- [63] H.-J. Kretzschmar and W. Wagner, *International steam tables-properties of water and steam based on the industrial formulation IAPWS-IF97.*, vol. 59. Berlin, Heidelberg: Springer-Verlag Berlin Heidelberg, 2008. doi: 10.1007/978-3-662-53219-5.
- [64] V. Ganapathy, *Industrial Boilers and Heat Recovery Steam Generators: Design, Applications, and Calculations.*, 2003.
- [65] W. Staniar, *Plant Engineering Handbook*, vol. 1 2 impr. 2001.
- [66] D. P. D. F.P. Incropera, *Introduction to Heat Transfer*, 3rd ed. John Wiley, 1996.
- [67] “Thin walled vessel and Thick walled cylinders,” *Freestudy.co.uk*.
<http://www.freestudy.co.uk/statics/complex/t1.pdf>
- [68] I. Journal, E. Science, T. Vol, M. Engineering, T. Tirunelveli, and P. Engineering, “FAILURE ANALYSIS ON T 92 STEEL TUBE AND COMPARED WITH PREDICTED NUMBER OF CYCLES TO FAILURE USING COFFIN-MANSON EQUATION,” vol. 2,

no. 10, pp. 5017–5033, 2010.

[69] J. Huang, K. Zhou, J. Xu, X. Xu, and J. Xie, “Failure evaluation of steam - side oxide scales in superheater tubes during unsteady thermal processes: A probabilistic method,” no. Xxx, pp. 1–11, 2014, doi: 10.1002/maco.201307338.

[70] G. R. Holcomb and G. R. Holcomb, “Materials at High Temperatures A review of the thermal expansion of magnetite A review of the thermal expansion of magnetite,” *Mater. High Temp.*, vol. 00, no. 00, pp. 1–8, 2018, doi: 10.1080/09603409.2018.1520953.

[71] J. P. Pan, S. H. Tu, G. L. Sun, X. W. Zhu, L. J. Tan, and B. Hu, “High-temperature creep properties and life predictions for T91 and T92 steels,” *IOP Conf. Ser. Mater. Sci. Eng.*, vol. 292, no. 1, 2018, doi: 10.1088/1757-899X/292/1/012098.

[72] N. A. Alang and K. Nikbin, “A new approach to predict creep rupture of Grade 92 steel under multiaxial stress states,” *Int. J. Mech. Sci.*, vol. 163, no. June, 2019, doi: 10.1016/j.ijmecsci.2019.105096.

[73] E. J. Mills, “Prediction of Creep Failure Time for Pressure Vessels,” pp. 5–10, 2015.

[74] BR. W. Bailey, “Design Aspect of Creep,” *J. Appl. Mech.*

[75] B. B. Jha, S. Ojha, and B. Misra, “Residual life estimation of high temperature tubings based on oxide scale thickness measurement,” *Remain. Life Assess. Aged Component Therm. Power Plants Petrochemical Ind.*, vol. 2, pp. 43–56, 2008.

[76] J. Li, H. Wei, and Z. Yuan, “Research on Remaining Life Evaluation Method of T92 Steel for Superheater Tube Based on Oxide Layer Growth,” *J. Fail. Anal. Prev.*, vol. 19, no. 3, pp. 802–808, 2019, doi: 10.1007/s11668-019-00662-6.

[77] W. Bendick and J. Gabrel, “Assessment of creep rupture strength for the new martensitic 9% Cr steels E911 and T/P92,” *Mater. High Temp.*, vol. 25, no. 3, pp. 139–148, 2008, doi: 10.3184/096034008X356330.

[78] J. L. Huang, K. Y. Zhou, J. Q. Xu, and X. H. Xu, “Probabilistic creep rupture life evaluation of T91 alloy boiler superheater tubes influenced by steam-side oxidation,” *Mater. Corros.*, vol. 65, no. 8, pp. 786–796, 2014, doi: 10.1002/maco.201206963.

[79] J. Qi, H. Xu, P. Lu, and K. Zhou, “Creep rupture life assessment of superheater tube with oxide formation in power plant,” *Mater. Corros.*, vol. 71, no. 12, pp. 2029–2037, 2020, doi: 10.1002/maco.202011728.

[80] B. Bicqué et al., “Mechanical behaviour of iron oxide scale: Experimental and numerical study To cite this version: HAL Id: hal-00514111 Mechanical behaviour of

iron oxide scale: experimental and numerical study,” 2012.

[81] E. I. Samuel, B. K. Choud, D. P. R. Palaparti, and M. D. Mathew, “Creep Deformation and Rupture Behaviour of P92 Steel at 923 K,” vol. 55, pp. 64–69, 2013, doi: 10.1016/j.proeng.2013.03.220.

[82] H. K. Kota Sawada, “CREEP DEFORMATION, RUPTURE STRENGTH, AND RUPTURE DUCTILITY OF GRADES T/P92 STEELS,” pp. 1–9, 2014.

[83] M. Nie et al., “Microstructure evolution and life assessment of T92 steel during long-term creep,” *J. Alloys Compd.*, vol. 588, pp. 348–356, 2014, doi: 10.1016/j.jallcom.2013.11.080.

A. APPENDIX

A.1 Properties of T92 alloy steel and steam side oxide

Table A.1: Geometry of T92 superheater tubes

D (mm)	d (mm)	L (mm)	N_W	S_L (mm)	S_T (mm)	m_S (Kg/h)	m_g (Kg/h)
50.8	43.8	1000	32	76.2	244	3600	2.34×10^6

Table A.2: Thermo-physical properties of metal and oxide

Materials	T (°C)	K ($W m^{-1} K^{-1}$)	ρ ($Kg m^{-3}$)	ν	E (MPa)
T92	600	26.69	7770	0.30	12.5×10^4
	650	26.53			
δ_{ox}	600	26.69	5010	0.29	12×10^4
	650	0.875			

Table A.3: Thermo- physical properties of steam

P_S (MPa)	T_S (°C)	C_S ($KJ Kg^{-1} K^{-1}$)	μ_S ($P_a S \times 10^{-6}$)	K_S ($W m^{-1} K^{-1} \times 10^{-3}$)
25	500	3.7661	30.80	99.02
25	550	3.2354	32.66	99.22
25	600	2.9679	34.55	102.1
25	650	2.8168	36.44	106.4
25	700	2.7267	38.31	111.5

Table A.4: Thermo- physical properties of flue gas

T_g (°C)	C_g ($J Kg^{-1} K^{-1}$)	μ_g ($P_a S$)	K_g ($W m^{-1} K^{-1}$)
800	1222	0.04283	0.06993
900	1242	0.04524	0.07468
1000	1259	0.04755	0.07911

Table A.5: Oxide scale and Temperature of boiler tube for a given time

Time(hr)	$c(m)$	$b(m)$	$a(m)$	$\delta_x(\mu m)$	$T_{metal(c)}(^{\circ}C)$	$T_{oxide(a)}(^{\circ}C)$	$T_{interface(b)}(^{\circ}C)$
2000	0.0254	0.021948	0.021852	96.0690	653.6	631.7	642.3
4000	0.0254	0.021971	0.021829	141.3280	657.9	631.3	646.8
6000	0.0254	0.021989	0.021811	178.6649	661.2	631	650.3
8000	0.0254	0.022006	0.021794	211.9621	664.3	630.7	653.5
10000	0.0254	0.022021	0.021779	242.8193	666.9	630.5	656.3

Table A.6: Creep parameter of T92 steel at temperature of 600°C of steam

K	n_{met}	n_{ox}	q	Inner diameter (m)	Outer diameter (m)	Steam pressure (MPa)	Gas pressure (MPa)
1.10×10^{-45}	5	3	0	0.021948	0.0254	25	0.1
				0.021971	0.0254		
				0.021989	0.0254		
				0.022006	0.0254		
				0.022021	0.0254		

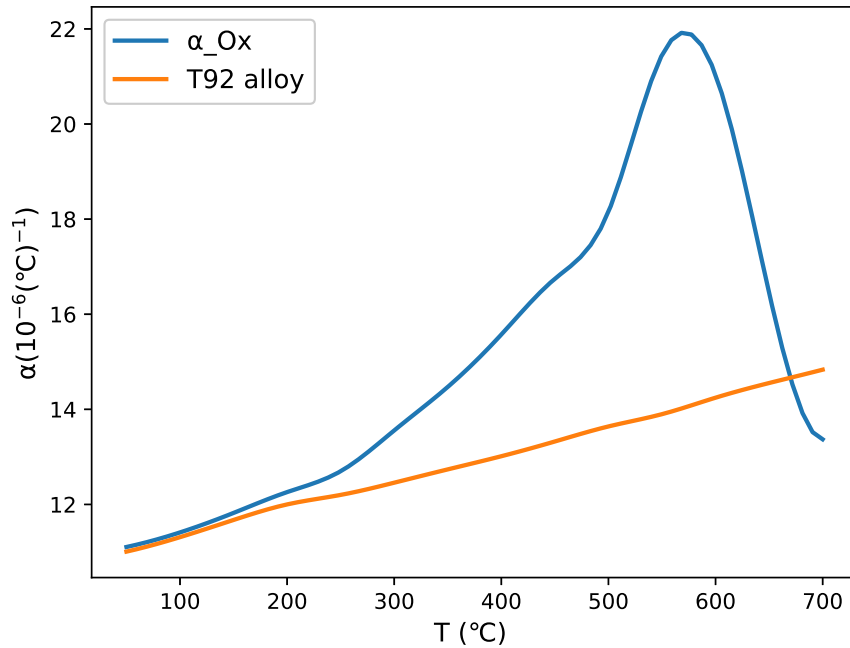


Figure A.1: Thermal expansion of T92 alloy and oxide scale at different temperature

B. APPENDIX

B.1 Python code for predicting oxide scale growth

```
1
2 #Analytical Analysis of oxide scale growth
3 #The code is help easily compute the growth of oxide scale at different
   temperature and working time
4
5 import math
6 import numpy as np
7
8 #pure constants
9 D=0.0508           #outer diameter of the tube
10 d=0.0438          #Initial inner diameter of the tube
11 L=1                #length of the tube
12 Nw=32             #number of tube
13 S1=0.0762         #tube pitch along the flow direction of flue gas
14 St=0.244          #the pitch in the perpendicular direction
15 ms=3600.0         #mass flow rate of steam
16 mg=2.34*(10**6)  #mass flow rate of gas
17 H=10              #height of flue gas
18 ro=D/2            #outer radius of the tube
19 ri=d/2            #Initial inner radius of the tube
20 A1 = 2*math.pi*ro #Area of the metal (Element 1)
21
22
23 #properties of metal
24 #0 is 600 and 1 is 650
25 def get_km(T):
26     if(T==0):
27         return 26.69
28     elif(T==1):
29         return 26.53
30 #Properties of oxide
31 def get_kox(T):
32     if(T==0):
33         return 0.84
34     elif(T==1):
35         return 0.875
```

```

36
37 # properties of steam
38 def get_μs(T):
39     if(T==0):
40         return 34.55 *(10**-6)
41     elif(T==1):
42         return 36.44*(10**-6)
43 def get_ks(T):
44     if(T==0):
45         return 102.1*(10**-3)
46     elif(T==1):
47         return 106.4*(10**-3)
48 def get_cs(T):
49     if(T==0):
50         return 2967.9
51     elif(T==1):
52         return 2816.8
53
54 #Properties of flue gas
55 #0 is 800 ,1 is 900 and 2 is 1000
56 def get_μg(T):
57     if(T==0):
58         return 0.04283
59     elif(T==1):
60         return 0.04524
61     elif(T==2):
62         return 0.04755
63 def get_kg(T):
64     if(T==0):
65         return 0.06993
66     elif(T==1):
67         return 0.07468
68     elif(T==2):
69         return 0.07911
70 def get_cg(T):
71     if(T==0):
72         return 1222
73     elif(T==1):
74         return 1242
75     elif(T==2):
76         return 1259
77
78 #get tempretures

```

```

79 def getTs(index):
80     if index==0:
81         return 600
82     elif index==1:
83         return 650
84 def getTg(index):
85     if index==0:
86         return 800
87     elif index==1:
88         return 900
89     elif index==2:
90         return 1000
91
92 # calculate length
93 def get_l(delta):
94     return ro-ri-delta
95
96 # calculate length2
97 def get_l2(delta):
98     return delta*2
99
100 # calculate the area of the oxide
101 def getA2(delta):
102     return 2*math.pi*(ri-delta)
103
104 # calculate steam convective heat transfer coefficient
105 def get_hs(ks,cs,μ,delta):
106     res=(4.0*ms)/(3600*math.pi*(d-(2*delta))*μs)
107     prs=(μs*cs)/ks
108     return 0.023*(ks/(d-(2*delta)))*((res)**0.8)*((prs)**0.4)
109
110
111 # calculate flue gas convective heat transfer coefficient
112 def get_hg(kg,cg,μg,delta):
113     reg = (D*mg)/(3600*Nw*H*(St-D)*μg)
114     prg = (μg*cg)/kg
115     return 0.33*12*(kg/D)*((reg)**0.6)*((prg)**0.33)
116
117
118 # calculate initial average temperture
119 def getIntitalAvgTemp(km,hg,hs,tg,ts):
120     l1 = get_l(0)
121     matrix1 = np.array([

```

```

122     [(km*A1/l1)+hg*A1, -1*(km*A1/l1)],
123     [-1*(km*A1/l1), (km*A1/l1)+hs*A1],
124 ]
125 # matrix1Inv = np.linalg.inv(matrix1)
126 matrix2 = np.array([
127     [hg*tg*A1],
128     [hs*ts*A1],
129 ])
130 resultMatrix = np.linalg.solve (matrix1,matrix2)
131 return resultMatrix[1][0]
132
133 def getAvgTemp(km,kox ,hg,hs ,tg,ts ,delta):
134     l1 = get_l(delta)
135     l2 = get_l2(delta)
136     A2 = getA2(delta)
137     matrix1 = np.array([
138         [(km*A1/l1)+(hg*A1) , -1*km*A1/l1, 0],
139         [-1*km*A1/l1, ((km*A1/l1)+(kox*A2/l2)) , -1*(kox*A2/l2) ],
140         [0, -1*(kox*A2/l2) , (kox*A2/l2)+(hs*A2) ]
141     ])
142     # matrix1Inv = np.linalg.inv(matrix1)
143     matrix2 = np.array([
144         [hg*tg*A1],
145         [0],
146         [hs*ts*A2]
147     ])
148     resultMatrix = np.linalg.solve(matrix1,matrix2)
149     return (resultMatrix[1][0]+resultMatrix[2][0])/2
150
151
152 # print(getAv, kligTemp(26.69, 0.84, 218, 841420, 800, 600, 1.25948*10**-6))
153
154 # print(getIntitalAvgTemp(26.69, get_hg(0.06993, 1222, 0.04283, 0), get_hs
155     (0.1021, 2967.9, 34.55*(10**-6) , 0), 800, 600))
156
157 # calculate delta by using tavg in meter
158 def getDelta(T_Avg,tFrom, tTo):
159     pFrom = (T_Avg+273.15)*(20+math.log10(tFrom))
160     pTo = (T_Avg+273.15)*(20+math.log10(tTo))
161     X_FROM = 10**(0.000564*pFrom-9.934)
162     X_TO = 10**(0.000564*pTo-9.934)
163     return ((X_TO-X_FROM)/2)*(10**-6) #converted to meter

```

```

164 # main iteration
165 def calc( $\mu$ s,ks,cs, g ,kg,cg,km,kox,ts,tg):
166     delta = 0
167     for timeIndex in range (100):
168         hg=get_hg(kg, cg,  $\mu$ g, delta)
169         hs=get_hs(ks, cs,  $\mu$ s, delta)
170         if(timeIndex==0):
171             #print("Initial")
172             T_Avg = getIntitalAvgTemp(km, hg, hs, tg, ts)
173             delta += getDelta(T_Avg, 1, 10)
174             #print(T_Avg)
175             #print("Initial")
176         else:
177             T_Avg = getAvgTemp(km, kox, hg, hs, tg, ts, delta)
178             delta += getDelta(T_Avg, ((timeIndex*10)), ((timeIndex+1)*10))
179             #print(delta)
180             print(T_Avg)
181
182
183 def run():
184     for i in range (1):
185          $\mu$ s = get_ $\mu$ s(i)
186         ks = get_ks(i)
187         cs = get_cs(i)
188         km = get_km(i)
189         kox = get_kox(i)
190         ts = getTs(i)
191         for j in range (1):
192              $\mu$ g = get_ $\mu$ g(j)
193             kg = get_kg(j)
194             cg = get_cg(j)
195             tg=getTg(j)
196             print("\nTs=",ts,"          Tg=",tg)
197             #print(""," $\mu$ s=", $\mu$ s, "ks=", ks, "cs=",cs, " $\mu$ g=", $\mu$ g, "kg=",kg, "cg
198             =" ,cg, "km=",km, "kox=",kox, ts, tg)
199             print("-----")
200         )
201         calc( $\mu$ s, ks, cs,  $\mu$ g, kg, cg, km, kox, ts, tg)
202
203 run()

```

B.2 Python code for Elastic radial and hoop stress-strain

```
1 #Analytical Analysis of Elastic Hoop and Radial stress and strain, at
   different oxide scale
2 #The code is help easily compute analytically only by substituting the
   radiuses
3
4 import math
5 import numpy as np
6 import scipy
7
8 # Table of boiler tube radius at dfferent oxide scale
9           #oxide scale thicknes ( $\mu\text{m}$ )
10 #Radius  96.0690   141.3280   178.6649   211.9621   242.8193
11
12 #a      0.021852   0.021829   0.021811   0.021794   0.021779
13 #b      0.021948   0.021971   0.021989   0.022006   0.022021
14 #c      0.0254    0.0254    0.0254    0.0254    0.0254
15
16 a=float(input('Enter the value of radial positions or radius a from the above
   table:'))
17 b=float(input('Enter the value of radial positions or radius b from the above
   table:'))
18 c=float(input('Enter the value of radial positions or radius c from the above
   table:'))
19
20           # Metal and oxide properties
21 Vox=0.29           # Poisons ratio of oxide
22 Vmet=0.3           #poison's ratio of Metal
23 Eox=1.2E+11        # Youngs modulus of Oxide
24 Emet=1.25E+11     # Youngs modulus of Metal
25 Pi=25000000        #Applied internal pressure
26 Po=100000          #Applied external pressure
27
28 # k the matrix value used to calculate the ineegral constants
29
30 K12=- (1-Vox) / ((1+Vox)*(a**2))
31 K24=- (1-Vmet) / ((1+Vmet)*(c**2))
32 K42=1/b**2
33 K44=-1/b**2
34 K32=- (1-Vox) / ((1+Vox)*(b**2))
35 K33=- (Emet/Eox)*((1-Vox)/(1-Vmet))
36 K34= (Emet/Eox)*((1-Vox)/((1+Vmet)*(b**2)))
```

```

37
38 B1=-((1-Vox)/Eox)*Pi
39 B2=-((1-Vmet)/Emet)*Po
40 B3=0
41 B4=0
42
43 K=np.array ([[1,K12,0,0],[0,0,1,K24],[1,K32,K33,K34],[1,K42,-1,K44]])
44 Kinv = np.linalg.inv (K)
45
46
47 B = np.array ([[B1],[B2],[B3],[B4]])
48 C = np.linalg.solve (K,B)
49
50 #C: values are the value of integral constant
51 #C11: integration constant at the position of inner surface of oxide scale
52 #C12: integration constant at the position of oxide/metal interface
53 #C21: integration constant at the position of oxide/metal interface
54 #C22: integration constant at the position of outer surface of metal tube
55
56 C11=C[0][0]
57 C12=C[1][0]
58 C21=C[2][0]
59 C22=C[3][0]
60
61 #σ_θ_ox and σ_θ_met: Hoop stress of oxide and metal at radial direction of
    the tube
62 #σ_r_ox and σ_r_met: Radial stress of oxide and metal at radial direction of
    the tube
63
64 #Symboles meaning
65
66 #σ_θ : Hoop stress          ox: Oxide part
67 #σ_r : Radial stress       met: Metal Part
68
69 σ_θ_ox_a=(Eox/(1-Vox**2))*(C11*(1+Vox)+C12*((1-Vox)/a**2))
70 σ_θ_ox_b=(Eox/(1-Vox**2))*(C11*(1+Vox)+C12*((1-Vox)/b**2))
71 σ_θ_met_b=(Emet/(1-Vmet**2))*(C21*(1+Vmet)+C22*((1-Vmet)/b**2))
72 σ_θ_met_c=(Emet/(1-Vmet**2))*(C21*(1+Vmet)+C22*((1-Vmet)/c**2))
73
74
75 σ_r_ox_a=(Eox/(1-Vox**2))*(C11*(1+Vox)-C12*((1-Vox)/a**2))
76 σ_r_ox_b=(Eox/(1-Vox**2))*(C11*(1+Vox)-C12*((1-Vox)/b**2))
77 σ_r_met_b=(Emet/(1-Vmet**2))*(C21*(1+Vmet)-C22*((1-Vmet)/b**2))

```

```

78  $\sigma_{r\_met\_c} = (E_{met} / (1 - \nu_{met}^{**2})) * (C21 * (1 + \nu_{met}) - C22 * ((1 - \nu_{met}) / c^{**2}))$ 
79
80 # $\epsilon_{\theta\_ox}$  and  $\epsilon_{\theta\_met}$ : Hoop strain of oxide and metal at radial direction of the
    tube
81 # $\epsilon_{r\_ox}$  and  $\epsilon_{r\_met}$ : Radial strain of oxide and metal at radial direction of
    the tube
82
83  $\epsilon_{\theta\_ox\_a} = C11 + C21 / a^{**2}$ 
84  $\epsilon_{\theta\_ox\_b} = C11 + C21 / b^{**2}$ 
85  $\epsilon_{\theta\_met\_b} = C21 + C22 / b^{**2}$ 
86  $\epsilon_{\theta\_met\_c} = C21 + C22 / c^{**2}$ 
87
88  $\epsilon_{r\_ox\_a} = C21 - C22 / a^{**2}$ 
89  $\epsilon_{r\_ox\_b} = C21 - C22 / b^{**2}$ 
90  $\epsilon_{r\_ox\_c} = C21 - C22 / c^{**2}$ 
91
92
93 print()

```

B.3 Python code for Thermo-Mechanical radial and hoop stress-strain

```

1 #Analytical Analysis of Thermo-mechanical Hoop and Radial stress and strain,
  at different oxide scale
2 #The code is help easily compute analytically only by substituting the
  radiuses
3
4 import math
5 import numpy as np
6 import scipy
7
8
9 # Table 1: Boiler tube radius at dfferent oxide scale
10
11 #oxide scale thicknes ( $\mu\text{m}$ )
12
13 #Radius      96.0690      141.3280      178.6649      211.9621      242.8193
14
15 #a           0.021852      0.021829      0.021811      0.021794      0.021779
16 #b           0.021948      0.021971      0.021989      0.022006      0.022021
17 #c           0.0254        0.0254        0.0254        0.0254        0.0254
18
19 # Table 2: Each surface temperature and thermal expansion cofficent at
  differnt oxide scale
20
21 #Oxide thickness  Ta      Tb      Tc       $\alpha_{\text{met}}$        $\alpha_{\text{ox}}$ 
22
23 # 96.0690        631.7   642.3   653.6   14.57E-6   18.31E-6
24 # 141.3280       631.3   646.8   657.9   14.6E-6    18.35E-6
25 # 178.6649       631     650.3   661.2   14.62E-6   18.38E-6
26 # 211.9621       630.7   653.5   664.3   14.63E-6   18.41E-6
27 # 242.8193       630.5   656.3   666.9   14.65E-6   18.43E-6
28
29
30 a=float(input('Enter the value of radial positions or radius a from the above
  Table 1:'))
31 b=float(input('Enter the value of radial positions or radius b from the above
  Table 1:'))
32 c=float(input('Enter the value of radial positions or radius c from the above
  Table 1:'))
33  $\alpha_{\text{met}}$ =float(input('Enter the value of  $\alpha_{\text{met}}$  for the required oxide thickness
  from the above Table 2:'))
34  $\alpha_{\text{ox}}$ =float(input('Enter the value of  $\alpha_{\text{ox}}$  for the required oxide thickness
  from the above Table 2:'))
35 Ta=float(input('Enter the value of Ta for the required oxide thicknessfrom
  the above Table 2:'))

```

```

32 Tb=float(input('Enter the value of Tb for the required oxide thickness from
    the above Table 2:'))
33 Tc=float(input('Enter the value of Tc for the required oxide thickness from
    the above Table 2:'))
34
35 # Metal and oxide properties
36
37 Vox=0.29 # Poisons ratio of oxide
38 Vmet=0.3 #poison's ratio of Metal
39 Eox=1.2E+11 # Youngs modulus of Oxide
40 Emet=1.25E+11 # Youngs modulus of Metal
41 Pi=25000000 #Applied internal pressure
42 Po=100000 #Applied external pressure
43 # k the matrix value used to calculate the ineegral constants
44
45 k12=- (1-2*Vox)/(a**2)
46 K24=- (1-2*Vmet)/(c**2)
47 K32=1/b**2
48 K34=-1/b**2
49 K42=- (1-2*Vox)/(b**2)
50 k43=- ((Emet/Eox)*((1+Vox)*(1-2*Vox)))/((1+Vmet)*(1-2*Vmet))
51 K44=((Emet/Eox)*((1+Vox)*(1-2*Vox)))/((1+Vmet)*(b**2))
52
53 B1=- ((1+Vox)*(1-2*Vox)/Eox)*Pi
54 B2= $\alpha_{met} * ((1+Vmet)/(1-Vmet)) * ((1-2*Vmet)/(c**2)) * (Tc-Tb) * (((c**2)-(b**2))/2) - ((1+Vmet)*(1-2*Vmet)/Emet) * Po$ 
55 B3=- $\alpha_{ox} * ((1+Vox)/(1-Vox)) * ((1)/(b**2)) * (Tb-Ta) * (((b**2)-(a**2))/2)$ 
56 B4= $\alpha_{ox} * ((1+Vox)/(1-Vox)) * ((1-2*Vox)/(b**2)) * (Tb-Ta) * (((b**2)-(a**2))/2)$ 
57
58 K=np.array ([[1,k12,0,0],[0,0,1,K24],[1,K32,-1,K34],[1,K42,k43,K44]])
59 Kinv = np.linalg.inv (K)
60
61 B = np.array([[B1],[B2],[B3],[B4]])
62 C = np.linalg.solve (K,B)
63
64 #C: values are the value of integral constant
65 #p11: integration constant at the position of iner surface of oxide scale
66 #q12: integration constant at the position of oxide/metal interface
67 #p21: integration constant at the position of oxide/metal interface
68 #q22: integration constant at the position of outer surface of metal tube
69
70 p11=C[0][0]
71 q12=C[1][0]

```

```

72 p21=C[2][0]
73 q22=C[3][0]
74
75 #Thermal_σ_θ_ox and σ_θ_met: Thermal Hoop stress of oxide and metal at radial
    direction of the tube
76 #Thermal_σ_r_ox and σ_r_met: Thermal Radial stress of oxide and metal at
    radial direction of the tube
77
78 Thermal_σ_θ_ox_a=Eox*((α_ox/((1-Vox)*(a**2)))*((Tb-Ta)*((a**2)-(a**2))/2)+(
    p11/((1+Vox)*(1-2*Vox)))+(q12/((1+Vox)*(a**2)))-((α_ox*(Tb-Ta))/(1-2*Vox))
    )
79 Thermal_σ_θ_ox_b=Eox*((α_ox/((1-Vox)*(b**2)))*((Tb-Ta)*((b**2)-(a**2))/2)+(
    p11/((1+Vox)*(1-2*Vox)))+(q12/((1+Vox)*(b**2)))-((α_ox*(Tb-Ta))/(1-2*Vox))
    )
80 Thermal_σ_θ_met_b=Emet*((α_met/((1-Vmet)*(b**2)))*((Tc-Tb)*((b**2)-(b**2))/2)
    +(p21/((1+Vmet)*(1-2*Vmet)))+(q22/((1+Vmet)*(b**2)))-((α_met*(Tc-Tb))
    /(1-2*Vmet)))
81 Thermal_σ_θ_met_c=Emet*((α_met/((1-Vmet)*(c**2)))*((Tc-Tb)*((c**2)-(b**2))/2)
    +(p21/((1+Vmet)*(1-2*Vmet)))+(q22/((1+Vmet)*(c**2)))-((α_met*(Tc-Tb))
    /(1-2*Vmet)))
82
83 Thermal_σ_r_ox_a=Eox*((-α_ox/((1-Vox)*(a**2)))*((Tb-Ta)*((a**2)-(a**2))/2)+(
    p11/((1+Vox)*(1-2*Vox)))-(q12/((1+Vox)*(a**2))))
84 Thermal_σ_r_ox_b=Eox*((-α_ox/((1-Vox)*(b**2)))*((Tb-Ta)*((b**2)-(a**2))/2)+(
    p11/((1+Vox)*(1-2*Vox)))-(q12/((1+Vox)*(b**2))))
85 Thermal_σ_r_met_b=Emet*((-α_met/((1-Vmet)*(b**2)))*((Tc-Tb)*((b**2)-(b**2))
    /2)+(p21/((1+Vmet)*(1-2*Vmet)))-(q22/((1+Vmet)*(b**2))))
86 Thermal_σ_r_met_c=Emet*((-α_met/((1-Vmet)*(c**2)))*((Tc-Tb)*((c**2)-(b**2))
    /2)+(p21/((1+Vmet)*(1-2*Vmet)))-(q22/((1+Vmet)*(c**2))))
87
88
89 #Thermal_ε_θ_ox and ε_θ_met: Thermal Hoop strain of oxide and metal at radial
    direction of the tube
90
91
92 Thermal_ε_θ_ox_a=((1+Vox)/(1-Vox))*(α_ox/(a**2))*((Tb-Ta)*((a**2)-(a**2))/2)
    +(p11)+(q12/(a**2))
93 Thermal_ε_θ_ox_b=((1+Vox)/(1-Vox))*(α_ox/(b**2))*((Tb-Ta)*((b**2)-(a**2))/2)
    +(p11)+(q12/(b**2))
94 Thermal_ε_θ_met_b=((1+Vmet)/(1-Vmet))*(α_met/(b**2))*((Tc-Tb)*((b**2)-(b**2))
    /2)+(p21)+(q22/(b**2))
95 Thermal_ε_θ_met_c=((1+Vmet)/(1-Vmet))*(α_met/(c**2))*((Tc-Tb)*((c**2)-(b**2))
    /2)+(p21)+(q22/(c**2))

```

```

96
97 #Thermal_ε_r_ox andε_r_met: Thermal Radial strain of oxide and metal at radial
    direction of the tube
98
99 Thermal_ε_r_ox_a=((1+Vox)/(1-Vox))*((-α_ox/(a**2))*((Tb-Ta)*((a**2)-(a**2))
    /2)+(α_ox*(Tb-Ta)))+p11-(q12/(a**2))
100 Thermal_ε_r_ox_b=((1+Vox)/(1-Vox))*((-α_ox/(b**2))*((Tb-Ta)*((b**2)-(a**2))
    /2)+(α_ox*(Tb-Ta)))+p11-(q12/(b**2))
101 Thermal_ε_r_met_b=((1+Vmet)/(1-Vmet))*((-α_met/(b**2))*((Tc-Tb)*((b**2)-(b
    **2))/2)+(α_met*(Tc-Tb)))+p21-(q22/(b**2))
102 Thermal_ε_r_met_c=((1+Vmet)/(1-Vmet))*((-α_met/(c**2))*((Tc-Tb)*((c**2)-(b
    **2))/2)+(α_met*(Tc-Tb)))+p21-(q22/(c**2))
103
104 print(Thermal_σ_θ_ox_a)
105 print(Thermal_σ_θ_ox_b)
106 print(Thermal_σ_θ_met_b)
107 print(Thermal_σ_θ_met_c)
108
109 print(Thermal_σ_r_ox_a)
110 print(Thermal_σ_r_ox_b)
111 print(Thermal_σ_r_met_b)
112 print(Thermal_σ_r_met_c)
113
114 print(Thermal_ε_θ_ox_a)
115 print(Thermal_ε_θ_ox_b)
116 print(Thermal_ε_θ_met_b)
117 print(Thermal_ε_θ_met_c)
118
119 print(Thermal_ε_r_ox_a)
120 print(Thermal_ε_r_ox_b)
121 print(Thermal_ε_r_met_b)
122 print(Thermal_ε_r_met_c)

```

B.4 Python code for Creep stress and strain rate

```
1
2 #Analytical Analysis of Creep Hoop and Radial stress and strain rate, at
   different oxide scale
3 #The code is help easily compute analytically only by substituting the
   radiuses
4
5 import math
6 import numpy as np
7 import scipy
8
9 # Table of boiler tube radius at dfferent oxide scale
10
   #oxide scale thicknes ( $\mu\text{m}$ )
11 #Radius    96.0690    141.3280    178.6649    211.9621    242.8193
12
13 #a    0.021852    0.021829    0.021811    0.021794    0.021779
14 #b    0.021948    0.021971    0.021989    0.022006    0.022021
15 #c    0.0254     0.0254     0.0254     0.0254     0.0254
16
17 #t is the working hour, for this research the working hour and the oxide
   scale is shown below
18 #      t           oxide scale
19 #    2000           96.0690
20 #    4000           141.3280
21 #    6000           178.6649
22 #    8000           211.9621
23 #   10000           242.8193
24
25 a=float(input('Enter the value of radial positions or radius a from the above
   table:'))
26 b=float(input('Enter the value of radial positions or radius b from the above
   table:'))
27 c=float(input('Enter the value of radial positions or radius c from the above
   table:'))
28 t=int(input("Enter the value of t of oxide scale from the above time vs oxide
   scale table:"))
29
30 # Metal and oxide properties
31
32 nox=3           #stress constan of oxide
33 nmet=5          #stress constant of Metal
34 Pi=25000000    #Applied internal pressure
```

```

35 Po=100000                                #Applied external pressure
36 kmet=1.1E-45                              #Creep parameter of material
37 q=0                                        #Creep parameter of material
38
39 # k the matrix value used to calculate the ineegral constants
40 k11=- (nox/2)*(a**(-2/nox))
41 k23=- (nmet/2)*(c**(-2/nmet))
42 k31=- (nox/2)*(b**(-2/nox))
43 k33=(nmet/2)*(b**(-2/nmet))
44 k42=1/b
45 k43=-1/b
46 B1=-Pi
47 B2=-Po
48 B3=0
49 B4=0
50
51 K=np.array ([[k11,1,0,0],[0,0,k23,1],[k31,1,k33,-1],[0,k42,k43,0]])
52 Kinv = np.linalg.inv (K)
53
54 B = np.array([[B1],[B2],[B3],[B4]])
55 C = np.linalg.solve (K,B)
56
57 #C: values are the value of integral constant
58 #C11: integration constant at the position of iner surface of oxide scale
59 #C12: integration constant at the position of oxide/metal interface
60 #C21: integration constant at the position of oxide/metal interface
61 #C22: integration constant at the position of outer surface of metal tube
62
63 C11=C[0][0]
64 C12=C[1][0]
65 C21=C[2][0]
66 C22=C[3][0]
67
68 #σr_ox and σθ_met: Radial and Hoop stress of metal at radial direction of
   the tube
69
70 σr_met_b=-((nmet/2)*(C21*b**(-2/nmet)))+C22
71 σr_met_c=-((nmet/2)*(C21*c**(-2/nmet)))+C22
72 σθ_met_b=σr_met_b+(C21/(b**(2/nmet)))
73 σθ_met_c=σr_met_c+(C21/(c**(2/nmet)))
74
75 σe_b=(1.732/2)*(σθ_met_b-σr_met_b)
76 σe_c=(1.732/2)*(σθ_met_c-σr_met_c)

```

```

77
78
79 #εrmet and εθmet: Radial and Hoop strain of metal at radial direction of
    the tube}
80
81 εθmet_b=kmet*((1.732/2)**(nmet+1))*((σθmet_b-σrmet_b)**nmet)*t
82 εθmet_c=kmet*((1.732/2)**(nmet+1))*((σθmet_c-σrmet_c)**nmet)*t
83
84 εrmet_b=-kmet*((1.732/2)**(nmet+1))*((σθmet_b-σrmet_b)**nmet)*t
85 εrmet_c=-kmet*((1.732/2)**(nmet+1))*((σθmet_c-σrmet_c)**nmet)*t
86
87
88 #εrate_rmet and εrate_θmet: Radial and Hoop strain rate of metal at
    radial direction of the tube}
89
90 εrate_θmet_b=(3/4)*kmet*(σe_b** (nmet-1))*(σθmet_b-σrmet_b)*(t**(1-q))
91 εrate_θmet_c=(3/4)*kmet*(σe_c** (nmet-1))*(σθmet_c-σrmet_c)*(t**(1-q))
92
93 εrate_rmet_b=-(3/4)*kmet*(σe_b** (nmet-1))*(σθmet_b-σrmet_b)*(t**(1-q))
94 εrate_rmet_c=-(3/4)*kmet*(σe_c** (nmet-1))*(σθmet_c-σrmet_c)*(t**(1-q))
95
96 print()

```
